

2 Elasticity Problems

Numerical experiments devoted to multi-component and multiscale media modelling are still one of the most important part of modern computational mechanics and engineering [98,161,272,312]. The main idea of this chapter in this context is to present a general approach to numerical analysis of elastostatic problems in 1D and 2D heterogeneous media [105,274,300,317] and the homogenisation method of periodic linear elastic engineering composite structures exhibiting randomness in material parameters [32,83,356,372,375]. As is shown below, the effective elasticity tensor components of such structures are obtained as the closed-form equations in the deterministic approach, which enables a relatively easy extension to the stochastic analysis by the application of the second order perturbation second central probabilistic moment analysis. On the other hand, the Monte Carlo simulation approach is employed to solve the cell problem. As is known from numerous books and articles in this area, the main difficulty in homogenisation is the lack of one general model valid for various composite structures; different nature homogenised constitutive relations are derived for beams, plates, shells etc. and even for the same type of engineering structure different effective relations are fulfilled for composites with constituents of different types (with ceramic, metal or polymer matrices and so forth). That is why numerous theoretical and numerical homogenisation models of composites are developed and applied in engineering practice.

All the theories in this field can be arbitrarily divided, considering especially the method and form of the final results, into two essentially different groups. The first one contains all the methods resulting in closed form equations characterizing upper and lower bounds [108,138,156,285,339] or giving direct approximations of the effective material tensors [122,123,248]. In alternative, so-called cell problems are solved to calculate, on the basis of averaged stresses or strains, the final global characteristics of the composite in elastic range [11,214,304,383], for thermoelastic analysis [117], for composites with elasto-plastic [50,57,58,146,332] or visco-elasto-plastic components [366], in the case of fractured or porous structures [38,361] or damaged interfaces [224,252,358]. The very recently even multiscale methods [236,340] and models have been worked out to include the atomistic scale effects in global composite characteristics [67,145]. The results obtained for the first models are relatively easy and fast in computation. However, usually these approximations are not so precise as the methods based on the cell problem solutions. In this context, the decisive role of symbolic computations and the relevant computational tools (MAPLE, MATHEMATICA, MATLAB, for instance) should be underlined [64,111,268]. By using the MAPLE program and any closed form equations for effective characteristics of composites as well as thanks to the stochastic second order perturbation technique (in practice of any finite order), the probabilistic moments of these characteristics can be derived and computed. The great value of such a computational technique lies in its usefulness

in stochastic sensitivity studies. The closed form probabilistic moments of the homogenised tensor make it possible to derive explicitly the sensitivity gradients with respect to the expected values and standard deviations of the original material properties of a composite.

Probabilistic methods in homogenisation [116,120,141,146,259,287,378] obey (a) algebraic derivation of the effective properties, (b) Monte–Carlo simulation of the effective tensor, (c) Voronoi–tessellations of the RVE together with the relevant FEM studies, (d) the moving–window technique. The alternative stochastic second order approach to the cell problem solution, where the SFEM analysis should be applied to calculate the effective characteristics, is displayed below. Various effective elastic characteristics models proposed in the literature are extended below using the stochastic perturbation technique and verified numerically with respect to probabilistic material parameters of the composite components. The entire homogenisation methodology is illustrated with computational examples of the two–component heterogeneous bar, fibre–reinforced and layered unidirectional composites as well as the heterogeneous plate. Thanks to these experiments, the general computational algorithm for stochastic homogenisation is proposed by some necessary modifications with comparison to the relevant theoretical approach.

Finally, it is observed that having analytical expressions for the effective Young modulus and their probabilistic moments, the model presented can be extended to the deterministic and stochastic structural sensitivity analysis for elastostatics or elastodynamics of the periodic composite bar structures. It can be done assuming ideal bonds between different homogeneous parts of the composites or even considering stochastic interface defects between them and introducing the interphase model due to the derivations carried out or another related microstructural phenomena both in linear and nonlinear range. In the same time, starting from the deterministic description of the homogenised structure, the effective behaviour related to any external excitations described by the stochastic processes can be obtained.

2.1 Composite Model. Interface Defects Concept

The main object of the considerations is the random periodic composite structure Y with the Representative Volume Element (RVE) denoted by Ω . Let us assume that Ω contain perfectly bonded, coherent and disjoint subsets being homogeneous (for classical fibre–reinforced composites there are two components, for instance) and let us assume that the scale between corresponding geometrical diameters of Ω and the whole Y is described by some small parameter $\epsilon > 0$; this parameter indexes all the tensors rewritten for the geometrical scale connected with Ω . Further, it should be mentioned that random periodic composites are considered; it is assumed that for an additional ω belonging to a suitable probability space there exists such a homothety that transforms Ω into the entire

composite Y . In the random case this homothety is defined for all probabilistic moments of input random variables or fields considered. Next, let us introduce two different coordinate systems: $\mathbf{y} = (y_1, y_2, y_3)$ at the microscale of the composite and $\mathbf{x} = (x_1, x_2, x_3)$ at the macroscale. Then, any periodic state function F defined on Y can be expressed as

$$F^\varepsilon(\mathbf{x}) = F\left(\frac{\mathbf{x}}{\varepsilon}\right) = F(\mathbf{y}) \quad (2.1)$$

This definition allows a description of the macro functions (connected with the macroscale of a composite) in terms of micro functions and vice versa. Therefore, the elasticity coefficients (being homogenised) can be defined as

$$C_{ijkl}^\varepsilon(\mathbf{x}) = C_{ijkl}(\mathbf{y}) \quad (2.2)$$

Random fields under consideration are defined in terms of geometrical as well as material properties of the composite. However the periodic microstructure as well as its macrogeometry is deterministic. Randomising different composite properties, the set of all possible realisations of a particular introduced random field have to be admissible from the physical and geometrical point of view, which is partially explained by the below relations. Let each subset Ω_a contain linear-elastic and transversely isotropic materials where Young moduli and Poisson coefficients are truncated Gaussian random variables with the first two probabilistic moments specified. There holds

$$0 < e(x; \omega) < \infty \quad (2.3)$$

$$E[e(x; \omega)] = \begin{cases} e_1; & x \in \Omega_1 \\ e_2; & x \in \Omega_2 \end{cases} \quad (2.4)$$

$$Cov(e_i(x; \omega); e_j(x; \omega)) = \begin{bmatrix} Var e_1 & 0 \\ 0 & Var e_2 \end{bmatrix}; i, j = 1, 2 \quad (2.5)$$

$$-1 < v(x; \omega) < \frac{1}{2} \quad (2.6)$$

$$E[v(x; \omega)] = \begin{cases} v_1; & x \in \Omega_1 \\ v_2; & x \in \Omega_2 \end{cases} \quad (2.7)$$

$$Cov(v_i(x; \omega); v_j(x; \omega)) = \begin{bmatrix} Var v_1 & 0 \\ 0 & Var v_2 \end{bmatrix}; i, j = 1, 2 \quad (2.8)$$

Moreover, it is assumed that there are no spatial correlations between Young moduli and Poisson coefficients and the effect of Gaussian variables cutting-off in the context of (2.3) and (2.6) does not influence the relevant probabilistic moments. This assumption will be verified computationally in the numerical

experiments; a discussion on the cross-property correlations has been done in [315]. Further, the random elasticity tensor for each component material can be defined as

$$C_{ijkl}(x; \omega) = \delta_{ij} \delta_{kl} \frac{v(x; \omega)}{(1+v(x; \omega))(1-2v(x; \omega))} e(x; \omega) + (\delta_{ik} \delta_{jl} + \delta_{il} \delta_{jk}) \frac{1}{2(1+v(x; \omega))} e(x; \omega); \quad i, j, k, l = 1, 2 \quad (2.9)$$

Considering all the assumptions posed above, the random periodicity of Y can be understood as the existence of such a translation which, applied to Ω , enables to cover the entire Y (as a consequence, the probabilistic moments of $e(x; \omega)$ and $v(x; \omega)$ are periodic too). Thus, let us adopt Y as a random composite if relevant properties of the RVE are Gaussian random variables with specified first two probabilistic moments; these variables are bounded to probability spaces admissible from mechanical and physical point of view.

Let us note that the probabilistic description of the elasticity simplifies significantly if the Poisson coefficient is assumed to be a deterministic function so that

$$v(x) = v_a, \text{ for } a=1, 2, \dots, n; \quad x \in \Omega_a \quad (2.10)$$

Finally, the random elasticity tensor field $C_{ijkl}(x; \omega)$ is represented as follows:

$$C_{ijkl}(x; \omega) = e(x; \omega) \left\{ \delta_{ij} \delta_{kl} \frac{v(x)}{(1+v(x))(1-2v(x))} + (\delta_{ik} \delta_{jl} + \delta_{il} \delta_{jk}) \frac{1}{2(1+v(x))} \right\} \quad (2.11)$$

Because of the linear relation between the elasticity tensor components and the Young modulus these components have the truncated Gaussian distribution and can thus be derived uniquely from their first two moments as

$$E[C_{ijkl}(x; \omega)] = A_{ijkl(a)}(x) \cdot E[e_a(x; \omega)] \quad (2.12)$$

for $i, j, k, l = 1, 2, a = 1, 2, \dots, n; \quad x \in \Omega_a$

and

$$\text{Var}(C_{ijkl}(x; \omega)) = A_{ijkl(a)}(x) A_{ijkl(a)}(x) \text{Var}(e_a(x; \omega)) \quad (2.13)$$

for $i, j, k, l = 1, 2, a = 1, 2, \dots, n; \quad x \in \Omega_a$,

with no sum over repeating indices at the right hand side.

There holds

$$A_{ijkl}(x) = \delta_{ij}\delta_{kl} \frac{\nu(x)}{(1+\nu(x))(1-2\nu(x))} + (\delta_{ik}\delta_{jl} + \delta_{il}\delta_{jk}) \frac{1}{2(1+\nu(x))} \quad (2.14)$$

$i, j, k, l = 1, 2$

General methodology leading to the final results of the effective elasticity tensor is to rewrite either strain energy (or complementary energy, for instance) or equilibrium equations for a homogeneous medium and the heterogeneous one. Next, the effective parameters are derived by equating corresponding expressions for the homogeneous and for the real structure. This common methodology is applied below, particular mathematical considerations are included in the next sections and only the final result useful in further general stochastic analysis is shown. The expected values for the effective elasticity tensor in the most general case can be obtained by the second order perturbation based extension as [162,208]

$$E[C_{ijkl}^{(eff)}(\mathbf{y})] = \int_{-\infty}^{+\infty} (C_{ijkl}^{(eff)0}(\mathbf{y}) + \Delta b^r C_{ijkl}^{(eff),r}(\mathbf{y}) + \frac{1}{2} \Delta b^r \Delta b^s C_{ijkl}^{(eff),rs}(\mathbf{y})) p_R(\mathbf{b}) d\mathbf{b} \quad (2.15)$$

Using classical probability theory definitions and theorems it is obtained that

$$\int_{-\infty}^{+\infty} p_R(b(\mathbf{y})) db = 1, \quad \int_{-\infty}^{+\infty} \Delta b p_R(b(\mathbf{y})) db = 0 \quad (2.16)$$

$$\int_{-\infty}^{+\infty} \Delta b^r \Delta b^s p_R(b(\mathbf{y})) db = Cov(b^r, b^s); \quad 1 \leq r, s \leq R \quad (2.17)$$

Therefore

$$E[C_{ijkl}^{(eff)}(\mathbf{y})] = C_{ijkl}^{(eff)0}(\mathbf{y}) + \frac{1}{2} C_{ijkl}^{(eff),rs} Cov(b^r, b^s) \quad (2.18)$$

Further, the covariance matrix $Cov(C_{ijkl}^{(eff)}; C_{pqmn}^{(eff)})$ of the effective elasticity tensor is calculated using its integral definition

$$\begin{aligned} & Cov(C_{ijkl}^{(eff)}; C_{pqmn}^{(eff)}) \\ &= \int_{-\infty}^{+\infty} (C_{ijkl}^{(eff)} - C_{ijkl}^{(eff)0}) (C_{pqmn}^{(eff)} - C_{pqmn}^{(eff)0}) g(b_i, b_j) db_i db_j \end{aligned} \quad (2.19)$$

whereas inserting the second order perturbation expansion it is found that

$$\begin{aligned}
&= \int_{-\infty}^{+\infty} \left\{ C_{ijkl}^{(eff)0} + \Delta b_r C_{ijkl}^{(eff),r} + \frac{1}{2} \Delta b_r \Delta b_s C_{ijkl}^{(eff),rs} - C_{ijkl}^{(eff)0} \right. \\
&\quad \left. \left(C_{mnpq}^{(eff)0} + \Delta b_r C_{mnpq}^{(eff),r} + \frac{1}{2} \Delta b_r \Delta b_s C_{mnpq}^{(eff),rs} - C_{mnpq}^{(eff)0} \right) \right\} g(b_i, b_j) db_i db_j
\end{aligned} \tag{2.20}$$

After all algebraic transformations and neglecting terms of order higher than second, there holds

$$\begin{aligned}
&Cov\left(C_{ijkl}^{(eff)}; C_{pqmn}^{(eff)} \right) \\
&= \int_{-\infty}^{+\infty} \Delta b_r C_{ijkl}^{(eff),r} \Delta b_s C_{mnpq}^{(eff),s} g(b_i, b_j) db_i db_j = C_{ijkl}^{(eff),r} C_{mnpq}^{(eff),s} Cov(b_r, b_s).
\end{aligned} \tag{2.21}$$

Then, starting from two-moment characterization of the effective elasticity tensor and the corresponding homogenisation models presented in (2.15) – (2.21), the stochastic second order probabilistic moment analysis of a particular engineering composites can be carried out. In the general case, these equations lead to a rather complicated description of probabilistic moments for the effective elasticity tensor particular components.

In the theory of elasticity the continuum is usually uniquely represented by its geometry and elastic properties; most often a character of these features is considered as deterministic. It has been numerically proved for the fibre composites that the influence of the elastic properties randomness on the deterministically represented geometry can be significant. The most general model of the linear elastic medium, and intuitively the nearest to the real material, is based on the assumption that both its geometry and elasticity are random fields or stochastic processes. The phenomenon of random, both interface [5,27,131,200, 225,242] and volumetric [74,316,342,353,388], non-homogeneities occur mainly in the composite materials. While the interface defects (technological inaccuracies, matrix cracks, reinforcement breaks or debonding) are important considering the fracturing of such composites, the volume heterogeneities generally follow the discrete nature of many media. The existing models of stochastic media (based on various kinds of geometrical tessellations) do not make it possible to analyse such problems and that is why a new formulation is proposed.

The main idea of the proposed model is a transformation of the stochastic medium into some deterministic media with random material parameters, more useful in the numerical analysis. Such a transformation is possible provided the probabilistic characteristics of geometric dimensions and total number of defects occurring at the interfaces are given, assuming that these random fields are Gaussian with non-negative or restricted values only. All non-homogeneities introduced are divided into two groups: the stochastic interface defects (SID), which have non-zero intersections with the interface boundaries, and the volumetric stochastic defects (VSD) having no common part with any interface or external composite boundary. Further, the interphases are deterministically

constructed around all interface boundaries using probabilistic bounds of geometric dimensions of the SID considered. Finally, the stochastic geometry is replaced by random elastic characteristics of composite constituents thanks to a probabilistic modification of the spatial averaging method (PAM). Let us note that the formulation proposed for including the SID in the interphase region has its origin in micro-mechanical approach to the contact problems rather than in the existing interface defects models.

Having so defined the composite with deterministic geometry and stochastic material properties, the stochastic boundary-value problem can be numerically solved using either the Monte Carlo simulation method, which is based on computational iterations over input random fields, or the SFEM based on second-order perturbation theory or based on spectral decomposition. The perturbation-based method has found its application to modeling of fibre-reinforced composites and, in view of its computational time savings, should be preferred.

Finally, let us consider the material discontinuities located randomly on the boundaries between composite constituents (interfaces) as it is shown in Figs. 2.1 and 2.2.

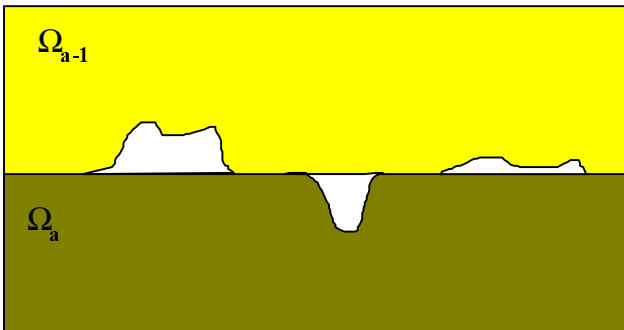


Figure 2.1. Interface defects geometrical sample

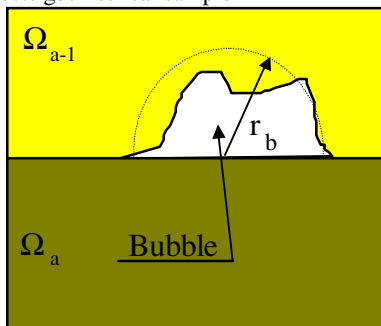


Figure 2.2. A single interface defect geometric idealization

Numerical model for such nonhomogeneities is based on the assumption that [193,194]:

- (1) there is a finite number of material defects on all composite interfaces; the total number of defects considered is assumed as a random parameter (with nonnegative values only) defined by its first two probabilistic moments;
- (2) interface defects are approximated by the semi-circles (bubbles) lying with their diameters on the interfaces; the radii of the bubbles are assumed to be the next random parameter of the problem defined by the expected value and the variance;
- (3) geometric dimensions of every defect belonging to any Ω_a are small in comparison with the minimal distance between the $\Gamma_{(a-2,a-1)}$ and $\Gamma_{(a-1,a)}$ boundaries for $a=3,\dots,n$ or with Ω_1 geometric dimensions;
- (4) all elastic characteristics specified above are assumed equal to 0 if $x \in D_a$, for $a=1,2,\dots,n$.

It should be underlined that the model introduced approximates the real defects rather precisely. In further investigations the semi-circle shape of the defects should be replaced with semi-elliptical [353] and their physical model should obey nucleation and growth phenomena [345,346] preserving a random character. However to build up the numerical procedure, the bubbles should be appropriately averaged over the interphases, which they belong to. Probabilistic averaging method is proposed in the next section to carry out this smearing.

Let us consider the stochastic material non-homogeneities contained in some $\Omega_a \subset \Omega$. The set of the defects considered D_a can be divided into three subsets D'_a , D''_a and D'''_a , where D'_a contains all the defects having a non-zero intersection with the boundary $\Gamma_{(a-1,a)}$, D''_a having zero intersection with $\Gamma_{(a-1,a)}$ and $\Gamma_{(a,a+1)}$, and D'''_a having a non-zero intersection with $\Gamma_{(a,a+1)}$. Further, all the defects belonging to subsets D'_a and D'''_a are called the stochastic interface defects (SID) and those belonging to D''_a the volumetric stochastic defects (VSD). Let us consider such Ω'_a , Ω''_a and Ω'''_a , where $\Omega_a = \Omega'_a \cup \Omega''_a \cup \Omega'''_a$, that with probability equal to 1, there holds $D'_a \subset \Omega'_a$, $D''_a \subset \Omega''_a$ and $D'''_a \subset \Omega'''_a$ (cf. Figure 2.3).

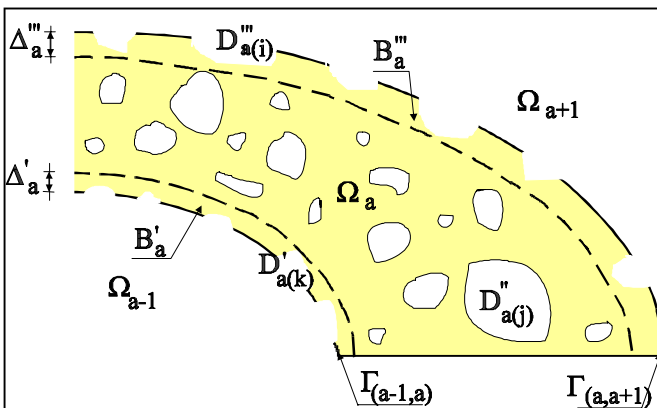


Figure 2.3. Interphase schematic representation

The subsets $\Omega'_a, \Omega''_a, \Omega'''_a$ can be geometrically constructed using probabilistic moments of the defect parameters (their geometric dimensions and total number). To provide such a construction let us introduce random fields $\Delta'_a(x; \omega)$ and $\Delta''_a(x; \omega)$ as upper bounds on the norms of normal vectors defined on the boundaries $\Gamma_{(a-1,a)}$ and $\Gamma_{(a,a+1)}$ and the boundaries of the SID belonging to D'_a , and D''_a , respectively. Next, let us consider the upper bounds of probabilistic distributions of $\Delta'_a(x; \omega)$ and $\Delta''_a(x; \omega)$ given as follows:

$$\Delta'_a = E[\Delta'_a(x; \omega)] + 3\sqrt{\text{Var}(\Delta'_a(x; \omega))} \quad (2.22)$$

$$\Delta''_a = E[\Delta''_a(x; \omega)] + 3\sqrt{\text{Var}(\Delta''_a(x; \omega))} \quad (2.23)$$

Thus, Ω'_a, Ω''_a can be expressed in the following form:

$$\Omega'_a = \{P(x_i) \in \Omega_a : d(P, \Gamma_{(a-1,a)}) \leq \Delta'_a\} \quad (2.24)$$

$$\Omega''_a = \{P(x_i) \in \Omega_a : d(P, \Gamma_{(a,a+1)}) \leq \Delta''_a\} \quad (2.25)$$

where $i=1,2$ and $d(P, \Gamma)$ denotes the distance from a point P to the contour Γ . Let us note that Ω''_a can be obtained as

$$\Omega''_a = \Omega_a - \Omega'_a \cup \Omega'''_a \quad (2.26)$$

Deterministic spatial averaging of properties Y_a on continuous and disjoint subsets Ω_a of Ω is employed to formulate the probabilistic averaging method. The averaged property $Y^{(av)}$ characterizing the region Ω is given by the following equation [65,129]:

$$Y^{(av)} = \frac{\sum_{a=1}^n Y_a |\Omega_a|}{|\Omega|}; \quad x \in \Omega \quad (2.27)$$

where $|\Omega|$ is the two-dimensional Lebesgue measure of Ω . Deterministic averaging can be transformed to the probabilistic case only if Ω is defined deterministically, and Y_a and Ω_a are uncorrelated random fields. The expected value of probabilistically averaged $Y^{(pav)}(\omega)$ on Ω can be derived as

$$E[Y^{(pav)}(\omega)] = \frac{1}{|\Omega|} \sum_{a=1}^n E[Y_a(\omega)] E[\Omega_a(\omega)] \quad (2.28)$$

and, similarly, the variance as

$$\text{Var}(Y^{(pav)}(\omega)) = \frac{1}{|\Omega|^2} \sum_{a=1}^n \text{Var}(Y_a(\omega)) \text{Var}(\Omega_a(\omega)) \quad (2.29)$$

Using the above equations Young moduli are probabilistically averaged over all Ω_a regions and their $\Omega'_a, \Omega''_a, \Omega'''_a$ subsets. Finally, a primary stochastic geometry of the considered composite is replaced by the new deterministic one. In this way, the n -component composite having m interfaces with stochastic interface defects on both sides of each interface and with volume non-homogeneities can be transformed to a $n+m$ -component structure with deterministic geometry and probabilistically defined material parameters. More detailed equations of the PAM can be derived for given stochastic parameters of interface defects (if these defects can be approximated by specific shapes – circles, hexagons or their halves for instance).

Let us suppose that there is a finite element number of discontinuities in the matrix region located on the fibre–matrix interface. These discontinuities are approximated by bubbles – semicircles placed with their diameters on the interface, see Figure 2.4. The random distribution of the assumed defects is uniquely defined by the expected values and variances of the total number and radius of the bubbles; it is shown below, there is a sufficient number of parameters to obtain a complete characterization of semicircles averaged elastic constants.

Using (2.28) and (2.29) one can determine the expected value and the variance of the effective Young modulus e_k , the terms included in the covariance matrix of this modulus and also the Poisson ratio. It yields for the expected value

$$E[e_{2c}] = E\left[\frac{S_{\Omega_{2c}} - S_b}{S_{\Omega_{2c}}} \cdot e_2\right] = E[e_2] \cdot \left(1 - \frac{1}{S_{\Omega_{2c}}} \cdot E[S_b]\right) \quad (2.30)$$

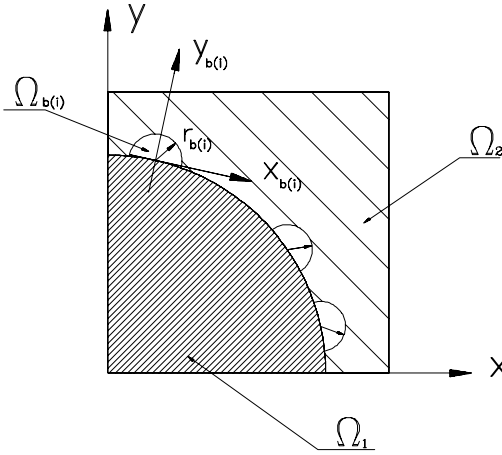


Figure 2.4. Bubble interface defects in the fibre-reinforced composite

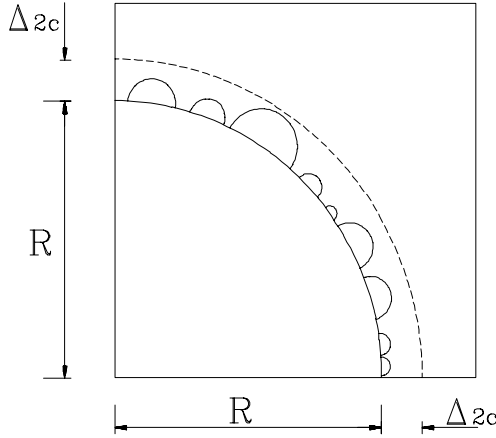


Figure 2.5. Interphase for bubble interface defects

As can be easily seen in the above relation, there holds

$$S_{\Omega_{2c}} = \pi \left\{ \left(R + E[r_{\Omega}] + 3\sqrt{\text{Var}[r_{\Omega}]} \right)^2 - R^2 \right\} \tag{2.31}$$

In a similar way the variance is derived as

$$\text{Var}[e_{2c}] = \text{Var} \left[\left(1 - \frac{S_b}{S_{\Omega_{2c}}} \right) \cdot e_2 \right] \tag{2.32}$$

It can be shown that this equation could have the following form:

$$\begin{aligned} \text{Var}[e_{2c}] = & \left\{ 1 - \frac{1}{S_{\Omega_{2c}}} E[S_b] \right\}^2 \text{Var}[e_2] \\ & + \frac{1}{S_{\Omega_{2c}}^2} \text{Var}[S_b] \text{Var}[e_2] + \frac{1}{S_{\Omega_{2c}}^2} \text{Var}[S_b] E^2[e_2] \end{aligned} \quad (2.33)$$

which, neglecting moments of higher than second order, can be reduced to

$$\text{Var}[e_{2c}] = \left\{ 1 - \frac{1}{S_{\Omega_{2c}}} E[S_b] \right\}^2 \text{Var}[e_2] + \frac{1}{S_{\Omega_{2c}}^2} \text{Var}[S_b] E^2[e_2] \quad (2.34)$$

Now the distribution parameters S_b have to be found. As can be seen

$$S_b = \frac{1}{2} \pi (r_b)^2 M_b \quad (2.35)$$

where M_b is the number of $\Omega_{b(i)}$ regions found in Ω_{2c} (according to Figures 2.4 and 2.5) and is equal to

$$M_b = 2\pi R m_b \quad (2.36)$$

Therefore, using fundamental properties of random variables it is obtained that

$$E[M_b] = 2\pi R \cdot E[m_b] \quad (2.37)$$

and

$$\text{Var}[M_b] = 4\pi^2 R^2 \cdot \text{Var}[m_b] \quad (2.38)$$

From the definition of the expected value one derives

$$E[S_b] = \frac{\pi}{2} E[(r_b)^2 M_b] = \frac{\pi}{2} \{ E^2[r_b] + \text{Var}[r_b] \} E[M_b] \quad (2.39)$$

Finally, the variance of S_b is found as

$$\text{Var}[S_b] = \text{Var}\left[\frac{\pi}{2} (r_b)^2 M_b \right] = \frac{\pi^2}{4} \text{Var}[(r_b)^2 M_b] \quad (2.40)$$

It can be shown that this expression may be transformed into the form:

$$\begin{aligned} \text{Var}[S_b] = & \frac{\pi^2}{4} \left(E^2[r_b] + \text{Var}[r_b] \right)^2 \text{Var}[M_b] \\ & + \frac{\pi^2}{2} \text{Var}[r_b] \left(E^2[M_b] + \text{Var}[M_b] \right) \left(2E^2[r_b] + \text{Var}[r_b] \right) \end{aligned} \quad (2.41)$$

Substituting the equations describing S_b distribution parameters into the relations describing the expected value and variance of the e_k modulus, we can similarly derive the data necessary for numerical analysis.

Using analogous equations, the stochastic interface defects in the fibre region can be approximated. So, let us assume a finite number of these discontinuities inserted into the contact zone. As already established, the fibre material has good resistance to degradation (much better than the matrix) and because of this, the defects in the Ω_1 region can be approximated as teeth with their sharp sides directed towards the fibre centre. A single discontinuity is, from the geometrical point of view, the superposition of two circular quadrants with the same radius (Figure 2.6). There holds

$$E[e_{1c}] = E[e_1] \left(1 - \frac{1}{S_{\Omega_{1c}}} E[S_t] \right) \quad (2.42)$$

and

$$\begin{aligned} \text{Var}[e_{1c}] = & \left\{ 1 - \frac{1}{S_{\Omega_{1c}}} E[S_t] \right\}^2 \text{Var}[e_1] \\ & + \frac{1}{S_{\Omega_{1c}}^2} \text{Var}[S_t] \text{Var}[e_1] + \frac{1}{S_{\Omega_{1c}}^2} \text{Var}[S_t] E^2[e_1] \end{aligned} \quad (2.43)$$

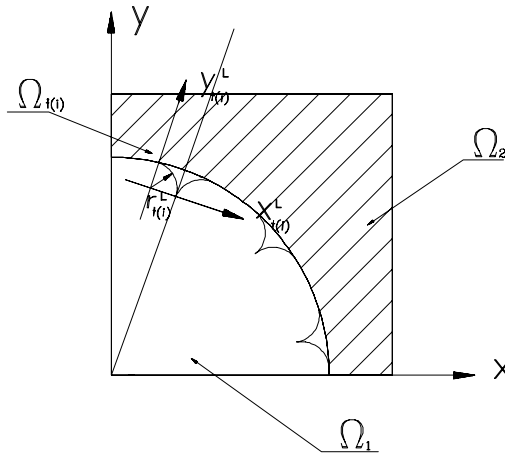


Figure 2.6. Teeth interface defects in fibre-reinforced composite

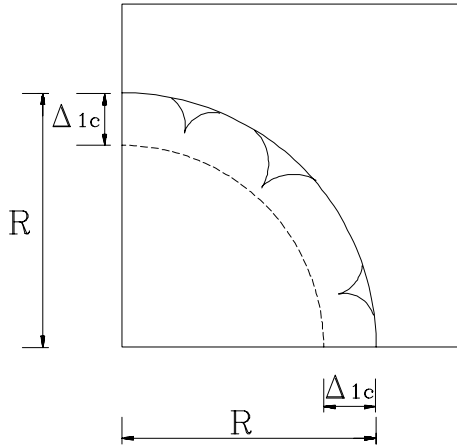


Figure 2.7. Interphase for teeth interface defects

The relations describing the discontinuity parameters will have a different form

$$S_t = \left(2 - \frac{\pi}{2}\right) r_t^2 M_t \quad (2.44)$$

so that

$$E[S_t] = \left(2 - \frac{\pi}{2}\right) E[r_t^2 M_t] = \left(2 - \frac{\pi}{2}\right) \{E^2[r_t] + \text{Var}[r_t]\} E[M_t] \quad (2.45)$$

and, finally

$$\begin{aligned} \text{Var}[S_t] &= \left(2 - \frac{\pi}{2}\right)^2 \left(E^2[r_t] + \text{Var}[r_t]\right)^2 \text{Var}[M_t] \\ &+ 2 \cdot \left(2 - \frac{\pi}{2}\right)^2 \text{Var}[r_t] \left(E^2[M_t] + \text{Var}[M_t]\right) \left(2E^2[r_t] + \text{Var}[r_t]\right) \end{aligned} \quad (2.46)$$

The Poisson ratio for the fibre interphase region can be obtained in analogous way. Finally, the covariance matrix of the Young modulus for this composite takes the following form:

$$\text{Cov}(e^{(i)}, e^{(j)}) = \begin{bmatrix} \text{Var}[e_1] & \text{Cov}[e_1, e_{1c}] & 0 & 0 \\ \text{Cov}[e_1, e_{1c}] & \text{Var}[e_{1c}] & 0 & 0 \\ 0 & 0 & \text{Var}[e_{2c}] & \text{Cov}[e_{2c}, e_2] \\ 0 & 0 & \text{Cov}[e_{2c}, e_2] & \text{Var}[e_2] \end{bmatrix} \quad (2.47)$$

Zeroing of the corresponding covariance matrix components can be achieved from the assumed mutual independence of the Young modulus in the fibre, its contact zone and associated regions for the matrix.

Special purpose numerical procedure has been implemented to check the influence of the interface defects parameters on the effective elastic parameters of the interphase. The expected values of the interface discontinuities in the matrix and fibre contact zone were assumed as 4, 10, 20 and 40 with the width of the observed interface varying between $4.0E-3$ and $2.0E-2$. The results of these computations are presented in Figures 2.8 to 2.13: the expected values of the homogenised Young modulus functions are given in Figures 2.8 and 2.9, the averaged Poisson ratio functions in Figures 2.10 and 2.11 and the variances of the Young modulus functions in Figures 2.12 and 2.13. All of these variables are marked on the vertical axis and the expected values of the interface defects radius are shown in the horizontal ones.

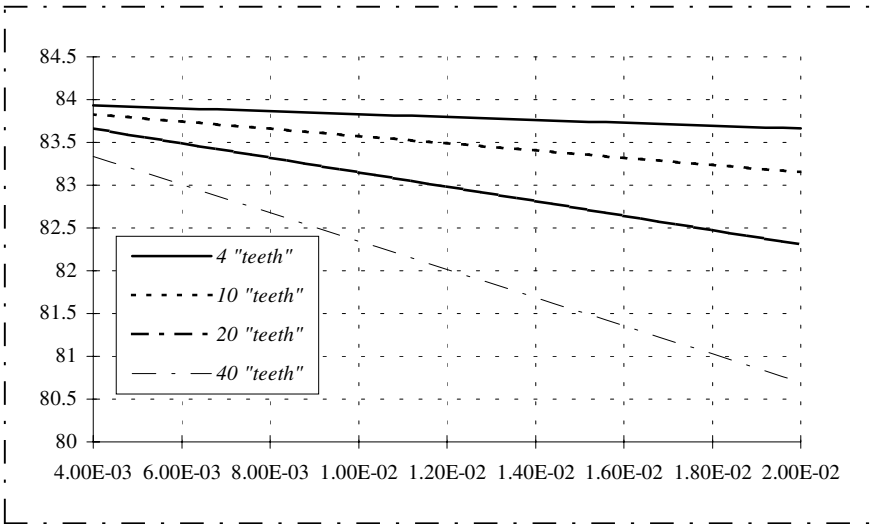


Figure 2.8. Expected values of probabilistically averaged Young modulus in fibre

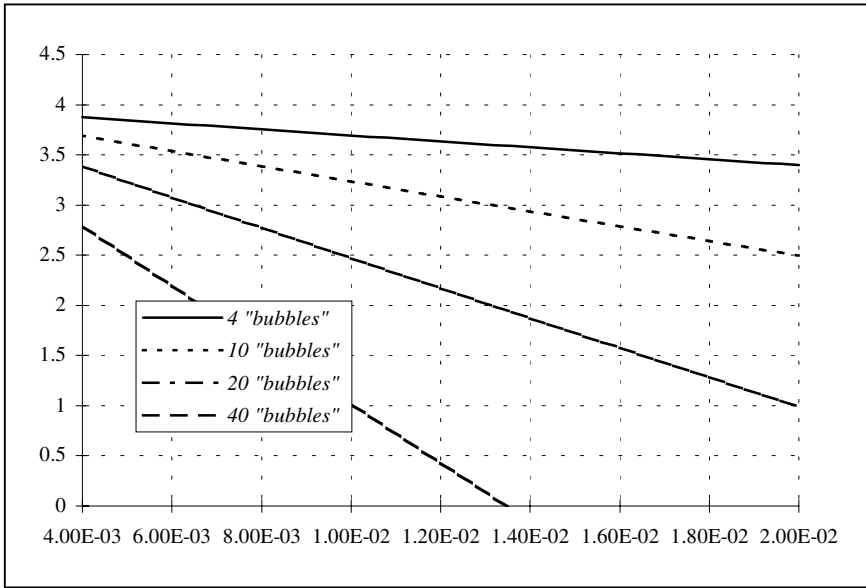


Figure 2.9. Expected values of probabilistically averaged Young modulus in matrix

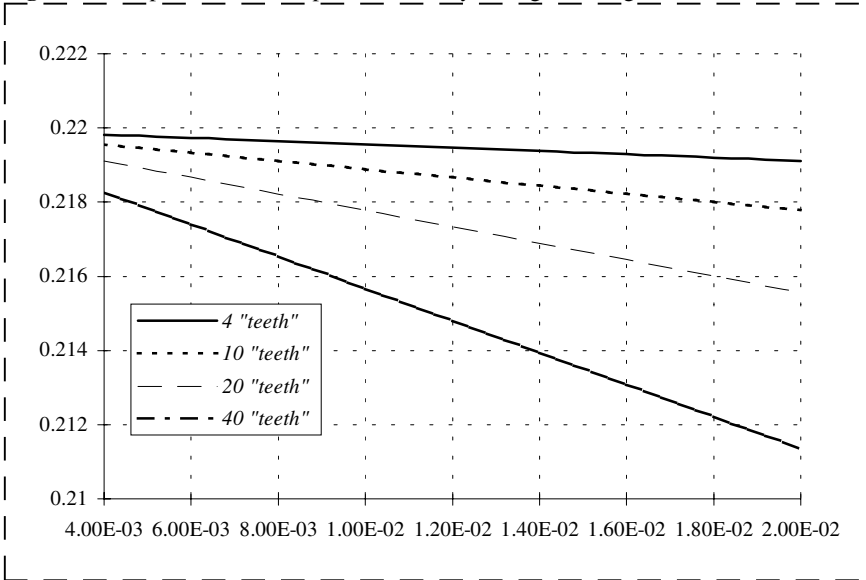


Figure 2.10. Probabilistically averaged Poisson ratio in fibre

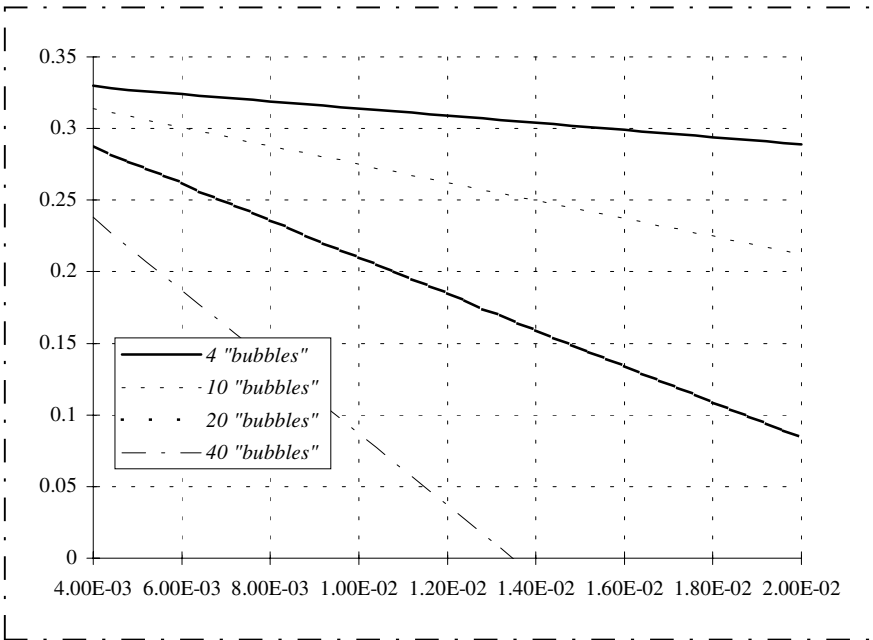


Figure 2.11. Probabilistically averaged Poisson ratio in matrix

As is expected, the resulting expected values of the homogenised Young modulus both in the matrix and the fibre regions, and similarly the Poisson ratio, are linear functions of the contact zone widths. The variances of the averaged Young modulus are second or higher order functions of this variable and this order is directly dependent on the number of interface defects.

Comparing Figures 2.8 with 2.9 and 2.12 with 2.13 it can be seen that the Young modulus in the matrix contact zone is, for the present problem, much more sensitive to variation of its parameters than the same modulus in the fibre interphase. Larger coefficient of variation of this modulus is obtained in the matrix interface region rather than in the fibre contact zone. On the other hand, the homogenised elastic properties are derived by averaging their values in both regions. Thus, greater changes in these properties can be expected in the matrix because of the larger volume of bubbles related to the fibre teeth.

Another interesting effect (cf. Figures 2.12 and 2.13) is the increase of variances of the homogenised Young modulus in the matrix contact zone for increasing width of this zone and the number of bubbles. The reverse effect occurs for the fibre side of the interface and its teeth. This is due to the fact that bubbles occupy more than half of a volume of the corresponding contact zone, and teeth less than a half.

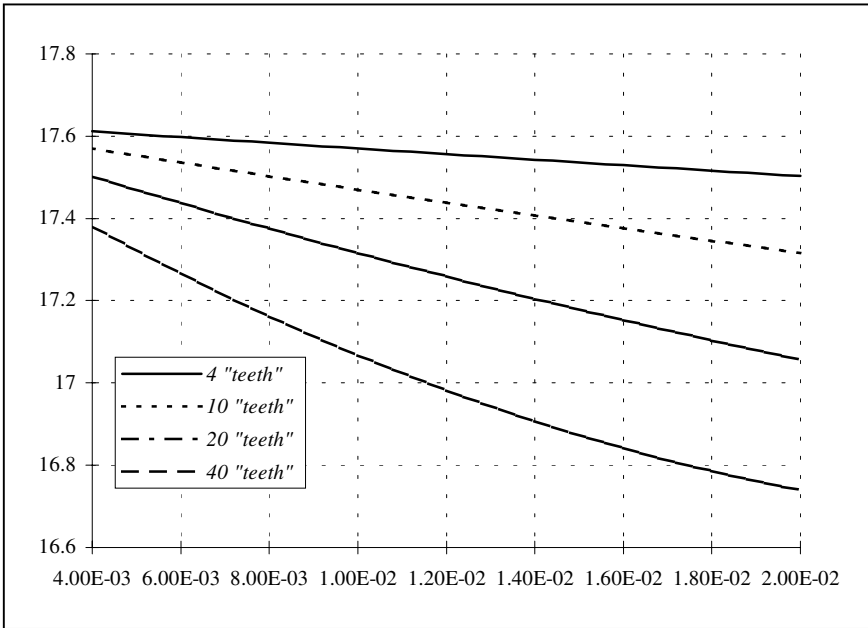


Figure 2.12. Variances of probabilistically averaged Young modulus in fibre

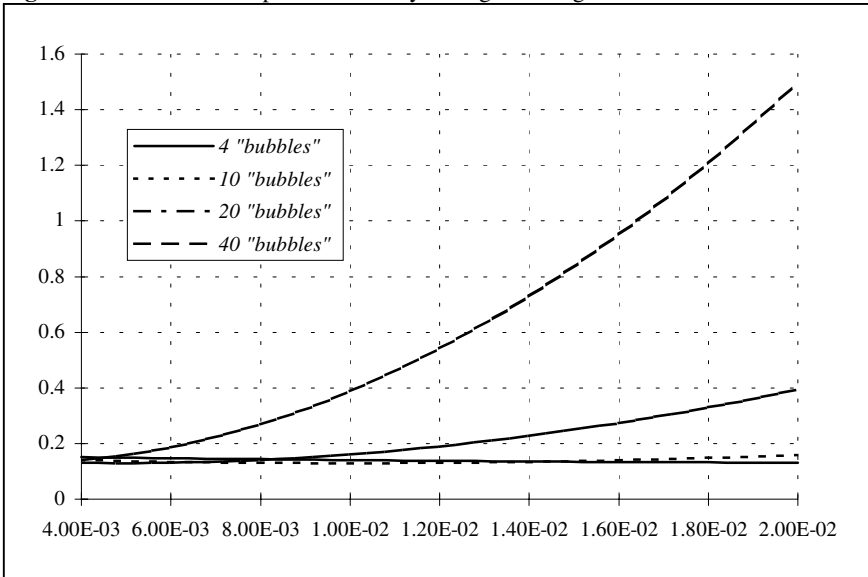


Figure 2.13. Variances of probabilistically averaged Young modulus in matrix

2.2 Elastostatics of Some Composites

Elastic properties and geometry of Ω so defined result in the random displacement field $u_i(x; \omega)$ and random stress tensor $\sigma_{ij}(x; \omega)$ satisfying the classical boundary-value problem typical for the linear elastostatics problem. Let us assume that there are the stress and displacement boundary conditions, $\partial\Omega_t$ and $\partial\Omega_u$ respectively, defined on Ω . Let C_{ijkl} be a random function of C^1 class defined on the entire Ω region. Let ρ denote the mass density of a material contained in Ω and ρf_i denote the vector of body forces per a unit volume. The boundary-differential equation system describing this equilibrium problem can be written as follows

$$\sigma_{ij}(x; \omega) = C_{ijkl}(x; \omega) \varepsilon_{kl}(x; \omega) \quad (2.48)$$

$$\varepsilon_{ij}(x; \omega) = \frac{1}{2} \left(\frac{\partial u_i(x; \omega)}{\partial x_j} + \frac{\partial u_j(x; \omega)}{\partial x_i} \right) \quad (2.49)$$

$$\sigma_{ij,j}(x; \omega) + \rho(\omega) f_i = 0 \quad (2.50)$$

$$E[u_i(x; \omega)] = E[\hat{u}_i(x; \omega)]; \quad x \in \partial\Omega_u \quad (2.51)$$

$$\text{Var}(u_i(x; \omega)) = 0; \quad x \in \partial\Omega_u \quad (2.52)$$

$$E[\sigma_{ij}(x; \omega)] n_j = E[t_i(x; \omega)]; \quad x \in \partial\Omega_t \quad (2.53)$$

$$\text{Var}(\sigma_{ij}(x; \omega)) n_j = 0; \quad x \in \partial\Omega_t \quad (2.54)$$

for $a=1,2,\dots,n$ and $i,j,k,l=1,2$.

Generally, the equation system posed above is solved using the well-established numerical methods. However it should first be transformed to the variational formulation. Such a formulation, based on the Hamilton principle, is presented in the next section. To have the formulation better illustrated, an example of the periodic superconducting coil structure is employed. The stochastic non-homogeneities simulate the technological inaccuracies of placing the superconducting cable in the RVE. Its periodicity cell in that case is subjected to horizontal uniform tension on its vertical boundaries to analyse the influence of the stochastic defects on the probabilistic moments of horizontal displacements. The stochastic variations of these displacements with respect to the thickness of the interphase constructed are verified numerically. Stochastic computational experiments are performed using the ABAQUS system and the program POLSAP specially adapted for this purpose.

2.2.1 Deterministic Computational Analysis

The main idea of the numerical experiments provided in this section is to illustrate the horizontal displacements fields and the shear stresses obtained for the deterministic problem of uniform extension of the periodicity cell quarter. Both Young modulus and Poisson ratio are assumed here as deterministic functions; for the purpose of the tests, the program ABAQUS [1] is used together with its graphical postprocessor. The periodicity cell quarter has been discretised by 224 rectangular 4-node plane strain isoparametric finite elements according to Figure 2.14.

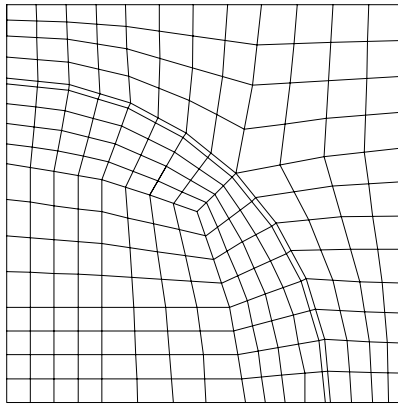


Figure 2.14. Discretisation of the fibre-reinforced composite cell quarter

The symmetry displacement boundary conditions are applied on the horizontal edges of the quarter as well as on the left horizontal edge, while the uniform extension is applied on the right vertical edge of the RVE. The standard deviations of the composite component Young moduli are taken as $\sigma(e_1) = 4.2 \text{ GPa}$, $\sigma(e_2) = 0.4 \text{ GPa}$ and the stochastic interface defect data are approximated by the following values: $E[n] = 3$, $\sigma(n) = 0.05 E[n] = 0.15$, $E[r] = 0.02 R$, $\sigma(r) = 0.1 R = 8.0 E - 4$. Probabilistically averaged values of the interphase elastic characteristics are obtained from these parameters as follows $E[e_k] = 3.82 \text{ GPa}$, $\text{Var}(e_k) = 1.48 \text{ GPa}$, $\nu_k = 0.324$ with the interphase thickness equal to $\Delta_k = 0.0104$. Four numerical experiments have been carried out for these parameters taking the values collected in Table 2.1.

Table 2.1. Young modulus values of the interphase for particular tests

Test number	1	2	3	4
e_k	e_2	$E[e_k]$	$E[e_k] - 3 \cdot \sigma(e_k)$	$E[e_k] + 3 \cdot \sigma(e_k)$

Horizontal displacement fields and the shear stress fields for particular experiments are presented in Figure 2.15 and 2.19 (test no 1), Figure 2.16 and 2.20 for test no 2, Figure 2.17, 2.21 for test no 3 and Figure 2.18 for test no 4.

Comparing these results, it is seen that a decrease of the Young modulus value lower than its expected value results in a jump of the horizontal displacements field within and around the interphase. This effect can be interpreted as the possibility of debonding of the composite components caused by the worsening of the interphase elastic parameters, which confirms the usefulness of the presented mathematical–numerical model in the interphase phenomena analysis. It should be underlined that in other models of interphase defects and contact effects at the interface, the horizontal displacements have discontinuous character too. On the other hand, increasing the Young modulus above its expected value does not introduce any sensible differences in comparison with the traditional deterministic model for the perfect interface.

Analysing the shear stresses fields $\sigma_{12}(x_i)$ collected in Figures 2.19 and 2.21 a jump of the respective values of stresses at the boundary between the fibre and the interphase region is observed in all cases. In the case of tests no. 1, 2 and 4 the shear stress fields have quite similar characters differing one from another in the interface regions placed near the horizontal and vertical edges of the periodicity cell quarter. The $\sigma_{12}(x_i)$ field obtained for test no. 3 has decisively different character: for almost the entire interface the jump of stresses between the matrix, interphase and fibre regions is visible. It may confirm the previous thesis based on the displacement results dealing with the usefulness of the model proposed for the analysis of the interface phenomena.

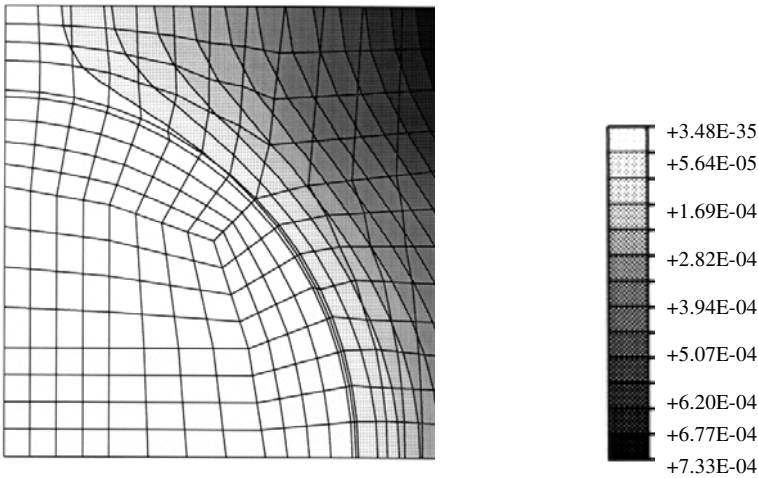


Figure 2.15. Horizontal displacements for test no. 1

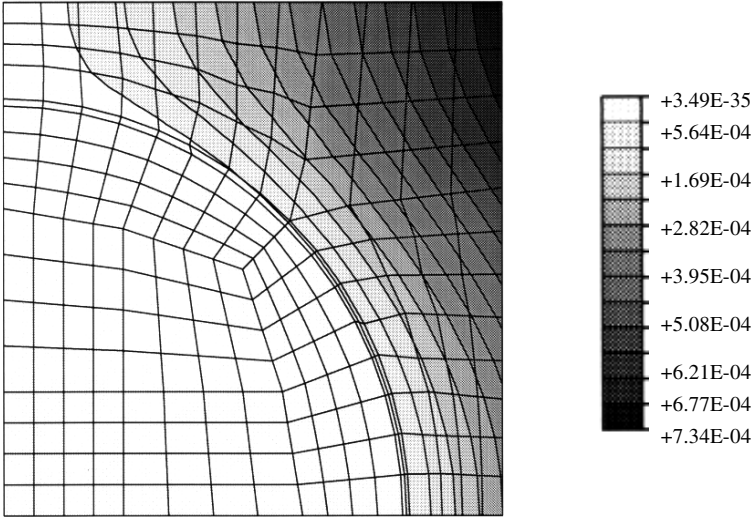


Figure 2.16. Horizontal displacements for test no. 2

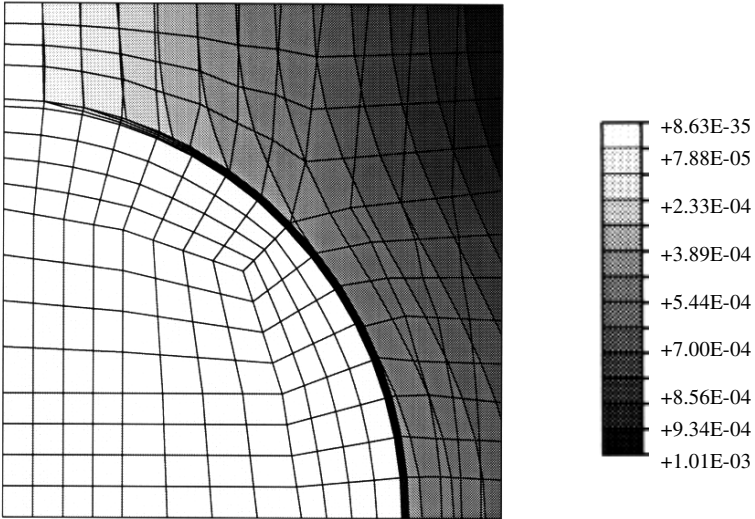


Figure 2.17. Horizontal displacements for test no. 3

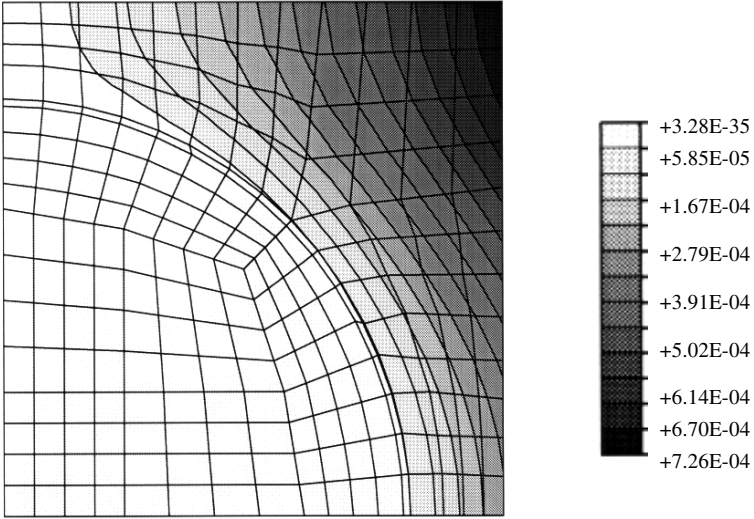


Figure 2.18. Horizontal displacements for test no. 4

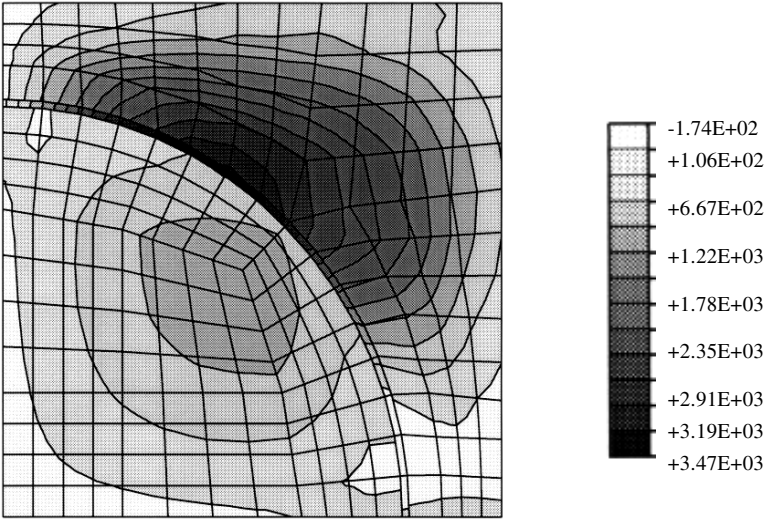


Figure 2.19. The shear stresses for test no. 1

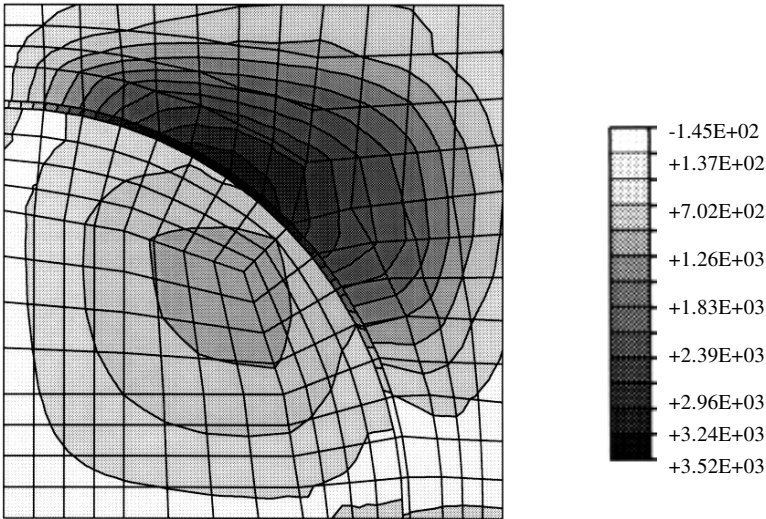


Figure 2.20. The shear stresses for test no. 2

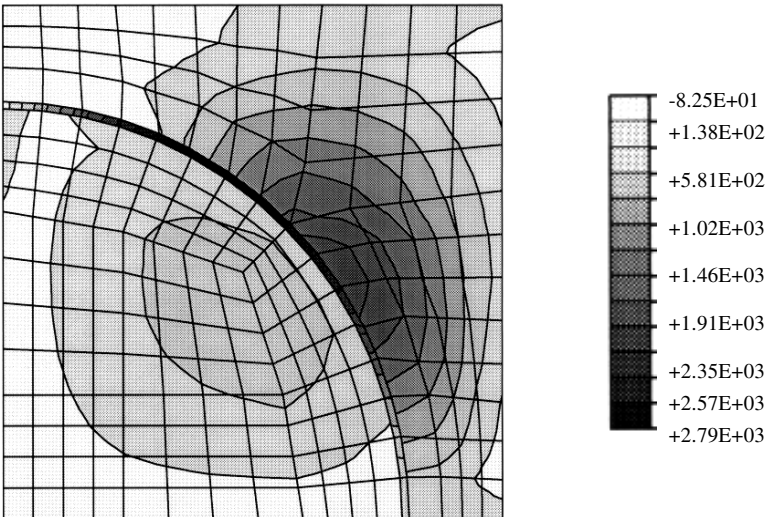


Figure 2.21. The shear stresses for test no. 3

The general purpose of the computational experiments performed is to verify the stochastic elastic behaviour of the composite materials with respect to probabilistic moments of the input random variables: both the Young moduli of the constituents as well as the stochastic interface defects parameters. The starting point for such analyses is a verification of the probabilistically averaged Young modulus in the interphase (example 1). This has been done by the use of the special FORTRAN subroutine, while the next tests have been carried out using the 4–node isoparametric rectangular plane strain element of the system POLSAP. Material parameters of the composite constituents are taken in examples 1 to 3 as

$E(e_1) = 84.0$ GPa, $\nu_1 = 0.22$, $\sigma(e_1) = 4.2$ GPa, $E(e_2) = 4.0$ GPa, $\sigma(e_2) = 0.4$ GPa, $\nu_2 = 0.34$ (expected values and standard deviations of the Young modulus and Poisson ratio, respectively).

2.2.2 Random Composite without Interface

Defects

The main aim of the numerical analysis is to verify numerically the elastic behaviour of a fibre composite when the Young modulus of composite components is Gaussian random variable. Moreover, numerical tests are carried out to state in what way, for various contents of fibre (with round section) in a periodicity cell, the random material properties of reinforcement and matrix influence the displacement and stress distribution in the cell. A quarter of a fibre composite periodicity cell is tested in numerical analysis and its discretisation is shown in Figure 2.22.

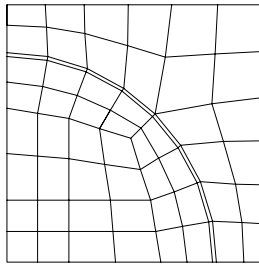


Figure 2.22. Discretisation of the periodicity cell quarter

Numerical implementation enabling the computations is made using a 4–node rectangular plane element of the program POLSAP (Plane Strain/Stress and Membrane Element). The composite structure is subjected to the uniform tension (100 kN/m) on a vertical cell boundary (60 finite elements with 176 degrees of freedom). Vertical displacements are fixed on the remaining cell external boundaries and the plane strain analysis is performed. Twelve numerical tests are carried out assuming the fibre contents of 30, 40 and 50 % and the resulting coefficients of variation are taken from Table 2.2.

Table 2.2. Coefficients of variation for different numerical tests

Test number	$\alpha(e_1)$	$\alpha(e_2)$
1	0.10	0.10
2	0.10	0.05
3	0.05	0.10
4	0.05	0.05

Each time the first two probabilistic moments of the displacements are observed at the interface and on the tensioned vertical edge. In the case of stress expectations, location and maximum value of reduced stress are examined. Figures 2.23 and 2.24 demonstrate radial displacement coefficients of variation of points belonging to the fibre–matrix boundary, which depend on the angle β describing their locations on this boundary.

The results of test no. 1 (Table 2.2) are presented in Figure 2.23, and the next figure shows the results of test no. 3; results of the remaining tests (no. 2 and 4) agree with them respectively. In both cases coefficients of variation for $\theta = 90^\circ$ are omitted on the graphs because of their large values. For fibre contents equal to 50%, they are approximately 1.5 times greater than for $\theta = 0^\circ$ (disproportion of the data would give an illegible picture). Therefore, it can be concluded that the randomness of displacements on the considered boundary depends mainly on the random character of fibre elastic properties, which means

$$\alpha[u(x)] \cong \alpha[e_1]; x \in \partial\Omega_{1,2} \quad (2.55)$$

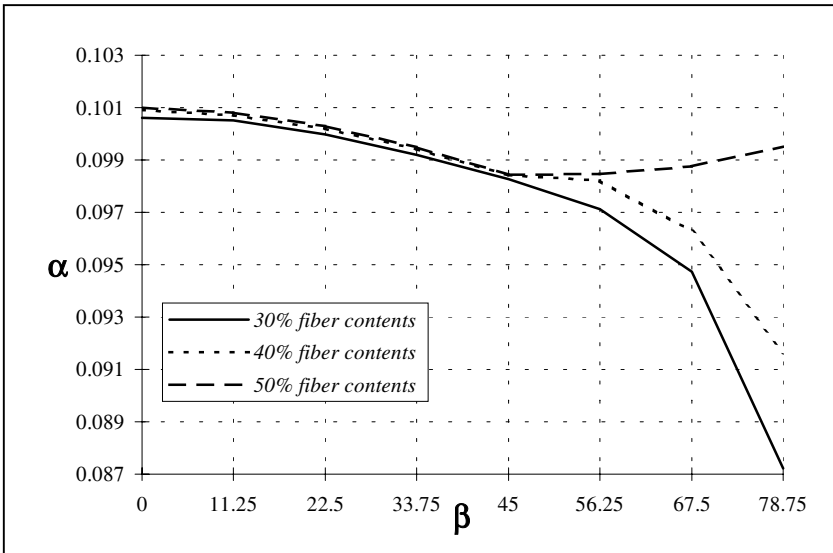


Figure 2.23. Coefficients of variation in test no. 1

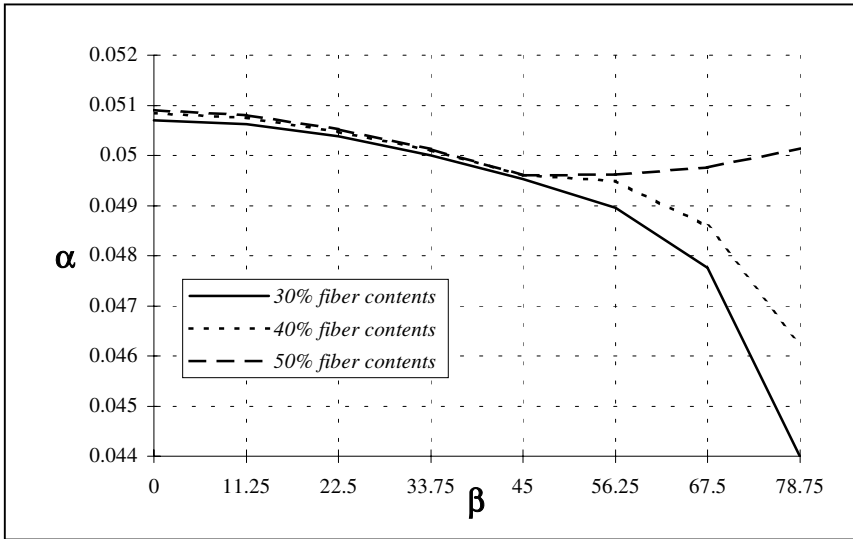


Figure 2.24. Coefficients of variation in test no. 3

Fibre contents in periodicity cell influence also displacement coefficients of variation on $\partial\Omega_{12}$. This influence is visible especially at $0^\circ \leq \theta \leq 45^\circ$. For 40% contents this decrease is not so sharp, and for 50% plane fraction the tendency is the opposite: the coefficient increases up to about 1.5 times of the value obtained at $\theta = 0^\circ$. In a physical way it may be interpreted as increasing the random measure of uncertainty about displacements perpendicular to the fibre boundary of the points belonging to its upper part with increasing fibre radius.

Figures 2.25–2.26 show displacement coefficients of the variation of horizontal points belonging to a vertical, uniformly tensioned edge of periodicity cell obtained in tests no. 1, 2, 3 and 4 respectively. Real numbers in decreasing order denote height on the vertical tensioned edge on the horizontal axes of these figures.

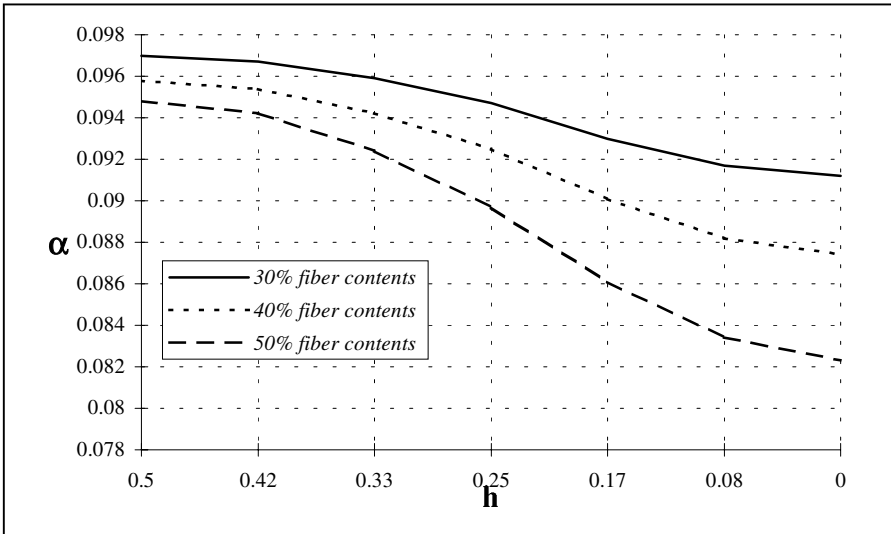


Figure 2.25. Coefficients of variation in test no. 1

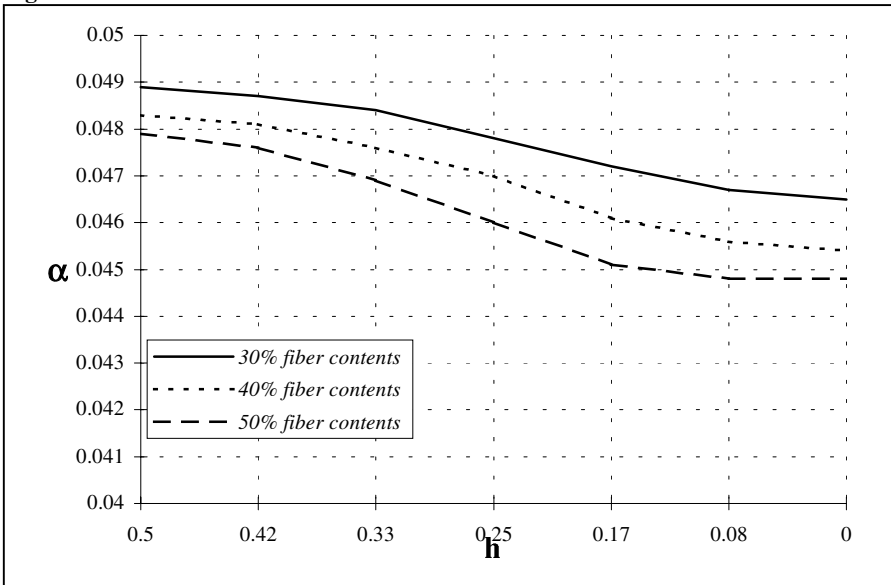


Figure 2.26. Coefficients of variation in test no. 2

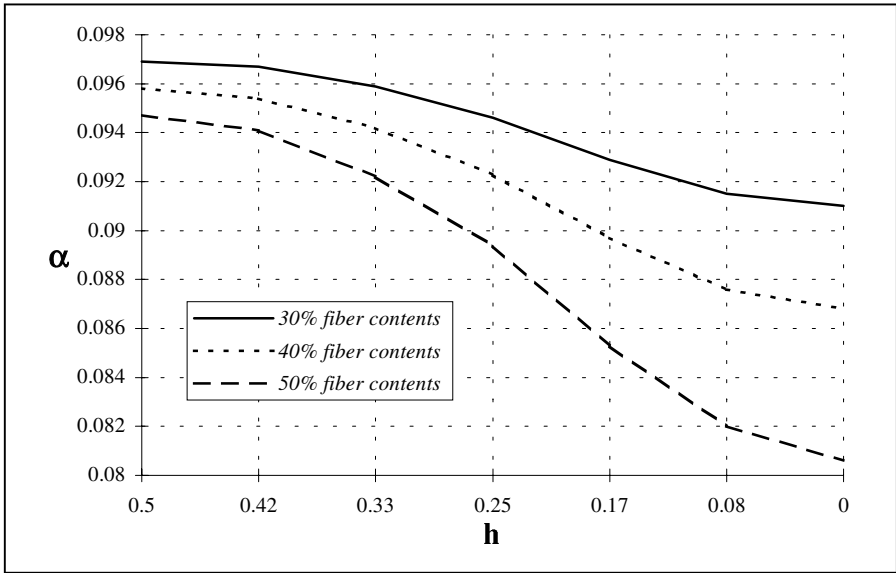


Figure 2.27. Coefficients of variation in test no. 3

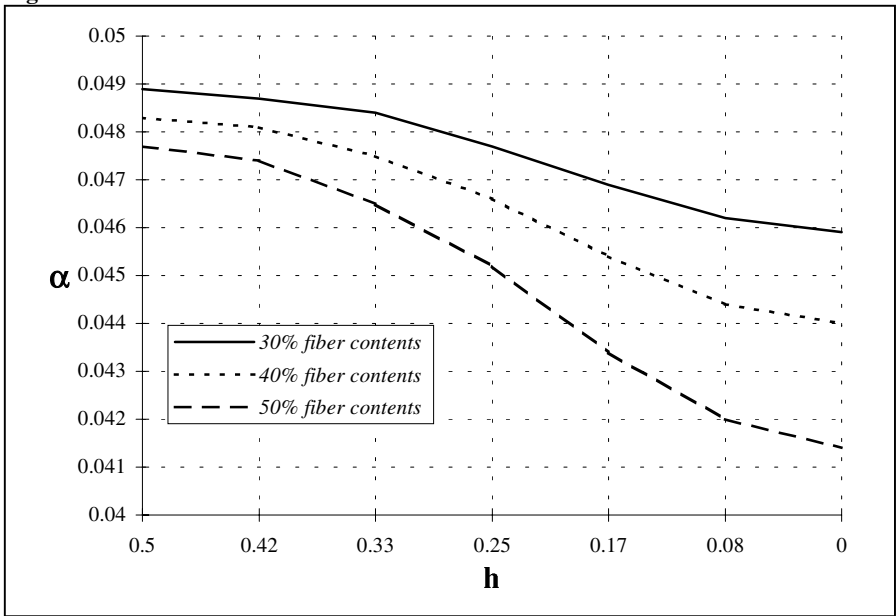


Figure 2.28. Coefficients of variation in test no. 4

The main conclusion from these results is that the random character of the matrix elastic properties influences the randomness of displacements at the tensioned edge of the composite specimen tested. Analogously to the previous observations it can be written that

$$\alpha[u(x)] \cong \alpha[e_2]; \quad x \in \partial\Omega_{\sigma} \quad (2.56)$$

Let us note that the random character of fibre stiffness has rather secondary influence here. The curves describing displacement variation coefficients on the edge are becoming less and less sharp together with an increase of the coefficients of variation of the fibre Young modulus. Increase of fibre contents in the periodicity cell, as expected, in all cases decreases variation coefficients of tensioned edge displacements, which physically can be interpreted as increasing stiffening of periodicity cell by the fibre.

Now, let us analyse expected values of maximum stresses (in MPa) in fibre and matrix specified in Figure 2.29. Darker bars show the maximal stresses in the matrix region, while lighter bars denote the fibre region, respectively.

Generally, it can be observed that the difference between the obtained expected values and the results of deterministic tests is approximately equal to the computational error. This difference would undoubtedly be much bigger if the formula describing these values included a component connected with elasticity tensor derivatives. The present version of computer program includes only the first two components, which correspond with expected values of displacement functions.

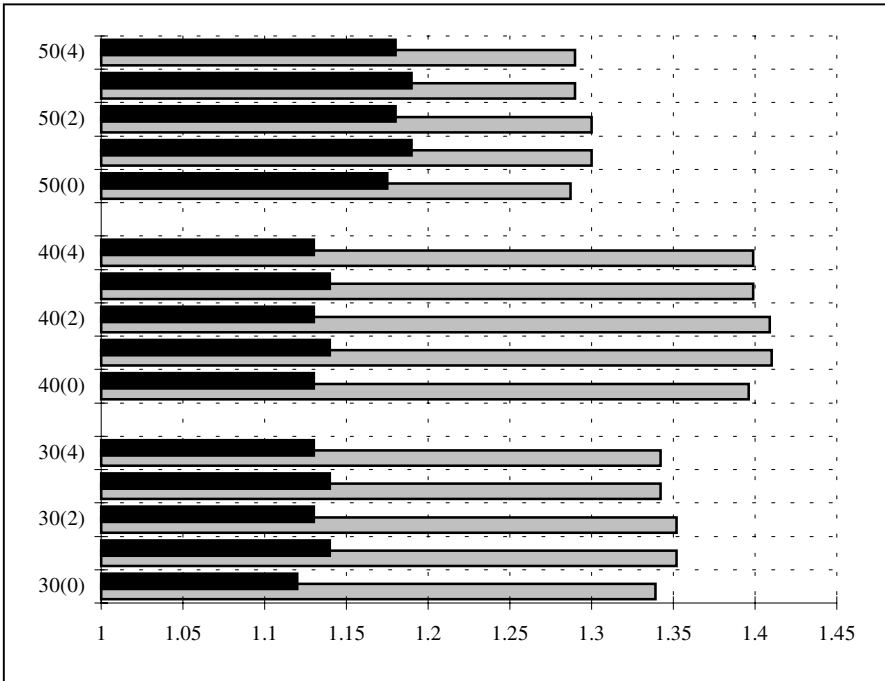


Figure 2.29. Expected values of maximal stresses

The results obtained lead to the conclusion that the most important factor influencing the value of maximum stresses is unquestionably the fibre radius, cf.

Figure 2.29. In the case of the matrix region, maximum stresses increase approximately in direct proportion to fibre radius increment

$$E[\sigma_{\max}(x)] \approx R; x \in \Omega_2 \quad (2.57)$$

To get an analogous relation for maximum stress appearing in the fibre, it is necessary to make a more precise numerical analysis. In tested examples with plane fractions of 30, 40 and 50% extremum appeared at 40% contents of fibre in the periodicity cell. Another factor, which influences the expected values of maximum stresses within a given material, is its coefficient of variation for the Young modulus. The following relation can be formulated:

$$E[\sigma_{\max}(x)] \approx \alpha[e_i]; x \in \Omega_i \quad (2.58)$$

Finally, it can be observed that there is a third-order influence of stronger material random changes of elastic features on maximum stresses in the matrix, especially with decreasing fibre contents in the RVE.

In the context of the present numerical analysis of maximum stresses it should be added that, apart from changes in the expected values of these stresses, a change of their locations was observed. In order to state the relation between the location of changes in the direction of the stress functions extremum and fibre radius increment it would be necessary to consider a wider range of this radius variation (equivalent to, for example, a surface fraction of 10 to 60%) with simultaneously increasing the number of tests (each 1 to 5% for example). The most essential thing would be, however, creating a mesh much more precise than the one used in the above tests, especially near the composite interface, where we have, of interest to us, maximum stresses.

2.2.3 Fibre-reinforced Composite with Stochastic Interface Defects

The subject of the third numerical example is the fibre-reinforced periodic composite, which has been discretised in Figure 2.30 as a cell quarter with smaller contact zones on the left and with larger ones on the right. The composite structure is subjected to uniform tension on the vertical cell boundary. Six numerical tests have been performed assuming interphases with different values of the total number of defects (in turn: 0%, 25% and 50% of the interface length). In each test, the first two probabilistic moments of the displacements are observed on the phase boundary and on the vertical edge subjected to tension and the coefficient of variation for displacements.

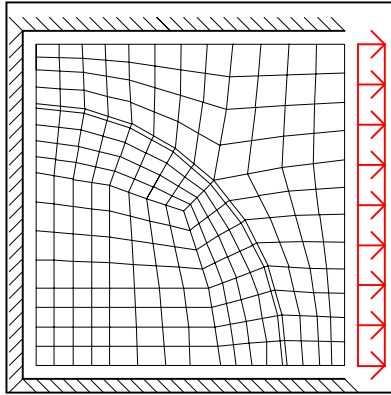


Figure 2.30. Quarter periodicity cell mesh for the SFEM analysis

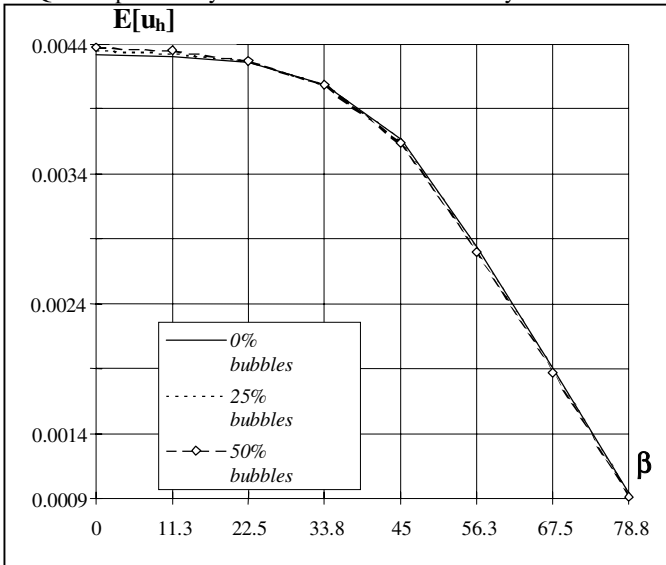


Figure 2.31. Expected values of horizontal displacement at the interface

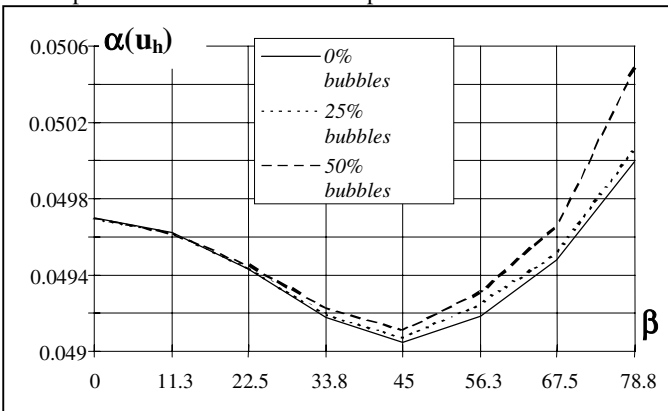


Figure 2.32. Coefficients of variation of horizontal displacements at the interface

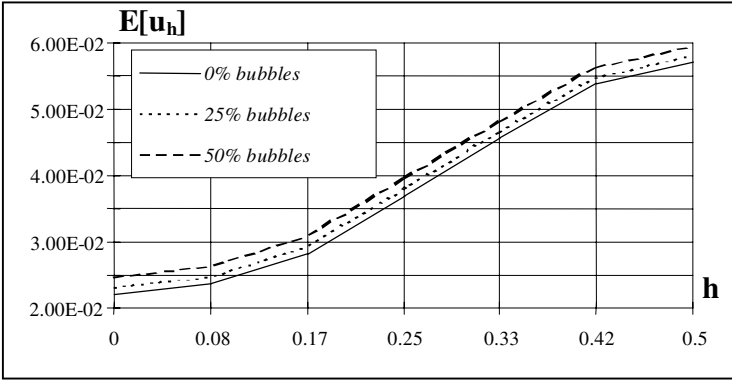


Figure 2.33. Expected values of horizontal displacements at the tensioned edge

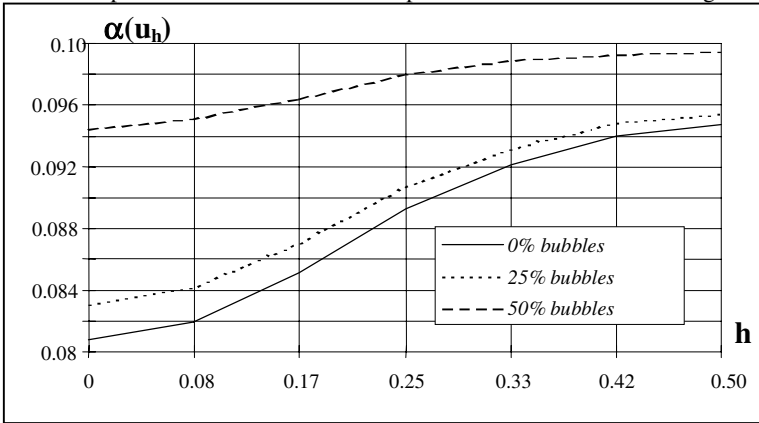


Figure 2.34. Coefficients of variation of horizontal displacements at the tensioned edge

The expected values of the displacements and their coefficients of variation are placed on the vertical axes of all figures. The angle β , which determines the location of a point on the fibre–matrix interface with respect to the x or y -coordinate on the tensioned edge, and which is marked on the vertical axes.

A further general observation is a direct proportionality between the number of interface defects and the volume of the contact zone as well as the expected values or coefficients of variation of these displacements. Small differences occur in the interface expected values of displacements for larger values of the angle β .

By comparing the coefficients of variation of the interface displacements (Figure 2.32 and 2.34) quite different forms for the relation between these coefficients and the angle β are observed. The model with a large contact zone shows a high sensitivity to the number of defects and the changes for the small contact zone are proportional. In the case of the coefficients of variation of the tensioned edge horizontal displacement both the models give approximately reversed effects. For example a small contact zone causes larger coefficients for smaller β values than for the larger ones (Figure 2.32). For both sizes of the contact

zones the changes in the coefficient α are inversely proportional to the increase in the number of discontinuities and show some similarity.

Finally, in both models the expected values of the displacement are quite similar with respect to their locations. In the large contact zone (Figure 2.31 and 2.33) the differences between the obtained expected values of displacements for 0%, 25% and 50% of discontinuities are more significant.

2.2.4 Stochastic Interface Defects in Laminated Composite

The two-component layered composite has been tested in this example. The discretisation into 72 finite elements and 233 degrees of freedom as well as the mixed boundary conditions is shown in Figure 2.35. Both layers have been uniformly extended in the opposite directions to verify the influence of interphase between them on the overall behaviour of the structure.

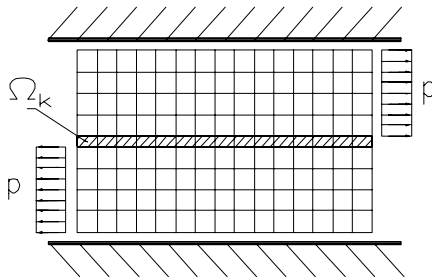


Figure 2.35. Two-layer laminate in the computational shear test

Ten numerical experiments have been carried out in the example: the deterministic problem (test-d) and the stochastic one without interface defects (test-s). In the next experiments the standard deviations of the defects are taken as $\sigma[r] = 0.1 \cdot E[r]$, $\sigma[n] = 0.1 \cdot E[n]$, and the expected values are shown in Table 2.3 (contribution of the boundary occupied by bubbles to the total boundary is given in brackets).

Table 2.3. The expected values of the interface defects tested

	Test 1	Test 2	Test 3	Test 4	Test 5	Test 6	Test 7	Test 8
$E[r]$	5.0E-2	5.0E-2	5.0E-2	5.0E-2	1.0E-1	1.0E-1	1.0E-1	1.0E-1
$E[n]$	5 (10%)	10 (20%)	15 (30%)	20 (40%)	5 (20%)	10 (40%)	15 (60%)	20 (80%)

The results of the analyses have been collected in Table 2.3, which shows the expected values and the coefficients of variation of the displacements and are

generally consistent with those obtained experimentally (in the range of expected values). The increases of the expected values in comparison to the results obtained in test-d and test-s are included also in this table. The coefficients of variation of the horizontal displacements for smaller and greater interphase are presented in Figure 2.36 and 2.37 as a function of the location of a point on the Ω_2 boundary. On the horizontal axis the height of the point (h) in decreasing order is presented: the coordinate 2.5 denotes the point belonging to the interface and Ω_1 region on the extended Ω_2 boundary, while the coordinate 5.0 denotes the point belonging to the upper Ω_2 boundary.

Table 2.4. The expected values and coefficients of variation of the displacements tested

	Test-d	test-s	test 1	test 2	test 3	test 4	test 5	test 6	test 7	Test 8
$E[q]$ (E-2)	1.924 2.610	1.939 2.633	2.049	2.089	2.134	2.188	2.686	2.844	3.065	3.408
$\Delta E[q]$ (%)	-0.8 -0.9	0.0 0.0	5.7	7.7	10.1	12.8	2.0	8.0	16.4	29.4
$\alpha[q]$	-	0.082	0.078	0.080	0.083	0.089	0.088	0.098	0.120	0.158

Generally, all the results computed show that the most sensitive region to the input random parameters is the point located on the weaker material (matrix) and the interphase on the extended Ω_2 boundary. Moreover, analysing the increases of the expected values of horizontal displacements on the tensioned boundary the significant influence of the stochastic interface defects introduced can be observed. In all tests performed the displacements obtained are greater than for the composites without defects between the composite constituents.

Moreover, the increases of the displacements analysed increase faster than the increases of the total length of the boundary occupied by the bubbles, which follows the stochastic nonlinearity of the model presented. The diagrams of the displacements have analogous characteristics to those obtained for the coefficients of variation presented later. However, considering the large disproportions between the values computed near the interphase and outside it, these graphs have been omitted.

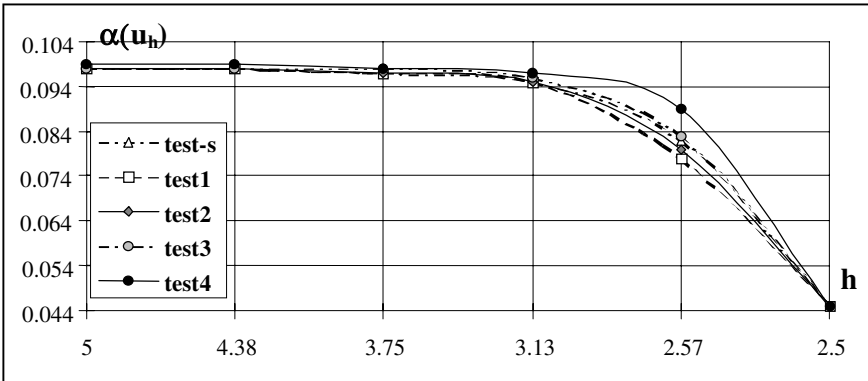


Figure 2.36. Coefficients of variation of horizontal displacements for shear test (I)

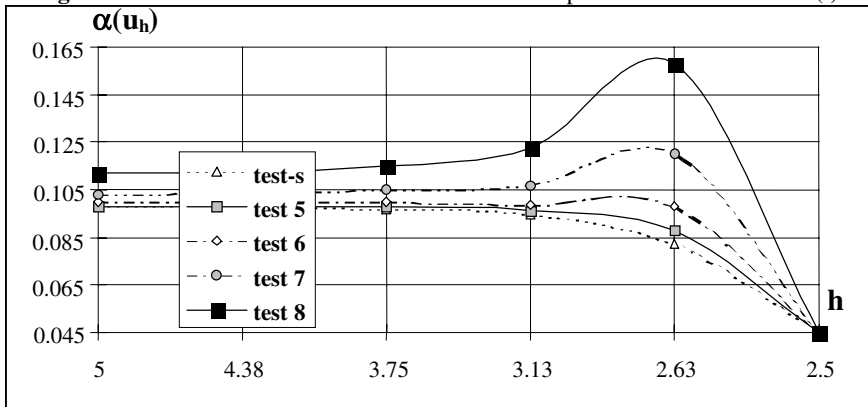


Figure 2.37. Coefficients of variation of horizontal displacements for shear test (II)

Comparing the coefficients of variation of the horizontal displacements it is seen that, especially in case of tests no. 5 to 8 (the interphase twice as large as for tests 1 to 4) the significant increase of these displacements is about 95% in case of test no. 8. These increases are analogous to the increases of expected values greater for displacements rather than the corresponding increases of total length of interface boundary occupied by the bubbles.

As can be expected, the statistical response of the laminate should depend on the contrast between stronger and weaker layer material properties, interphase elastic parameters, the total number of layers in the composite etc. Essentially different situation can be observed when both material properties and external load are introduced as random variables [273].

2.2.5 Superconducting Coil Cable Probabilistic Analysis

The main ideas of the experiment [193] are as follows: (i) comparison of the stochastic behaviour of the superconducting coil cable in the original geometry with the model in which the technological nonhomogeneities have been probabilistically averaged; (ii) verification of the model sensitivity to the assumed thickness of the interphase introduced.

The example of the RVE analysed is presented in Figures 2.38 and 2.39 (all geometric dimensions are given in mm). A single discontinuity is modelled by complementing two circle quarters (teeth with their sharp sides directed to the interior of the superconducting cable). Their radii are equal to 1.5 mm for defects on the interface superconducting cable–tube and 2.0 mm for defects on the interface cable–jacket. The periodicity cell is subjected to a horizontal uniform tension on its vertical boundaries; due to symmetry only one quarter of this cell is employed. Displacement boundary conditions on all the remaining external boundaries are assumed to satisfy the symmetry conditions.

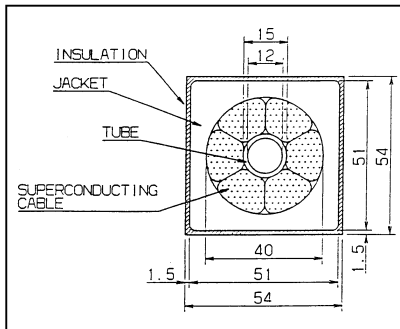


Figure 2.38. Superconducting coil cable RVE geometry

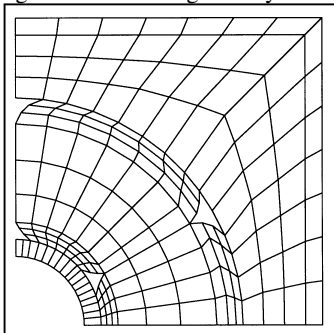


Figure 2.39. Quarter periodicity cell mesh for the superconductor

The elastic properties and their probabilistic characteristics of the RVE components, the expected values and the standard deviations of Young moduli, Poisson ratios and Kirchhoff moduli are collected in Table 2.5.

Table 2.5. Elastic characteristics of composite components

Material	$E[e]$ [GPa]	$\sigma(e)$ [GPa]	ν	G [GPa]
Tube	205.0	8.0	0.265	81.0
Superconductor	182.0	0.0	0.300	70.0
Jacket	126.0	12.0	0.311	48.0
Insulation	36.0	0.0	0.210	11.0

The following tests are performed: deterministic test including defects non-averaged (test 1), an experiment without defects (test 2), an experiment with defects averaged in the interphase (test 3) or over the finite elements which they belong to (test 4). The first two probabilistic moments of the displacements are observed in each test on the interface determined by a radius equal to 9.0 mm (between the lower superconductor interphase and the superconductor region). Four additional tests are performed in test 3 to verify the results variations with respect to the interphase thicknesses: test 3A, where the thickness is equal to the expected value of the relevant geometric dimensions of interface defects, test 3D with thickness given by eqn (2.22) and tests 3B and 3C with the intermediate thicknesses.

The results of these computations due to tests numbered 1 to 4 are presented in Figures 2.40 and 2.41: the expected values of the horizontal displacements and their coefficients of variation. The first two moments are marked on the vertical axes of these figures, while the angle β , which determines the location of a point on the interface considered with respect to the x -coordinate on the horizontal axes. The results of tests 3A to 3D are collected in Table 2.6 presented below the figures. The expected values of displacements observed (in mm) are given in the upper row of each table cell and the coefficients of variation in the lower one.

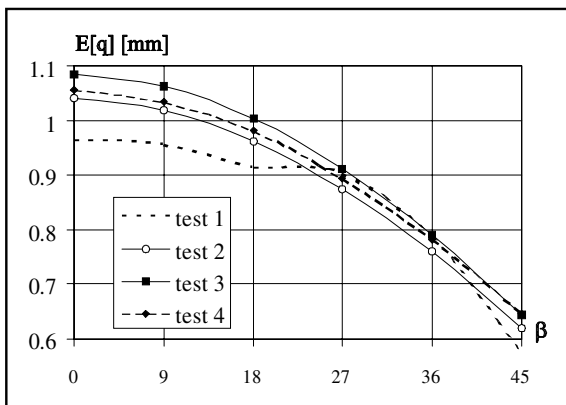


Figure 2.40. Expected values of horizontal displacements at the tensioned edge

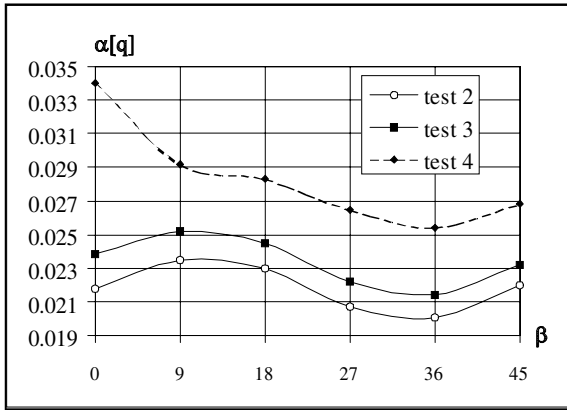


Figure 2.41. Coefficients of variation of horizontal displacements at the tensioned edge

Table 2.6. The expected values and the coefficients of variation of horizontal displacements

β [°]	Test 3A	Test 3B	Test 3C	Test 3D
0	1.066 0.0241	1.069 0.0237	1.078 0.0235	1.085 0.0233
9	1.047 0.0239	1.053 0.0238	1.057 0.0234	1.062 0.0232
18	0.985 0.0236	0.993 0.0234	0.994 0.0231	1.003 0.0230
27	0.895 0.0239	0.897 0.0235	0.908 0.0234	0.910 0.0231
36	0.783 0.0241	0.784 0.0238	0.784 0.0235	0.790 0.0232
45	0.631 0.0212	0.634 0.0212	0.639 0.0213	0.645 0.0214

Generally, it can be observed that in all stochastic tests the expected values of horizontal displacements are greater than the corresponding values obtained from deterministic tests, which follow equation (1.134). The greatest expected values of displacements observed are obtained for test 4: from 50% (for $\beta \approx 0^\circ$) to 100% (for $\beta \approx 80^\circ$) greater than in the remaining tests. Analogous observation can be done for the coefficients of variation. Generally, these facts follow the great variances of the Young moduli in finite elements containing defects averaged in comparison to the remaining elements.

On the basis of these results it can be stated that the observed probabilistic moments of displacements are strongly sensitive to the scale of the composite structure, which probabilistic averaging is applied in. A rapid decrease of the total area of the region averaged results in a significant increase of the effective Young modulus and much smaller increases of the expected values for the displacements. Further, the expected values obtained in test 2 (without including interface defects in any form) give the most exact results of the horizontal displacements computed

in the deterministic model. However, for $\beta \approx 30^\circ$, which corresponds to the defects location, the best approximation is obtained in test 3 (with interphase zones introduced).

Finally, let us consider the stochastic variations of the interface horizontal displacements to the interphase zone thicknesses illustrated by the results collected in Table 2.6. It can be observed that increasing thickness causes a small increase of the horizontal displacements and a decrease of the coefficients of variation. The decrease (or increase) has a linear character and the maximum increment is no greater than 2% of the values considered. It confirms the possibility of using the model presented in the numerical analysis of stochastic non-homogeneities (especially interface defects) in composite materials. To verify the applicability of the model presented this sensitivity should be discussed as a function of interface defects and elastic properties of composite component stochastic parameters.

Let us note that the SFEM methodology can be applied in further analyses for numerical modelling of random both uncoupled and coupled thermal, electric or magnetic fields in various superconducting structures [221,385]. A common application of the stochastic perturbation technique with computational plasticity algorithms will enable us to perform modelling of interface debonding in the case of laminates and fibre-reinforced composites, which will essentially extend our knowledge of composites behaviour in relation to the existing models [251,384,386].

2.3 Homogenisation Approach

Homogenisation methods present some specific approach to such computational analysis of composite materials, where the homogeneous medium equivalent to the real composite is proposed. The assumptions decisive for these methods are introduced in the context of numerous equivalence criteria; usually it is assumed that internal energies per unit mass stored in both systems are to be equal. A concept of the Representative Volume Element (RVE) for the composite is most frequently used together with the corresponding assumption on a scale parameter relating dimensions of the RVE to the entire composite – it has to tend to 0, which is usually unrealistic for most of engineering composites. It is evident now that the spatial distribution of the reinforcement (uniaxially periodic, with rectangular, hexagonal, triangular periodicity or completely random according to Gaussian or Poisson distributions) is of decisive importance for the effective material tensors [52]. There exist some mathematical approaches, where the scale parameter is assumed to be some small and positively defined [370]. It gives a less restrictive model, but such an approach has no general corresponding FEM computational implementations in the existing software. The essential differences between these two methodologies are especially apparent in homogenisation of dynamic and transient heat transfer problems, where dispersive effects are observed under the last assumption only.

Most of the homogenisation methods have one common point – the necessity of use of the so-called homogenisation functions. These functions are the solutions of the cell problem on the RVE under periodic boundary conditions, where some additional conditions can be imposed on external boundaries or/and interfaces between the composite constituents. Some exceptions can be obtained for the 1D homogenisation problems, where effective thermal (and/or elastic) parameters may be derived directly. Let us note that if some further assumptions on composite microgeometry are introduced (a composite has a specified number of components in the periodicity cell and the shapes and/or location of the components are given), then the closed form equations for the effective material properties for either 2 or 3D structures can be derived [6,65,253].

2.3.1 Unidirectional Periodic Structures

Let us consider a unidirectional heterogeneous bar in unstressed and unstrained state, with periodic structure and with elastic properties piecewise constant. An example of the structure under considerations is presented below (Figures 2.42 and 2.43).

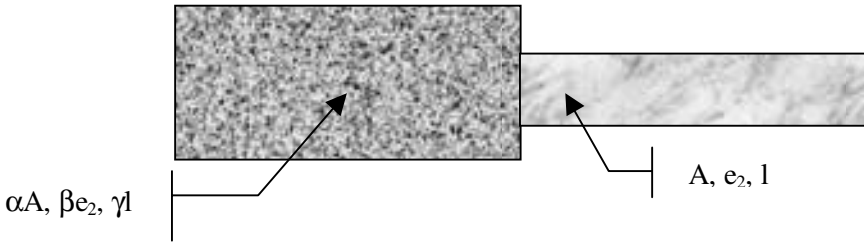


Figure 2.42. RVE of two-component composite bar

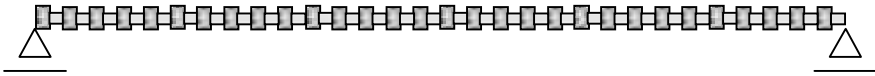


Figure 2.43. Unidirectional periodic two-component composite beam

Using the parameter ε the displacements and stresses are asymptotically expanded in the bar as follows [30,43,133,308]:

$$u^\varepsilon(\mathbf{x}) = u^0(\mathbf{x}, \mathbf{y}) + \varepsilon u^1(\mathbf{x}, \mathbf{y}) + \varepsilon^2 u^2(\mathbf{x}, \mathbf{y}) + \dots \quad (2.59)$$

and

$$\sigma^\varepsilon(\mathbf{x}) = \sigma^0(\mathbf{x}, \mathbf{y}) + \varepsilon \sigma^1(\mathbf{x}, \mathbf{y}) + \varepsilon^2 \sigma^2(\mathbf{x}, \mathbf{y}) + \dots \quad (2.60)$$

where $u^{(i)}(\mathbf{x}, \mathbf{y})$, $\sigma^{(i)}(\mathbf{x}, \mathbf{y})$ are periodic, too; the coordinate \mathbf{x} is introduced in the macro scale (Figure 2.43), with \mathbf{y} in the micro scale (cf. Figure 2.42). Introducing these expansions into classical Hooke law it is found that

$$\begin{aligned} \sigma^\varepsilon(\mathbf{x}) &= \sigma^0(\mathbf{x}, \mathbf{y}) + \varepsilon \sigma^1(\mathbf{x}, \mathbf{y}) + \varepsilon^2 \sigma^2(\mathbf{x}, \mathbf{y}) + \dots \\ &= e(\mathbf{y}) \left\{ \frac{\partial u^0(x, y)}{\partial x} + \frac{1}{\varepsilon} \frac{\partial u^0(x, y)}{\partial y} + \varepsilon \frac{\partial u^1(x, y)}{\partial x} + \frac{\partial u^1(x, y)}{\partial y} + \dots \right\} \end{aligned} \quad (2.61)$$

whereas the equilibrium equation

$$\frac{\partial \sigma^\varepsilon}{\partial x} + \gamma^\varepsilon = 0 \quad (2.62)$$

results in

$$\frac{\partial \sigma^0}{\partial \mathbf{x}} + \frac{1}{\varepsilon} \frac{\partial \sigma^0}{\partial \mathbf{y}} + \varepsilon \frac{\partial \sigma^1}{\partial \mathbf{x}} + \frac{\partial \sigma^1}{\partial \mathbf{y}} + \varepsilon^2 \frac{\partial \sigma^2}{\partial \mathbf{x}} + \varepsilon \frac{\partial \sigma^2}{\partial \mathbf{y}} + \dots + \gamma(\mathbf{y}) = 0 \quad (2.63)$$

Hence, the following zeroth, first and second order constitutive equations are derived:

$$0 = e(\mathbf{y}) \frac{\partial u^0}{\partial \mathbf{y}} \quad (2.64)$$

$$\sigma^0 = e(\mathbf{y}) \left\{ \frac{\partial u^0}{\partial \mathbf{x}} + \frac{\partial u^1}{\partial \mathbf{y}} \right\} \quad (2.65)$$

$$\sigma^1 = e(\mathbf{y}) \left\{ \frac{\partial u^1}{\partial \mathbf{x}} + \frac{\partial u^2}{\partial \mathbf{y}} \right\} \quad (2.66)$$

Applying an analogous methodology, the equilibrium equation is expanded as

$$\frac{\partial \sigma^0}{\partial \mathbf{y}} = 0 \quad (2.67)$$

$$\frac{\partial \sigma^0}{\partial \mathbf{x}} + \frac{\partial \sigma^1}{\partial \mathbf{y}} + \gamma(\mathbf{y}) = 0 \quad (2.68)$$

It is observed that zeroth order displacements and stresses depend on the macroscale coordinate only $u^0 = u^0(\mathbf{x})$ and $\sigma^0 = \sigma^0(\mathbf{x})$, so that it can be written that

$$\sigma^0(\mathbf{x}) = e(\mathbf{y}) \left(\frac{\partial u^0(\mathbf{x})}{\partial \mathbf{x}} + \frac{\partial u^1(\mathbf{x}, \mathbf{y})}{\partial \mathbf{y}} \right) \quad (2.69)$$

Integrating both sides of (2.69) over the periodicity cell of a bar, there holds

$$\sigma^0(x) = \left(|\Omega| / \int_{\Omega} \frac{dy}{e(y)} \right) \frac{\partial u^0(x)}{\partial x} \quad (2.70)$$

which leads to the following description of the homogenised (effective) Young modulus

$$e^{(eff)} = \frac{|\Omega|}{\int_{\Omega} \frac{dy}{e(y)}} \quad (2.71)$$

Such a formulation makes it possible to derive the closed form equations for the expected values and covariances of the homogenised Young moduli using classical definitions of probabilistic moments or by an application of perturbation theory. It is possible to derive such equations for particular engineering examples only if the bar has a geometrical characteristics piecewise constant within its length. Let us consider further the RVE built up with n piecewise constant components defined on Ω by the use of design parameters (e_i, A_i, l_i) where $e_i = \text{const.}$ for $y \in l_i$ and such that $e_i \neq e_j$ for $i, j = 1, \dots, n$. Hence, the integration in formula (2.71) can be replaced by

$$e^{(eff)} = \frac{1}{\sum_{i=1}^n \frac{A_i l_i}{e_i}} \quad (2.72)$$

where the variables A_i, l_i denote the cross-sectional area and the length of the i th structural element. After some algebraic transformations relation (2.72) can be transformed to

$$e^{(eff)} = \frac{\prod_{i=1}^n e_i}{\sum_{i=1}^n A_i l_i e_1 e_2 \dots e_{i-1} e_{i+1} \dots e_n} \quad (2.73)$$

which can be efficiently implemented in any FEM computer program. Let us note that an analogous procedure can be applied successfully for the transient heat transfer problem Young moduli are to be replaced here by the relevant coefficients of heat conduction.

If the general beam structure is to be homogenised, the equilibrium and constitutive equations should be enriched with transversal effect components but, for the composite beams having constant Poisson ratio within its length and various Young moduli, the formulation posed above is quite sufficient for the needs of computational analyses. Moreover, it should be underlined that the homogenisation model for 2D and 3D problems is carried out similarly but the effective elasticity tensor is to be introduced instead of the Young modulus only. As a result, it is not possible to derive any closed form algebraic equations describing the effective properties of a composite, which significantly complicates numerical analysis. On the other hand, the randomness in multidimensional composite structures appears usually in their geometry, too, which must be implemented in the FEM analysis using some special finite element types.

Finally, considering further applications of the homogenisation approach in the elastodynamics of engineering structures, the effective mass density of a composite can be derived according to the spatial averaging method as [28,265]

$$\rho^{(eff)} = \frac{1}{|\Omega|} \int_{\Omega} \rho(y) dy. \quad (2.74)$$

Let us mention that this relation is used for any space configuration and periodicity conditions of a composite. Since that, having a homogenised elastostatic problem, especially in random case, further extension to the elastodynamic analysis in the context of a stochastic second order perturbation technique does not seem to be very complicated. The expected values for the effective Young modulus can be obtained by the second order perturbation second probabilistic moment analysis as [162]

$$E[e^{(eff)}(\mathbf{y})] = \int_{-\infty}^{+\infty} \left(e^{(eff)0}(\mathbf{y}) + \Delta b^r e^{(eff),r}(\mathbf{y}) + \frac{1}{2} \Delta b^r \Delta b^s e^{(eff),rs}(\mathbf{y}) \right) p_R(b) db \quad (2.75)$$

Using classical probability theory definitions and theorems

$$\int_{-\infty}^{+\infty} p_R(b(\mathbf{y})) db = 1, \quad \int_{-\infty}^{+\infty} \Delta b p_R(b(\mathbf{y})) db = 0 \quad (2.76)$$

$$\int_{-\infty}^{+\infty} \Delta b^r \Delta b^s p_R(b(\mathbf{y})) db = Cov(b^r, b^s); \quad 1 \leq r, s \leq R \quad (2.77)$$

one can determine that

$$E[e^{(eff)}(\mathbf{y})] = e^{(eff)0}(\mathbf{y}) + \frac{1}{2} e^{(eff),rs}(\mathbf{y}) Cov(b^r, b^s) \quad (2.78)$$

Further, using the analogous methodology the covariance matrix for the effective Young modulus $Cov(e^{(eff)})$ is derived

$$Cov(e_i^{(eff)}; e_j^{(eff)}) = \int_{-\infty}^{+\infty} \left(e_i^{(eff)}(\mathbf{y}) - e_i^{(eff)0}(\mathbf{y}) \right) \left(e_j^{(eff)}(\mathbf{y}) - e_j^{(eff)0}(\mathbf{y}) \right) g(b_i, b_j) db_i db_j$$

and, using the classical perturbation approach, there holds

$$\begin{aligned} &= \int_{-\infty}^{+\infty} \left\{ \left(e_i^{(eff)0}(\mathbf{y}) + \Delta b_r e_i^{(eff),r}(\mathbf{y}) + \frac{1}{2} \Delta b_r \Delta b_s e_i^{(eff),rs}(\mathbf{y}) - e_i^{(eff)0}(\mathbf{y}) \right) \right. \\ &\quad \left. \times \left(e_j^{(eff)0}(\mathbf{y}) + \Delta b_u e_j^{(eff),u}(\mathbf{y}) + \frac{1}{2} \Delta b_u \Delta b_v e_j^{(eff),uv}(\mathbf{y}) - e_j^{(eff)0}(\mathbf{y}) \right) \right\} g(b_i, b_j) db_i db_j \end{aligned}$$

After all possible algebraic transformations and by neglecting the terms of order greater than the second, it is obtained that

$$\begin{aligned} \text{Cov}(e_i^{(eff)}; e_j^{(eff)}) &= \int_{-\infty}^{+\infty} \Delta b_r e_i^{(eff),r}(\mathbf{y}) \Delta b_s e_j^{(eff),s}(\mathbf{y}) g(b_i, b_j) db_i db_j \\ &= e_i^{(eff),r}(\mathbf{y}) e_j^{(eff),s}(\mathbf{y}) \text{Cov}(b_r, b_s) \end{aligned} \quad (2.79)$$

For the particular case of the two–component composite structure there holds

$$e^{(eff)} = \frac{\Omega}{\frac{A_1 l_1}{e_1} + \frac{A_2 l_2}{e_2}} = \frac{(A_1 l_1 + A_2 l_2) e_1 e_2}{e_2 A_1 l_1 + e_1 A_2 l_2} \quad (2.80)$$

Let us consider the case of a 1D bar structure with two homogeneous components having deterministically defined geometry (cross–sections and lengths) and with Young moduli assumed to be the input random variables. The zeroth, first and second order derivatives of the effective elasticity with respect to the Young moduli of the composite constituents are obtained by analytical derivation:

- zeroth order components

$$e^{(eff)0} = \frac{(A_1 l_1 + A_2 l_2) E[e_1] E[e_2]}{E[e_2] A_1 l_1 + E[e_1] A_2 l_2} \quad (2.81)$$

- first order components

$$\frac{\partial e^{(eff)}}{\partial e_1} = \frac{A_1 l_1 (A_1 l_1 + A_2 l_2) E^2[e_2]}{(E[e_2] A_1 l_1 + E[e_1] A_2 l_2)^2} \quad \frac{\partial e^{(eff)}}{\partial e_2} = \frac{A_2 l_2 (A_1 l_1 + A_2 l_2) E^2[e_1]}{(E[e_2] A_1 l_1 + E[e_1] A_2 l_2)^2} \quad (2.82)$$

- second order components

$$\frac{\partial^2 e^{(eff)}}{\partial e_1^2} = \frac{-2 A_1 l_1 A_2 l_2 (A_1 l_1 + A_2 l_2) E^2[e_2]}{(E[e_2] A_1 l_1 + E[e_1] A_2 l_2)^3} \quad (2.83)$$

$$\frac{\partial^2 e^{(eff)}}{\partial e_2^2} = \frac{-2 A_1 l_1 A_2 l_2 (A_1 l_1 + A_2 l_2) E^2[e_1]}{(E[e_2] A_1 l_1 + E[e_1] A_2 l_2)^3} \quad (2.84)$$

$$\frac{\partial^2 e^{(eff)}}{\partial e_1 \partial e_2} = \frac{2 A_1 l_1 A_2 l_2 (A_1 l_1 + A_2 l_2) E[e_1] E[e_2]}{(E[e_2] A_1 l_1 + E[e_1] A_2 l_2)^3} \quad (2.85)$$

Then, the resulting covariance matrix of the effective elastic behaviour for the two component composite structure is described as follows:

$$\begin{cases} \text{Cov}(e_1^{(eff)}, e_1^{(eff)}) = \text{Cov}(e_1, e_1) \frac{\partial e^{(eff)}}{\partial e_1} \frac{\partial e^{(eff)}}{\partial e_1} \\ \text{Cov}(e_1^{(eff)}, e_2^{(eff)}) = \text{Cov}(e_1, e_2) \frac{\partial e^{(eff)}}{\partial e_1} \frac{\partial e^{(eff)}}{\partial e_2} \\ \text{Cov}(e_2^{(eff)}, e_2^{(eff)}) = \text{Cov}(e_2, e_2) \frac{\partial e^{(eff)}}{\partial e_2} \frac{\partial e^{(eff)}}{\partial e_2} \end{cases} \quad (2.86)$$

To obtain the stochastic finite element model let us introduce the displacement field approximation. The zeroth, first and second order stiffness matrices for the homogenised bar structures may be written out by analogy to the previous considerations:

- zeroth order stiffnesses

$$\mathbf{K}^{(eff)0} = \left(\frac{e^{(eff)} A}{l} \right)^0 \begin{bmatrix} 1 & -1 \\ -1 & 1 \end{bmatrix} = \sum_{j=1}^m e^{(eff)j0} \frac{A^{(m)}}{l^{(m)}} \begin{bmatrix} 1 & -1 \\ -1 & 1 \end{bmatrix} \quad (2.87)$$

with m denoting the total number of bar intervals with constant cross-sectional area $A^{(m)}$;

- first order stiffnesses

$$\begin{aligned} \mathbf{K}^{(eff),e} &= \frac{\partial \mathbf{K}}{\partial e^{(eff)}} = \frac{A}{l} \begin{bmatrix} 1 & -1 \\ -1 & 1 \end{bmatrix} \\ \mathbf{K}^{(eff),A} &= \frac{\partial \mathbf{K}^{(eff)}}{\partial A} = \frac{e^{(eff)}}{l} \begin{bmatrix} 1 & -1 \\ -1 & 1 \end{bmatrix} \\ \mathbf{K}^{(eff),l} &= \frac{\partial \mathbf{K}^{(eff)}}{\partial l} = -\frac{e^{(eff)} A}{l^2} \begin{bmatrix} 1 & -1 \\ -1 & 1 \end{bmatrix} \end{aligned} \quad (2.88)$$

- second order stiffness

$$\begin{aligned}
\mathbf{K}^{(eff),e^{(eff)}e^{(eff)}} &= \frac{\partial^2 \mathbf{K}^{(eff)}}{\partial (e^{(eff)})^2} = \mathbf{0}, & \mathbf{K}^{(eff),AA} &= \frac{\partial^2 \mathbf{K}^{(eff)}}{\partial A^2} = \mathbf{0} \\
\mathbf{K}^{(eff),ll} &= \frac{\partial^2 \mathbf{K}^{(eff)}}{\partial l^2} = -\frac{2e^{(eff)}A}{l^3} \begin{bmatrix} 1 & -1 \\ -1 & 1 \end{bmatrix} \\
\mathbf{K}^{(eff),e^{(eff)}A} &= \frac{\partial^2 \mathbf{K}^{(eff)}}{\partial e^{(eff)} \partial A} = \frac{1}{l} \begin{bmatrix} 1 & -1 \\ -1 & 1 \end{bmatrix} \\
\mathbf{K}^{(eff),e^{(eff)}l} &= \frac{\partial^2 \mathbf{K}^{(eff)}}{\partial e^{(eff)} \partial l} = -\frac{A}{l^2} \begin{bmatrix} 1 & -1 \\ -1 & 1 \end{bmatrix} \\
\mathbf{K}^{(eff),Al} &= \frac{\partial^2 \mathbf{K}^{(eff)}}{\partial A \partial l} = -\frac{e^{(eff)}}{l^2} \begin{bmatrix} 1 & -1 \\ -1 & 1 \end{bmatrix}
\end{aligned} \tag{2.89}$$

Hence, the canonical set of the second order SFEM equations can be rewritten as follows:

$$\mathbf{K}^{(eff)0} \mathbf{q}^{(eff)0} = \mathbf{Q}^{(eff)0} \tag{2.90}$$

$$\mathbf{K}^{(eff)0} \mathbf{q}^{(eff),r} = -\mathbf{K}^{(eff),r} \mathbf{q}^{(eff)0} \tag{2.91}$$

$$\mathbf{K}^{(eff)0} \mathbf{q}^{(eff)(2)} = -2\mathbf{K}^{(eff),r} \mathbf{q}^{(eff),s} \mathbf{Cov}(e_r^{(eff)}, e_r^{(eff)}) \tag{2.92}$$

which makes it possible to compute $\mathbf{q}^{(eff)0}$, $\mathbf{q}^{(eff),r}$ and $\mathbf{q}^{(eff),rs}$ and to calculate the first probabilistic moments of displacements as

$$E[\mathbf{q}^{(eff)}] = \mathbf{q}^{(eff)0} + \frac{1}{2} \mathbf{q}^{(eff),rs} \mathbf{Cov}(e_r^{(eff)}, e_r^{(eff)}) \tag{2.93}$$

$$\mathbf{Cov}(\mathbf{q}^{(eff)r}, \mathbf{q}^{(eff)s}) = \mathbf{q}^{(eff),r} \mathbf{q}^{(eff),s} \mathbf{Cov}(e_r^{(eff)}, e_r^{(eff)}) \tag{2.94}$$

The expected values and cross-covariances of the stresses are obtained in comparison to the heterogeneous model as

$$\begin{aligned}
E[\boldsymbol{\sigma}_{ij}^{(eff)e}] \\
= \left\{ C_{ijkl}^{(eff)(e)0} (q^{(eff)0} + \frac{1}{2} q^{(eff),rs}) + C_{ijkl}^{(eff)(e),r} q^{(eff),s} \right\} B_{kl}^{(e)} Cov(e_r^{(eff)}, e_s^{(eff)})
\end{aligned} \tag{2.95}$$

and

$$\begin{aligned}
Cov(\boldsymbol{\sigma}_{ij}^{(eff)e}, \boldsymbol{\sigma}_{ij}^{(eff)f}) &= B_{kl}^{(e)} B_{mn}^{(f)} Cov(e_r^{(eff)}, e_s^{(eff)}) \\
&\times \left\{ C_{ijkl}^{(eff)(e)0} C_{ijmn}^{(eff)(f)0} q^{(eff),r} q^{(eff),s} + C_{ijkl}^{(eff)(e),r} C_{ijmn}^{(eff)(f),s} q^{(eff)0} q^{(eff)0} \right. \\
&\left. C_{ijkl}^{(eff)(e),r} C_{ijmn}^{(eff)(f)0} q^{(eff),s} q^{(eff)0} + C_{ijkl}^{(eff)(e)0} C_{ijmn}^{(eff)(f),r} q^{(eff),s} q^{(eff)0} \right\}
\end{aligned} \tag{2.96}$$

The first computational example deals with Young moduli defined as deterministic function and cross-sectional area being a random field, while in the

second Young moduli of the constituents are only randomised. Due to the homogenisation method presented, the effective Young modulus is obtained in the form of a random field in both cases. Since the fact that homogenisation is only the intermediate tool to analyse composite structures, the expected values and standard deviations of displacements for homogenised structures are compared against those obtained for real, multi-component structure models.

The results of these analyses make it possible to modify the theoretically established probabilistic homogenisation algorithm to approximate expected values as well as covariances in the most efficient way. Neglecting the fact that effective material characterisation presented above is derived assuming periodicity of a composite, we try to use this approach in composites having small number of the RVEs on their lengths.

The first numerical experiment deals with the homogenisation of a beam clamped at both sides and subjected to uniformly distributed vertical static load (see Figure 2.44), analogously to the computational illustration demonstrated in [208].

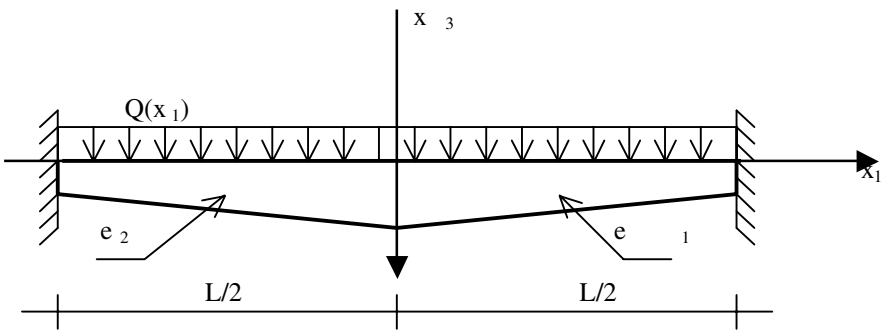


Figure 2.44. Clamped beam homogenised

Young moduli of the composite beam constituents discretised here by the use of 100 finite elements, are assumed to be deterministic variables, so that $e_1/e_2 = \{1.00; 1.25; \dots; 3.00\}$, while $e_2 = 2.0$ GPa and $\nu_1 = \nu_2 = 0.30$. The mesh nodes are numbered sequentially from the left to right edge. The cross-sectional area of the beam A_r is an input random field defined as

$$E[A_r] = A^0 \left(1.0 + \frac{0.3}{L} x_r \right); r = 1, \dots, 50 \quad \text{and} \quad A^0 = 5.0 \times 10^{-3}$$

$$\mu(A_r, A_s) = \exp \left(-\frac{|x_r - x_s|}{\lambda} \right); \lambda = 0.10; \alpha = 0.07; r, s = 1, \dots, 100$$

Other data are taken as follows:

$$Q(x_1) = f + \gamma A^0 \text{ for } f=49.61 \text{ and } \gamma=7.7126$$

while

$$I_{x_2} = I_{x_3} = \beta(A_r)^2; I_{x_1} = I_{x_2} + I_{x_3}; \beta = \frac{1}{6}; L=1.0$$

It is observed that starting from deterministically defined Young moduli the effective Young modulus random field is obtained as a result of the cross-sectional area randomness.

The main purpose of the SFEM-based tests is to verify the variability of the two-moment statistical response of the structure with respect to probabilistic input random fields. The results of the analysis are collected in Figures 2.45–2.48. The first two figures report expected values (vertical axes) as functions of location around the midpoint of a beam (horizontal axes); variable NN denotes here the node number where node 51 is the central point. The models outlined in the legend correspond to different composite configurations related to e_1/e_2 value – model 2R is equivalent to computational analysis of the beam in its real heterogeneous configuration with the Young moduli relation taken as 1.25. Thee data labelled as model 2H denote SFEM analysis results for the same homogenised model. The data obtained for model 1 denote the homogeneous beam with $e_1=e_2$, while ‘j’ from ‘model jR’ or ‘model jH’ is equivalent to the relation taken from the set $\{1.00;1.25;\dots;3.00\}$, accordingly.

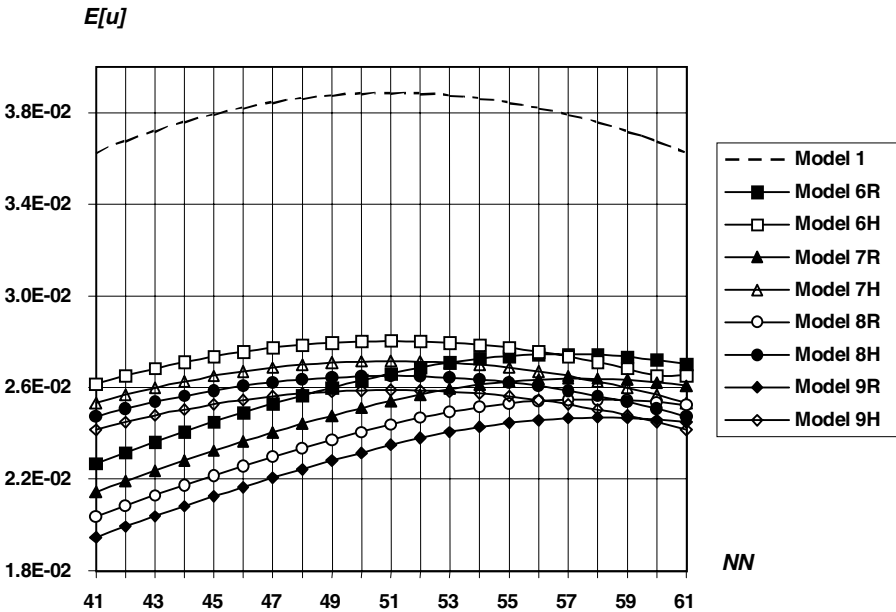


Figure 2.45. Expected values of the beam displacements

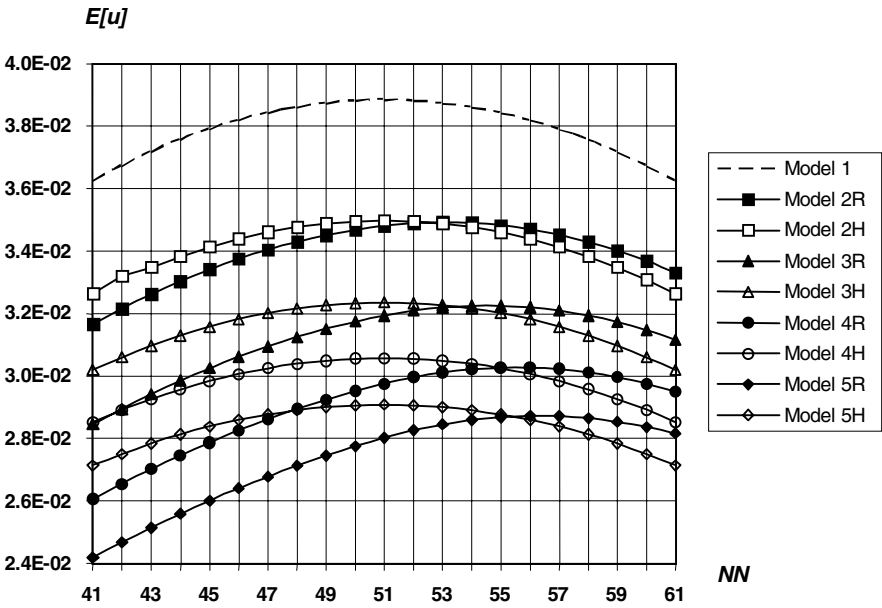


Figure 2.46. Expected values of the beam displacements

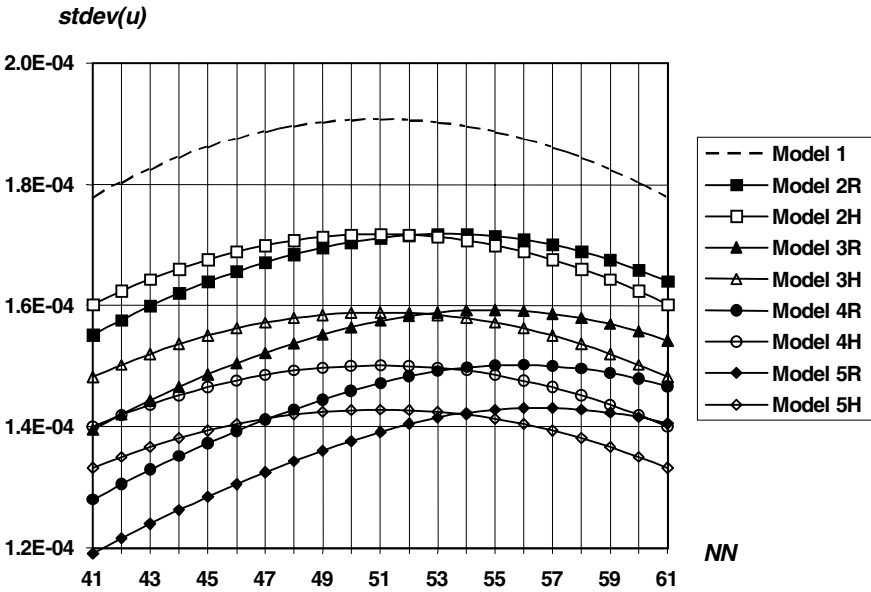


Figure 2.47. Standard deviations of the beam displacements

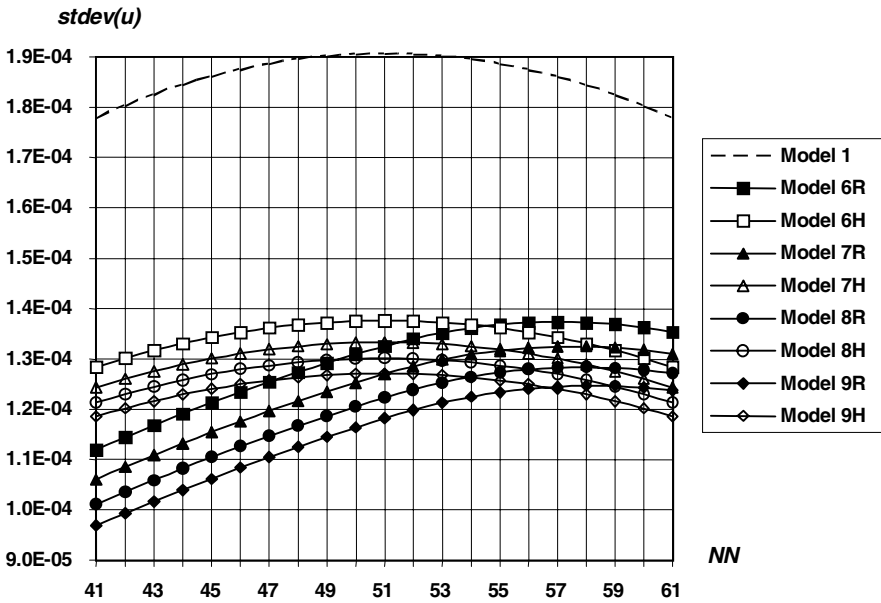


Figure 2.48. Standard deviations of the beam displacements

Analysing the results presented in Figures 2.45 and 2.46 as well as 2.47 and 2.48 it is seen that the homogenised structure approximates the real one with satisfactory precision, which is observed especially for smaller values of the relation e_1/e_2 . It can be seen that this approximation effectiveness has the same character for the expected values and standard deviations of displacements analysed. It is characteristic that while probabilistic moments of structural displacements are symmetric for symmetric boundary conditions imposed on the homogenised beam then for a real composite beam this field has not the symmetric character at all with greater values under the weaker part of a beam. Further, relating standard deviations to the corresponding expected values, it is observed that output coefficients of variance for displacements are equal to 0.05 (in real and homogenised beam) which, taking into account limitations of the perturbation technique, enable one to confirm the usefulness of this methodology for such an analysis. It should be underlined that neglecting the bending effects in homogenisation procedure has no effect on the differences observed because the Poisson ratio of both composite components is the same while the 3D beam finite element used is quite appropriate for that analysis.

Two-component linear elastic composite bar is built up with two homogeneous components with the following material and geometrical data: $E[e_1]=3000$, $A_1=4$, $l_1=15$, $E[e_2]=2500$, $A_2=2$, $l_2=10$ are considered (see Figure 2.49). The covariance matrix of Young moduli variables is assumed to be equal:

$$Cov(e_r, e_s) = \begin{bmatrix} 90,000 & 75,000 \\ \text{symm.} & 62,500 \end{bmatrix} \times 10^3$$

while the external loads $Q_1=200$ and $Q_2=250$ are applied to the structure:

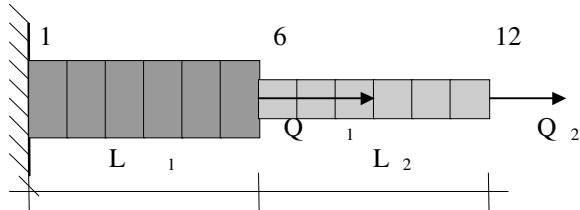


Figure 2.49. Two-component bar structure

The expected value and the covariance matrix of the effective Young modulus are calculated first and next, probabilistic moments of displacements and stresses for the original composite are computed. We compare these results against those determined for the homogenised structure. The input data and the results of computations are collected in Table 2.7 given below – the components of covariance matrix are equivalent to 10% standard deviation of the input Young moduli according to the following relation:

$$Cov(e_i, e_j) = \begin{bmatrix} \sigma_1^2 & \sigma_1 \sigma_2 \\ \text{symm.} & \sigma_2^2 \end{bmatrix}$$

Table 2.7.

Probabilistic data and intermediate results for computational experiments

Model no	Input data (1 st probabilistic moments)	Input data (2 nd probabilistic moments)
1	$E[e_1, e_2] = \{3000, 2500\}$	$Cov(e_r, e_s) = \begin{bmatrix} 90,000 & 75,000 \\ \text{symm.} & 62,500 \end{bmatrix} \times 10^3$
2	$E[e^{(eff)}] = 2857, 1437$	$Cov(e_r^{(eff)}, e_s^{(eff)}) = \begin{bmatrix} 41,649 & 16,659 \\ \text{symm.} & 6,663 \end{bmatrix} \times 10^3$
3	$E[e^{(eff)}] = 2857, 1437$	$Cov(e_r^{(eff)}, e_s^{(eff)}) = \begin{bmatrix} 90,000 & 75,000 \\ \text{symm.} & 62,500 \end{bmatrix} \times 10^3$

Next, the first two probabilistic moments of horizontal displacements are analysed along the bar. The results obtained for the stiffer part show better approximation by model 2 (with covariance matrix homogenised), while for a weaker part by model 3 (with original covariance matrix). Quite a different situation is observed for the standard deviations – those resulting from model 3

approximate those obtained in model 1 very well, while the results of model 2 are definitely smaller.

Table 2.8. Expected values and standard deviations of beam displacements

Node Number (NN)	Expected values			Standard deviations		
	Model 1	Model 2	Model 3	Model 1	Model 2	Model 3
1	0	0	0	0	0	0
2	0.0789	0.0825	0.0829	7.81E-03	5.89E-03	8.61E-03
3	0.1578	0.1649	0.1659	1.56E-02	1.18E-02	1.72E-02
4	0.2367	0.2474	0.2488	2.34E-02	1.77E-02	2.58E-02
5	0.3156	0.3298	0.3318	3.13E-02	2.35E-02	3.45E-02
6	0.3945	0.4123	0.4147	3.91E-02	2.94E-02	4.31E-02
7	0.4734	0.4947	0.4976	4.69E-02	3.53E-02	5.17E-02
8	0.5786	0.586	0.5895	5.73E-02	3.80E-02	5.97E-02
9	0.6838	0.6772	0.6813	6.77E-02	4.06E-02	6.76E-02
10	0.7891	0.7684	0.7732	7.81E-02	4.32E-02	7.56E-02
11	0.8943	0.8596	0.865	8.85E-02	4.59E-02	8.36E-02
12	0.9995	0.9509	0.9569	9.90E-02	4.85E-02	9.16E-02
13	1.1045	1.0421	1.0487	0.1094	0.0511	9.95E-02

Taking into account the results of computational experiments presented in Table 2.8, the following algorithm is proposed to model strictly periodic composite beams using homogenisation-based SFEA.

<u>Input random variables definition</u>
$E[b_r], Cov(b^r, b^s)$
<u>Initial boundary value problem</u>
$\sigma_{ij,j}^\varepsilon + \gamma^\varepsilon = 0$
→ solve:
$\mathbf{K}^{(\varepsilon)0} \mathbf{q}^{(\varepsilon)0} = \mathbf{Q}^0$
$\mathbf{K}^{(\varepsilon)0} \mathbf{q}^{(\varepsilon),r} = -\mathbf{K}^{(\varepsilon),r} \mathbf{q}^{(\varepsilon)0}$
$\mathbf{K}^{(\varepsilon)0} \mathbf{q}^{(\varepsilon)(2)} = (-2\mathbf{K}^{(\varepsilon),r} \mathbf{q}^{(\varepsilon),s} - \mathbf{K}^{(\varepsilon),rs} \mathbf{q}^{(\varepsilon)0}) Cov(b^r, b^s)$
<u>Evaluation of effective Young moduli parameters</u>
$E[e^{(eff)}] Cov(e^{(eff)r}, e^{(eff)s})$
<u>Homogenised boundary value problem:</u>
$\sigma_{ij,j}^{(eff)} + \gamma^{(eff)} = 0$
<u>1st SFEM solution (zeroth order homogenised displacements):</u>
→ solve:
$\mathbf{K}^{(eff)0} \mathbf{q}_{[1]}^{(eff)0} = \mathbf{Q}^0$
$\mathbf{K}^{(eff)0} \mathbf{q}_{[1]}^{(eff),r} = -\mathbf{K}^{(eff),r} \mathbf{q}_{[1]}^{(eff)0}$

$$\mathbf{K}^{(eff)0} \mathbf{q}_{[1]}^{(eff)(2)} = \left(-2\mathbf{K}^{(eff),r} \mathbf{q}_{[1]}^{(eff),s} - \mathbf{K}^{(eff),rs} \mathbf{q}_{[1]}^{(eff)0} \right) \text{Cov}(e^{(eff)r}, e^{(eff)s})$$

2nd SFEM solution (first and second order homogenised displacements)
 → solve:

$$\mathbf{K}^{(eff)0} \mathbf{q}_{[2]}^{(eff)0} = \mathbf{Q}^0$$

$$\mathbf{K}^{(eff)0} \mathbf{q}_{[2]}^{(eff),r} = -\mathbf{K}^{(eff),r} \mathbf{q}_{[2]}^{(eff)0}$$

$$\mathbf{K}^{(eff)0} \mathbf{q}_{[2]}^{(eff)(2)} = \left(-2\mathbf{K}^{(eff),r} \mathbf{q}_{[2]}^{(eff),s} - \mathbf{K}^{(eff),rs} \mathbf{q}_{[2]}^{(eff)0} \right) \text{Cov}(b^r, b^s)$$

Final evaluation of displacements probabilistic moments

$$E[q_{\beta}^{(eff)}] = q_{\beta[1]}^{(eff)0} + q_{\beta[2]}^{(eff)(2)}$$

$$\text{Cov}(q_{\alpha}^{(eff)}, q_{\beta}^{(eff)}) = q_{\alpha[2]}^{(eff),r} q_{\beta[2]}^{(eff),s} \text{Cov}(b^r, b^s)$$

Figure 2.50. Algorithm of homogenisation-based SFEM analysis

It should be underlined that such a stochastic second order homogenisation scheme has its basis in the computational observations only. However its results are in good agreement with those observed for the real composite model subjected to the same boundary conditions.

2.3.2 2D and 3D Composites with Uniaxially Distributed Inclusions

This class of composites is equivalent to all 2D and 3D periodic heterogeneous structures where isotropic homogeneous constituents are distributed periodically along the x_3 axis, which in practice is observed in case of the periodic laminates. Further, it should be mentioned that the effective elasticity tensor components valid for these structures can be reduced to the periodic bar structure shown above only if the 1D case is considered. The following system of partial differential equations is considered here to calculate probabilistic moments of the effective elasticity tensor [159]:

$$\left(C_{ijkl} \left(\frac{x_3}{\delta} \right) u_{k,l}^{\delta} \right)_{,j} = f_i(\mathbf{x}), \quad \mathbf{u}^{\delta}(\mathbf{x}) = \mathbf{u}^o(\mathbf{x}), \quad \mathbf{x} \in \partial\Omega. \quad (2.97)$$

According to the general theory, the homogenised formulation of the problem has the following form:

$$\left(C_{ijkl}^{(eff)} u_{k,l} \right)_{,j} = f_i(\mathbf{x}), \quad \mathbf{u}(\mathbf{x}) = \mathbf{u}^o(\mathbf{x}), \quad \mathbf{x} \in \partial\Omega. \quad (2.98)$$

where the effective coefficients $C_{ijkl}^{(eff)}$ are given by the formula. The homogenisation functions $\chi^{kl}(\mathbf{y})$ are determined as the solution of the local problem on the RVE

$$\frac{\partial}{\partial y_j} \left(C_{ijkl}(y_3) \frac{\partial}{\partial y_i} (\chi_k^{mn}) + C_{ijmn}(y_3) \right) = 0; \mathbf{x} \in \Omega \quad (2.99)$$

for any $\chi^{mn}(\mathbf{y})$ periodic on the RVE. Since the heterogeneity distribution is observed along y_3 axis only, a solution should be of the form $\chi^{mn}(\mathbf{y}) = \chi^{mn}(y_3)$. It yields the following problem for determination of $\chi^{mn}(y_3)$

$$\frac{\partial}{\partial y_3} \left(C_{i3k3}(y_3) \frac{\partial}{\partial y_3} (\chi_k^{mn}) + C_{i3mn}(y_3) \right) = 0, \quad \mathbf{x} \in \Omega \quad (2.100)$$

for any $\chi^{mn}(y_3)$ being periodic on the RVE. Therefore, (2.100) is ordinary differential equations system, which can be solved explicitly as

$$C_{i3k3}(y_3) \chi_{k,3}^{mn} + C_{i3mn}(y_3) = A_i. \quad (2.101)$$

If the elasticity tensor components C_{i3k3} are invertible, then

$$\chi_{k,3}^{mn} = -\{C_{k3j3}\}^{-1} C_{j3mn} + \{C_{k3j3}\}^{-1} A_j \quad (2.102)$$

The periodicity condition results in $\langle \chi_{,3}^{mn} \rangle_{\Omega} = 0$ which introduced in (2.102) yields

$$0 = -\langle \{C_{k3j3}\}^{-1} C_{j3mn} \rangle_{\Omega} + \langle \{C_{k3j3}\}^{-1} \rangle_{\Omega} A_j \quad (2.103)$$

Therefore

$$A_i = \langle \{C_{i3k3}\}^{-1} \rangle_{\Omega}^{-1} \langle \{C_{k3j3}\}^{-1} C_{j3mn} \rangle_{\Omega} \quad (2.104)$$

and there holds

$$\chi_{k,3}^{mn} = -\{C_{k3j3}\}^{-1} C_{j3mn} + \{C_{k3j3}\}^{-1} \langle \{C_{j3q3}\}^{-1} \rangle_{\Omega}^{-1} \langle \{C_{q3p3}\}^{-1} C_{p3mn} \rangle_{\Omega} \quad (2.105)$$

Taking into account that the state functions depend on y_3 axis only, the effective parameters are expressed as

$$C_{ijkl}^{(eff)} = \left\langle C_{ijkl} + C_{ijm3} \chi_{m,3}^{kl} \right\rangle_{\Omega} \quad (2.106)$$

Finally, the homogenised elasticity tensor components are given by

$$\begin{aligned} C_{ijkl}^{(eff)} = & \left\langle C_{ijkl} \right\rangle_{\Omega} - \left\langle C_{ijm3} \left\{ C_{m3p3} \right\}^{-1} C_{p3kl} \right\rangle_{\Omega} \\ & + \left\langle C_{ijm3} \left\{ C_{m3p3} \right\}^{-1} \right\rangle_{\Omega} \left\langle \left\{ C_{p3n3} \right\}^{-1} \right\rangle_{\Omega} \left\langle \left\{ C_{n3q3} \right\}^{-1} C_{q3kl} \right\rangle_{\Omega} \end{aligned} \quad (2.107)$$

In case of isotropic and linear elastic constituent materials of this composite, it is obtained after some algebraic manipulation [159,177]

$$C_{1111}^{(eff)} = C_{2222}^{(eff)} = \left\langle \frac{(1-\nu)e}{(1+\nu)(1-2\nu)} \right\rangle_{\Omega} - \left\langle \frac{(1-2\nu)e}{1-\nu^2} \right\rangle_{\Omega} + \frac{\left\langle \frac{1-2\nu}{1-\nu} \right\rangle_{\Omega}^2}{\left\langle \frac{(1+\nu)(1-2\nu)}{(1-\nu)e} \right\rangle_{\Omega}} \quad (2.108)$$

$$C_{3333}^{(eff)} = \frac{1}{\left\langle \frac{(1+\nu)(1-2\nu)}{(1-\nu)e} \right\rangle_{\Omega}} \quad (2.109)$$

$$C_{1133}^{(eff)} = C_{3311}^{(eff)} = C_{2233}^{(eff)} = C_{3322}^{(eff)} = \frac{\left\langle \frac{1-2\nu}{1-\nu} \right\rangle_{\Omega}}{\left\langle \frac{(1+\nu)(1-2\nu)}{(1-\nu)e} \right\rangle_{\Omega}} \quad (2.110)$$

$$C_{1122}^{(eff)} = C_{2211}^{(eff)} = \left\langle \frac{e}{(1-\nu)} \right\rangle_{\Omega} - \left\langle \frac{(1-2\nu)e}{1-\nu^2} \right\rangle_{\Omega} + \frac{\left\langle \frac{1-2\nu}{1-\nu} \right\rangle_{\Omega}}{\left\langle \frac{(1+\nu)(1-2\nu)}{(1-\nu)e} \right\rangle_{\Omega}} \quad (2.111)$$

$$C_{1212}^{(eff)} = C_{2121}^{(eff)} = \left\langle \frac{e}{(1+\nu)} \right\rangle_{\Omega}, \quad C_{1212}^{(eff)} = C_{2121}^{(eff)} = \left\langle \frac{1}{1+\nu} \right\rangle_{\Omega} \quad (2.112)$$

while the remaining components are equal to 0. The layered structure analysed in this experiment has material characteristics corresponding to a glass-epoxy composite: $E[e_1]=84.0$ GPa, $\sigma[e_1]=8.4$ GPa, $\nu_1=0.22$ and $E[e_2]=4.0$ GPa, $\sigma[e_2]=0.4$ GPa, $\nu_2=0.34$; the volume ratios are taken as equal. The results of

computational analysis are collected as deterministic quantities, expected values and coefficients of variation computed for the particular components in Table 2.9 below.

Table 2.9. Effective materials characteristics

Effective elasticity tensor components	Deterministic	Expected value	Variation
$C_{1111}=C_{2222}$	29.2316 GPa	29.2260 GPa	0.0767
C_{3333}	10.4662 GPa	10.4566 GPa	0.0954
$C_{1133}=C_{3311}=C_{2233}=C_{3322}$	6.1479 GPa	6.1424 GPa	0.0954
$C_{1122}=C_{2211}$	34.3657 GPa	34.3601 GPa	0.0794
$C_{1212}=C_{2121}$	50.7785 GPa	50.7785 GPa	0.0936
$C_{2323}=C_{3232}$	51.5489 GPa	51.5608 GPa	0.0968

Comparing the results presented in Table 2.9 it is seen that there is no difference between the deterministic result and the corresponding expected values for effective tensor components, while the coefficient of variation has values generally smaller or almost equal to the corresponding input variables value 0.1. To verify the variability of the tensor with respect to input Young moduli expected values, the MAPLE plot3d option for $E[C_{2323}^{(eff)}]$ and $\alpha(C_{2323}^{(eff)})$ has been applied; the remaining components show almost the same tendencies. The range of variability for both the composite components Young moduli is taken as $\pm 10\%$ of the original values and, as can be observed in Figures 2.51 and 2.52, Young modulus of the weaker material appears to be the decisive parameter for the overall elastic characteristics of this composite in terms of a homogenisation method applied. Further, it can be noticed that an increase of the coefficient of variation $\alpha(C_{2323}^{(eff)})$ results from decreasing matrix Young modulus, while the inverse relation is observed in case of $E[C_{2323}^{(eff)}]$.

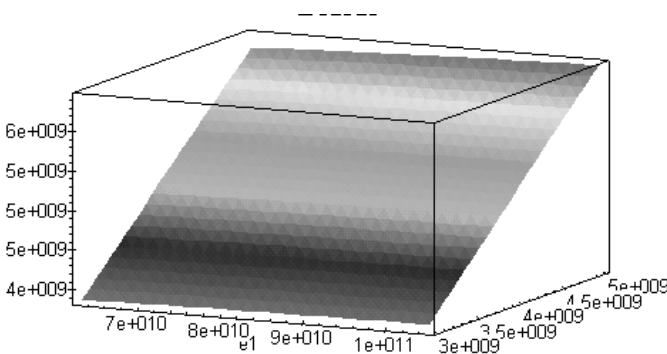


Figure 2.51. Expected values for C_{2323} component

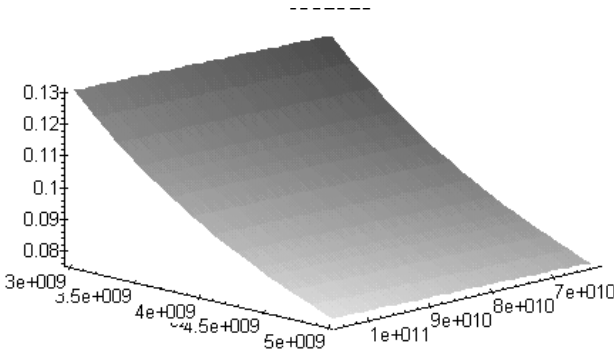


Figure 2.52. Coefficients of variation for C_{2323} component

It should be underlined that the model for one dimensionally distributed inhomogeneity is valid after some minor simplifications for the heat conduction homogenisation of the same composites, since probabilistic numerical algorithm has a quite general character.

2.3.3 Fibre-Reinforced Composites

2.3.3.1 Algebraic Equations for Homogenised Characteristics

It should be emphasised that the homogenisation procedure can be applied to the fibre-reinforced composite with anisotropic constituents, too. The effective elasticity tensor in terms of different transverse and longitudinal Young moduli and Poisson ratios can be calculated explicitly using the Mori-Tanaka or the self-consistent analytical homogenisation technique as follows [18,31]:

$$\begin{Bmatrix} \sigma_{11} \\ \sigma_{22} \\ \sigma_{33} \\ \sigma_{23} \\ \sigma_{31} \\ \sigma_{12} \end{Bmatrix} = \begin{Bmatrix} n & l & l & 0 & 0 & 0 \\ & k+m & k-m & 0 & 0 & 0 \\ & & k+m & 0 & 0 & 0 \\ & & & m & 0 & 0 \\ & sym. & & & p & 0 \\ & & & & & p \end{Bmatrix} \begin{Bmatrix} \epsilon_{11} \\ \epsilon_{22} \\ \epsilon_{33} \\ \epsilon_{23} \\ \epsilon_{31} \\ \epsilon_{12} \end{Bmatrix} \tag{2.113}$$

where the following description for the constants k, l, m, n and p is applied:

$$p = \frac{2c_f p_m p_f + c_m (p_m p_f + p_m^2)}{2c_f p_m + c_m (p_f + p_m)} \quad (2.114)$$

$$m = \frac{m_m m_f (k_m + 2m_m) + k_m m_m (c_f m_f + c_m m_m)}{k_m m_m + (k_m + 2m_m)(c_f m_m + c_m m_f)} \quad (2.115)$$

$$k = \frac{c_f k_f (k_m + m_m) + c_m m_m (k_f + m_m)}{c_f (k_m + m_m) + c_m (k_f + m_m)} \quad (2.116)$$

$$l = \frac{c_f l_f (k_m + m_m) + c_m l_m (k_f + m_m)}{c_f (k_m + m_m) + c_m (k_f + m_m)} \quad (2.117)$$

$$n = c_m n_m + c_f n_f + (l - c_f l_f - c_m l_m) \frac{l_f - l_m}{k_f - k_m} \quad (2.118)$$

There holds for matrix and fibre

$$\left\{ \begin{array}{l} k = \left[\frac{1}{G_T} - \frac{4}{E_T} + \frac{4v_L^2}{E_L} \right]^{-1} \\ l = 2kv_L \\ n = E_L + 4kv_L^2 = E_L + \frac{l^2}{k} \\ m = G_T, p = G_L \end{array} \right. \quad (2.119)$$

where c_f and c_m denote fibre and matrix volume fractions of a composite measured in the direction transverse to the fibres. The indices L and T denote longitudinal and transversal elastic characteristics for the components. It can be observed that closed form relations for effective elasticity tensor components are obtained in this case without the necessity of a cell problem solution.

Two alternative ways of fibre–reinforced composite homogenisation have been proposed below. Since the fact that the computational illustration for the SFEM solution of the cell problem is shown in [192], then only the second order perturbation based model is discussed here. The composite taken to illustrate probabilistic moments of relevant material properties is exactly the same as in the previous example. The final equations for the effective characteristics for a layered and fibre–reinforced composite do not contain any shape parameters – different forms of the reinforcement lead, according to some mathematical considerations, to different equations rewritten however for the same parameters: material properties and volume ratios of the constituents only. That is why such a comparative studies, especially in terms of the random spaces of the material properties analysed, are important.

The deterministic and the corresponding expected values as well as coefficients of variation are collected in Table 2.10 for the components of the effective tensor k , l , m , n and p , separately. Generally, it can be observed that, as previously noted, expected values are almost equal to relevant deterministic quantities and the

resulting coefficients of variation are almost equal to the corresponding input probabilistic coefficients. Further, comparing the data collected in Tables 2.9 and 2.10 it can be noted that the layered structure has greater effective elastic characteristics than the fibre-reinforced composite with the same constituents – this observation is very important considering practical applications and optimisation of composites.

Table 2.10. Effective materials characteristics

Effective elasticity tensor components	Deterministic	Expected value	Variation
k	6.8350 GPa	6.8216 GPa	0.0902
l	5.2983 GPa	5.2898 GPa	0.0909
m	3.5892 GPa	3.5840 GPa	0.0927
n	46.9052 GPa	46.9000 GPa	0.0938
p	4.0195 GPa	4.0121 GPa	0.0907

Further, see Figures 2.53–2.62, the parameter variability of the expected values of the effective parameters k , l , m , n and p (Figures 2.53, 2.55, 2.57, 2.59 and 2.61) as well as their variances (Figures 2.54, 2.56, 2.58, 2.60 and 2.62) is computed with respect to expected values of the Young moduli of the components. It is seen that the expected values of all these parameters show greater sensitivity with respect to stronger material Young moduli; all the changes are significant especially for decreasing values of both moduli. As can be predicted from these figures, the sensitivity gradients of all the parameters have positive signs – an increase of any effective constant k , l , m , n and p results from the increase of Young moduli of fibre or/and matrix. In further computational studies, the probabilistic moments so computed may be applied in the FEM–based probabilistic computational simulation for an engineering composite by using the Monte Carlo simulation technique or, as is done in the first example, the SFEM approach.

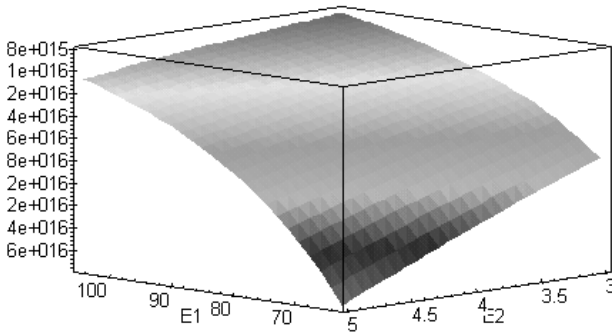


Figure 2.53. Expected values of the component k

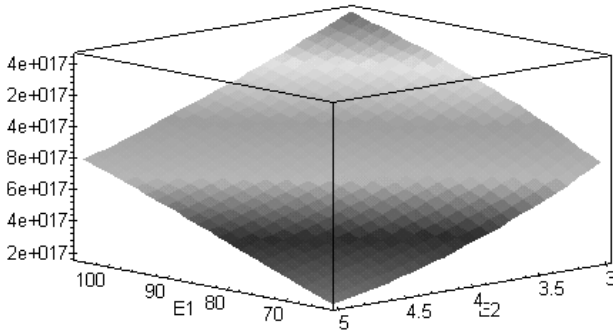


Figure 2.54. Variance of the component k

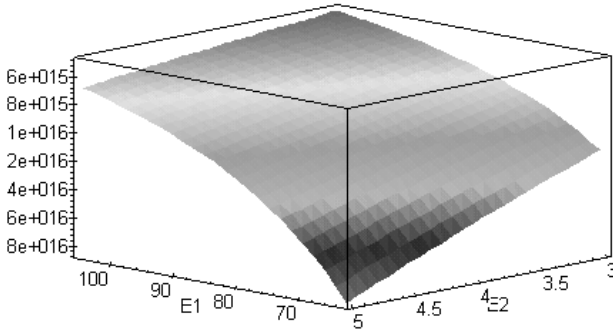


Figure 2.55. Expected values of the component l

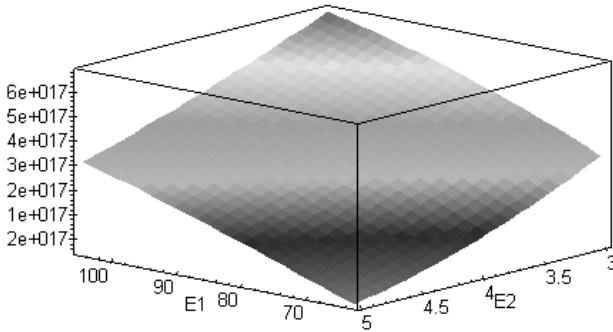


Figure 2.56. Variance of the component l

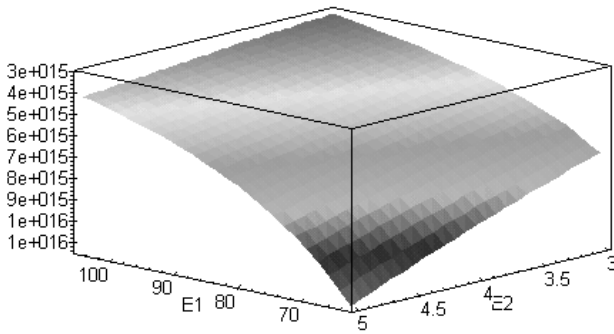


Figure 2.57. Expected values of the component m

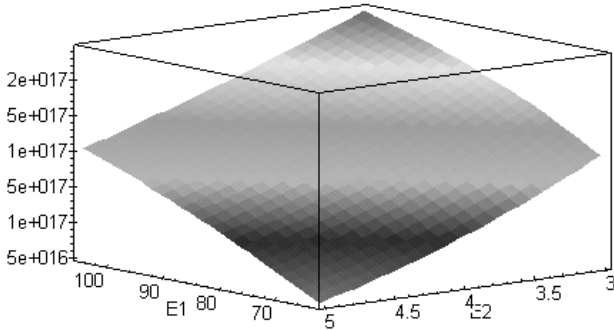


Figure 2.58. Variance of the component m

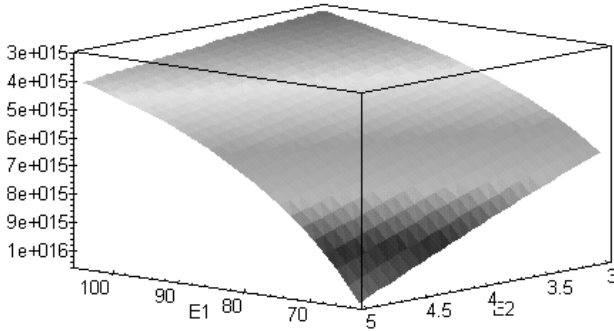


Figure 2.59. Expected values of the component n

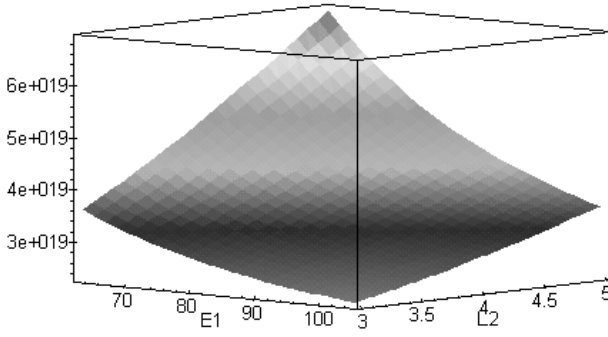


Figure 2.60. Variance of the component n

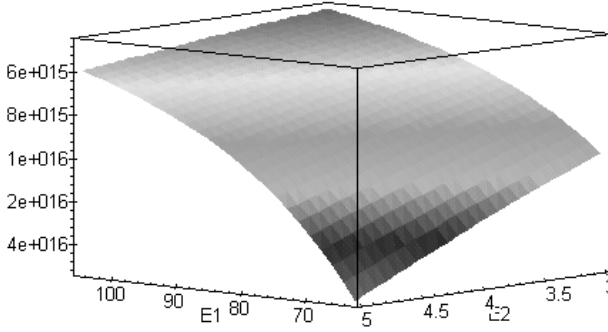


Figure 2.61. Expected values of the component p

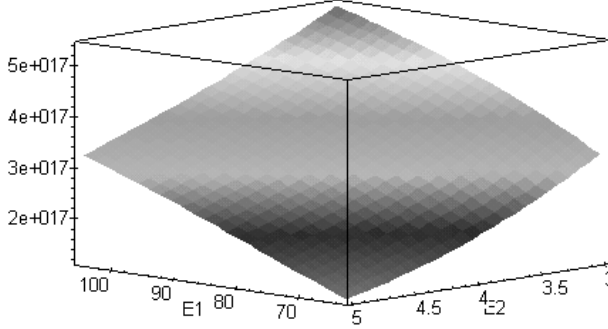


Figure 2.62. Variance of the component p

2.3.3.2 Asymptotic Homogenisation Method

2.3.3.2.1 Deterministic Approach to the Problem

The homogenisation of the n -component periodic composites in the context of linear deterministic elastostatic problem is studied here; the effective modules method worked out previously for two-component heterogeneous media is now extended on the n -component composites to homogenise multi-component materials in general form. The approach proposed enables particularly, as is demonstrated, to calculate effective elastic characteristics for composites with some interphases between the constituents. As it is known, the interphase in engineering practice may be considered as the next homogeneous component of the composite with small volume in comparison to the rest of a structure that increases contact between reinforcement and matrix and can be crucial for the composite macro-behaviour [59,255,270,314]. One of the interphase computational modelling method is based on the special (both elastic and elastoplastic) interface finite elements [238,260,318].

On the other hand, there are some approaches in the mechanics of composite materials, where the interphase is the hypothetical region containing all interface defects that appear between the original components of a composite. Usually, the interphase is introduced with thickness and material parameters constant within its region; ultrasonic emission seems to be the most efficient experimental method in this field. Numerical studies based on this formulation and collected in this chapter show the sensitivity of the periodic composite effective parameters to strengthening and weakening, in the context of elastic parameters, of the interphase. Due to the fact that the observations correspond with engineering practice, it may confirm the usefulness of the method to homogenise n -component heterogeneous media.

Very important aspect of the method proposed is that the effective modules method in present extended version enables to homogenize the composite materials with the microdefects appearing in the constituents – they have the dimensions relatively small with comparison to the components. Next, we observe that the method presented can be relatively easily transformed to the probabilistic case where material properties as well as the periodicity cell geometry may be treated as random; the Monte Carlo simulation method is the most recommended technique. This formulation may be used to formulate and to compute the deterministic or stochastic sensitivity, in a phenomenological or structural sense, to both material and geometrical parameters of the composite that enable one to find out the most decisive parameters for the entire computational homogenisation procedure.

The linear problem of elasticity is formulated for the n -component composite shown in Figure 2.64 with the Representative Volume Element given in Figure 2.63 as follows:

$$\left\{ \begin{array}{l} \frac{\partial \sigma_{ij}^\varepsilon}{\partial x_j} = 0 \\ \sigma_{ij}^\varepsilon n_j = p_i; \mathbf{x} \in \partial \Omega_\sigma \\ u_i^\varepsilon = 0; \mathbf{x} \in \partial \Omega_u \\ \sigma_{ij}^\varepsilon = C_{ijkl}^\varepsilon(\mathbf{x}) \varepsilon_{kl}^\varepsilon \\ \varepsilon_{kl}^\varepsilon = \frac{1}{2} (u_{k,l}^\varepsilon + u_{l,k}^\varepsilon) \end{array} \right. \quad i,j,k,l=1,2 \quad (2.120)$$

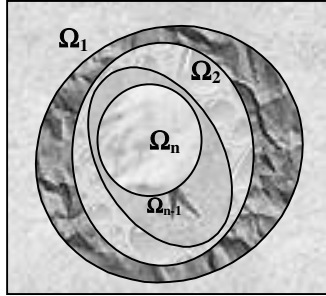


Figure 2.63. Cross-section of periodic composite structure

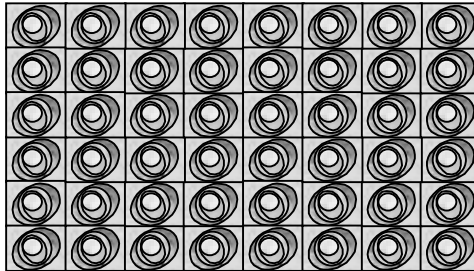


Figure 2.64. The RVE of plane composite

Let us assume that all interfaces of the composite are perfect in the sense that

$$[u_i^\varepsilon] = 0, \quad [\sigma_{ij}^\varepsilon n_j^\Gamma] = 0 \quad (2.121)$$

where the symbol $[.]$ denotes a jump of the respective function values at the interface. The homogenisation problem is to find the limit of solution \mathbf{u}^ε with ε tending to 0. For this purpose let us consider a bilinear form $a^\varepsilon(\mathbf{u}, \mathbf{v})$ defined as follows:

$$a^\varepsilon(\mathbf{u}, \mathbf{v}) = \int_{\Omega} C_{ijkl}^\varepsilon\left(\frac{\mathbf{x}}{\varepsilon}\right) \varepsilon_{ij}(\mathbf{u}) \varepsilon_{kl}(\mathbf{v}) d\Omega \quad (2.122)$$

and the linear form:

$$L(\mathbf{v}) = \int_{\Omega} F_i v_i d\Omega + \int_{\partial\Omega_{\sigma}} p_i v_i d(\partial\Omega) \quad (2.123)$$

both in a Hilbert space

$$V = \left\{ \mathbf{v} \mid \mathbf{v} \in (H^1(\Omega))^3, \mathbf{v} \Big|_{\partial\Omega_u} = 0 \right\} \quad (2.124)$$

characterised by the norm

$$\|\mathbf{v}\|^2 = \int_{\Omega} \boldsymbol{\varepsilon}_{ij}(\mathbf{v}) \boldsymbol{\varepsilon}_{ij}(\mathbf{v}) d\Omega \quad (2.125)$$

A variational statement equivalent to the equilibrium problem (2.120) is to find $\mathbf{u}^{\varepsilon} \in V$ fulfilling the equation

$$a^{\varepsilon}(\mathbf{u}^{\varepsilon}, \mathbf{v}) = L(\mathbf{v}) \quad (2.126)$$

for any $\mathbf{v} \in V$. Let us introduce for this purpose a space of periodic functions $P(\Omega) = \left\{ \mathbf{v}, \mathbf{v} \in (H^1(\Omega))^3 \right\}$ so that the trace of \mathbf{v} is equal on opposite sides of Ω . Let us denote for any $\mathbf{u}, \mathbf{v} \in P(\Omega)$

$$a_y(\mathbf{u}, \mathbf{v}) = \int_{\Omega} C_{ijkl}(\mathbf{y}) \boldsymbol{\varepsilon}_{ij}(\mathbf{u}) \boldsymbol{\varepsilon}_{kl}(\mathbf{v}) d\Omega \quad (2.127)$$

and introduce a homogenisation function $\chi_{(ij)k} \in P(\Omega)$ as a solution for the local problem on a periodicity cell:

$$a_y\left(\left(\chi_{(ij)k} + y_j \delta_{ki}\right) \mathbf{n}_k, \mathbf{w}\right) = 0 \quad (2.128)$$

for any $\mathbf{w} \in P(\Omega)$; δ_{ki} denotes the Kronecker delta while \mathbf{n}_k is the unit coordinate vector. Assuming finally that:

$$C_{ijkl} \in L^{\infty}(\mathfrak{R}^3) \quad (2.129)$$

$$C_{ijkl} = C_{klij} = C_{jikl} \quad (2.130)$$

$$\exists C_0 > 0; C_{ijkl} \xi_{ij} \xi_{kl} \geq C_0 \xi_{ij} \xi_{ij}, \quad \forall_{i,j} \xi_{ij} = \xi_{ji} \quad (2.131)$$

we may introduce a homogenisation theorem as follows:

Homogenisation theorem

The solution \mathbf{u}^{ε} of problem (2.126) converges weakly in space V

$$\mathbf{u}^\varepsilon \rightarrow \mathbf{u} \quad (2.132)$$

if the tensor $C_{ijkl}^\varepsilon(\mathbf{y})$ is Ω -periodic and its components fulfil conditions (2.129–2.131). Solution \mathbf{u} is the unique one for the problem

$$\mathbf{u} \in V : D(\mathbf{u}, \mathbf{v}) = L(\mathbf{v}) \quad (2.133)$$

for any $\mathbf{v} \in V$ and

$$D(\mathbf{u}, \mathbf{v}) = \int_Y D_{ijkl} \varepsilon_{ij}(\mathbf{u}) \varepsilon_{kl}(\mathbf{v}) dY \quad (2.134)$$

where

$$D_{ijkl} = \frac{1}{|\Omega|} a_y \left((\chi_{(ij)p} + y_i \delta_{pj}) \mathbf{n}_p, (\chi_{(kl)q} + y_l \delta_{qk}) \mathbf{n}_q \right) \quad (2.135)$$

As a result of this theorem, a limit for $\varepsilon \rightarrow 0$ gives a homogeneous elastic material described by the tensor [163]:

$$C_{ijkl}^{(eff)} = \frac{1}{|\Omega|} \int_{\Omega} \left(C_{ijkl}(\mathbf{y}) + C_{ijmn}(\mathbf{y}) \varepsilon_{mn}^y(\chi_{(kl)}(\mathbf{y})) \right) H \Omega \quad (2.136)$$

The most important result is that neither the local problem nor the statement (2.136) really depend on the stress boundary conditions since that solution obtained has a general character. To show formally these results, the local problem is rewritten in its differential form

$$\frac{\partial}{\partial x_j} \left(C_{ijkl} \left(\frac{\mathbf{x}}{\varepsilon} \right) \varepsilon_{kl} \left(\mathbf{u}_i^\varepsilon \right) \right) + F_i = 0; \quad \frac{\mathbf{x}}{\varepsilon} = \mathbf{y} \in \Omega; \quad u_i^\varepsilon = 0 \text{ for } \mathbf{y} \in \partial \Omega \quad (2.137)$$

Next, similarly to the stochastic perturbation approach, an asymptotic expansion is employed in terms of the parameter ε as follows:

$$u_i^\varepsilon(\mathbf{x}) = u_i^{(0)}(\mathbf{x}, \mathbf{y}) + \varepsilon u_i^{(1)}(\mathbf{x}, \mathbf{y}) + \varepsilon^2 u_i^{(2)}(\mathbf{x}, \mathbf{y}) + \dots \quad (2.138)$$

where $u_i^{(m)}(\mathbf{x}, \mathbf{y})$ are periodic in \mathbf{y} with a periodicity cell Ω . The main idea of this expansion is presented schematically in Figure 2.65: to better illustrate the meaning of (2.133) only a quarter of the composite is shown.

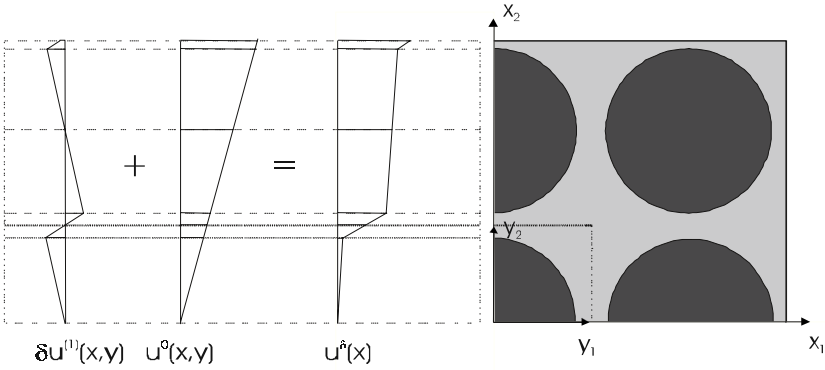


Figure 2.65. First order asymptotic expansion of displacements in a composite

Let us note that differentiation separates the coordinates \mathbf{x} and \mathbf{y} , so that

$$\varepsilon_{ij}(\mathbf{v}) = \varepsilon_{ij}^x(\mathbf{v}) + \frac{1}{\varepsilon} \varepsilon_{ij}^y(\mathbf{v}) \tag{2.139}$$

where the strain tensors $\varepsilon_{ij}^x(\mathbf{v})$, $\varepsilon_{ij}^y(\mathbf{v})$ correspond to small deformations

$$\varepsilon_{ij}^x(\mathbf{v}) = \frac{1}{2} \left(\frac{\partial v_i}{\partial x_j} + \frac{\partial v_j}{\partial x_i} \right), \quad \varepsilon_{ij}^y(\mathbf{v}) = \frac{1}{2} \left(\frac{\partial v_i}{\partial y_j} + \frac{\partial v_j}{\partial y_i} \right). \tag{2.140}$$

Thus, (2.132) can be rewritten as follows:

$$\left(\varepsilon^{-2} L_1 + \varepsilon^{-1} L_2 + L_3 \right) \left(u_i^{(0)} + \varepsilon u_i^{(1)} + \varepsilon^2 u_i^{(2)} + \dots \right) + F_i = 0 \tag{2.141}$$

where

$$L_1 u_i = \frac{\partial}{\partial y_j} \left(C_{ijkl}(\mathbf{y}) \frac{\partial u_k}{\partial y_l} \right) \tag{2.142}$$

$$L_2 u_i = C_{ijkl}(\mathbf{y}) \frac{\partial}{\partial x_j} \left(\frac{\partial u_k}{\partial y_l} \right) + \frac{\partial}{\partial y_j} \left(C_{ijkl}(\mathbf{y}) \right) \frac{\partial u_k}{\partial x_l} \tag{2.143}$$

$$L_3 u_i = C_{ijkl}(\mathbf{y}) \frac{\partial}{\partial x_j} \left(\frac{\partial u_k}{\partial x_l} \right) \tag{2.144}$$

Next, we equate to 0 the terms with the same order of ε , obtaining an infinite sequence of equations. The relations adequate to its zeroth, first and second orders can be written as

$$L_1 u_i^{(0)} = 0 \quad (2.145)$$

$$L_1 u_i^{(1)} + L_2 u_i^{(0)} = 0 \quad (2.146)$$

$$L_1 u_i^{(2)} + L_2 u_i^{(1)} + L_3 u_i^{(0)} + F_i = 0 \quad (2.147)$$

The displacements fields $u_i^{(0)}$, $u_i^{(1)}$ and $u_i^{(2)}$ can be found from these equations recurrently only if \mathbf{x} and \mathbf{y} are independent variables. Let us note also that the equation

$$L_1 u_i + P_i = 0 \quad (2.148)$$

with u_i being Ω -periodic function has a unique solution for

$$\langle P \rangle = \frac{1}{|\Omega|} \int_{\Omega} P_i 1_i d\mathbf{y} = 0 \quad (2.149)$$

Further, if the unique solution $\mathbf{u}(\mathbf{x}, \mathbf{y})$; $\mathbf{x} \in \Omega$ of (2.148) is constant then for all \mathbf{x} (where \mathbf{x} plays here the role of parameter) we have $u_0 = \text{const}$. Considering this fact it can be obtained that

$$u_i^{(0)}(\mathbf{x}, \mathbf{y}) = u_i(\mathbf{x}) \quad (2.150)$$

which can be observed in Figure 2.65 as well. It can be observed that the first term of the expansion of \mathbf{u} does not depend on the micro variable \mathbf{y} and can be considered as a mean displacement altered by the higher order terms only. Thus, (2.146) takes the following form:

$$L_1 u_i^{(1)}(\mathbf{x}, \mathbf{y}) + \frac{\partial}{\partial y_j} (C_{ijkl}(\mathbf{y})) \frac{\partial}{\partial x_l} (u_k^{(0)}(\mathbf{x})) = 0 \quad (2.151)$$

The solution is obtained by separation of \mathbf{x} and \mathbf{y}

$$u_i^{(1)}(\mathbf{x}, \mathbf{y}) = \chi_{(kl)i}(\mathbf{y}) \frac{\partial}{\partial x_l} (u_k^{(0)}(\mathbf{x})) + u_i(\mathbf{x}) \quad (2.152)$$

The last two equations give the formulation for the Ω -periodic functions $\chi_{(kl)i}(\mathbf{y})$

$$\frac{\partial}{\partial y_j} \left(C_{ijmn}(\mathbf{y}) \frac{\partial \chi_{(kl)m}(\mathbf{y})}{\partial y_n} \right) + \frac{\partial}{\partial y_j} (C_{ijkl}(\mathbf{y})) = 0 \quad (2.153)$$

which completes our consideration of general homogenisation method for linear elastostatic problems.

It is relatively easy to see that the local problems for homogenisation functions $\chi_{(kl)i}(\mathbf{y})$ reduce to the equations given above for any region Ω_a where $1 \leq a \leq n$ for the so-called fibre-like composite materials where one component is placed into the next one, etc. Let us denote by $\Gamma_{(k-1,k)}$ the interface between components Ω_{a-1} and Ω_a . Then the following conditions are true for $a=2, \dots, n$ and $x \in \Gamma_{(a-1,a)}$:

$$[\chi_i^{kl}] = 0 \tag{2.154}$$

and

$$\sigma_{ij}(\chi_{(pq)}) n_j = [C_{pqij}]_{\Gamma_{(a-1,a)}} n_j = F_{(pq)i} |_{\Gamma_{(a-1,a)}} \tag{2.155}$$

$$[C_{pqij}]_{\Gamma_{(a-1,a)}} = C_{pqij}^{(a)} - C_{pqij}^{(a-1)}; \quad \mathbf{x} \in \Gamma_{(a-1,a)} \tag{2.156}$$

Summing up all the considerations on the homogenisation problem (2.126), we compute the effective elasticity tensor components given by (2.136) using the homogenisation functions $\chi_{(kl)i}$ being a solution of a classical well-posed boundary value problem with periodicity conditions on the external boundaries of Ω . The stress boundary conditions are equal to the difference of constitutive tensor components at the particular composite interface. The variational formulation necessary for a finite element formulation of the local problem can be introduced as follows:

$$\sum_{a=1}^n \int_{\Omega_a} C_{ijkl} \varepsilon_{kl}(\chi_{(pq)}) \varepsilon_{ij}(\mathbf{v}) d\Omega = - \sum_{a=2}^n \int_{\Gamma_{(a-1,a)}} \sigma_{ij}(\chi_{(pq)}) n_j v_i d\Gamma + \int_{\Omega} f_i v_i d\Omega \tag{2.157}$$

which by neglecting body forces leads to

$$\sum_{a=1}^n \int_{\Omega_a} C_{ijkl} \varepsilon_{kl}(\chi_{(pq)}) \varepsilon_{ij}(\mathbf{v}) d\Omega = - \sum_{a=2}^n \int_{\Gamma_{(a-1,a)}} F_{(pq)i} v_i d\Gamma \tag{2.158}$$

Having determined the homogenisation functions for the n -component composite, the effective elasticity tensor components from (2.136) are calculated as the result.

The general configuration of the n -component composite denotes that there are m interfaces in the periodicity cell where $m \in N$ and $m \geq n - 1$. It can be observed that for coherent components, as was assumed at first, the case of $m=n-1$ (minimum value of m) is equivalent to the fibre-like composite characterised in the previous section or the composite where $n-1$ components are embedded into

one matrix. In that case the variational formulation of the homogenisation problem has the following form:

$$\sum_{a=1}^n \int_{\Omega_a} C_{ijkl} \varepsilon_{kl}(\chi_{(pq)}) \varepsilon_{ij}(\mathbf{v}) d\Omega = - \sum_{a=2}^{n-1} \int_{\Gamma_{(1,a)}} F_{(pq)i} v_i d\Gamma \quad (2.159)$$

Moreover, it can be seen that the n -component composite in a general configuration generates, due to the component permutation scheme, the bounded set of $(n-1)!$ various effective elasticity tensors. If some components are disjoint, the total number of these subsets must be included in the permutation procedure. It would be interesting to calculate, due to the homogenisation method presented, the upper and lower bounds of the effective elasticity tensor components for such a set of permutations.

Next, it is observed that in the general case the effective elasticity tensor components can be calculated by the following modification of (2.159):

$$\sum_{a=1}^n \int_{\Omega_a} C_{ijkl} \varepsilon_{kl}(\chi_{(pq)}) \varepsilon_{ij}(\mathbf{v}) d\Omega = - \sum_{r=1}^m \int_{\Gamma_r} \mathbf{F}_{(pq)} \mathbf{v} d\Gamma \quad (2.160)$$

where the RHS summation is carried out along all interfaces detected in the composite periodicity cell. Further, if any interface shows some finite number of nonsmoothness, the integration over such contour to be replaced with the sum of integrals defined on partially smooth curves composing the interface.

Finally, it is observed that the effective modules method of homogenisation formulated by (2.158) – (2.159) enables one to calculate effective properties for the composites including microdefects or interface defects; it can be done by equating the appropriate material characteristics to 0 for these regions. For this purpose, the computational procedure applied in numerical experiments can be linked with the program for digital processing of composite cross-section images.

Now let us consider the Finite Element Method discretisation of the homogenisation problem. Let us introduce the following approximation of homogenisation functions $\chi_{(rs)i}$ ($i, r, s=1,2$) at any point of the considered continuum Ω in terms of a finite number of generalised coordinates $q_{(rs)\alpha}$ and the shape functions $\varphi_{i\alpha}$

$$\chi_{(rs)i} = \varphi_{i\alpha} q_{(rs)\alpha}, \quad i, r, s = 1, 2, \quad \alpha = 1, \dots, N \quad (2.161)$$

In the same way the strain $\varepsilon_{ij}(\chi_{(rs)})$ and stress $\sigma_{ij}(\chi_{(rs)})$ tensors are rewritten as

$$\varepsilon_{ij}(\chi_{(rs)}) = B_{ij\alpha} q_{(rs)\alpha} \quad (2.162)$$

$$\sigma_{ij(rs)} = \sigma_{ij}(\chi_{(rs)}) = C_{ijkl} \varepsilon_{kl}(\chi_{(rs)}) = C_{ijkl} B_{kl\alpha} q_{(rs)\alpha} \quad (2.163)$$

where $B_{kl\alpha}$ represents the shape functions derivatives. Introducing (2.162) – (2.163) into the virtual work equation in its variational form it is found that

$$\int_{\Omega} \delta \chi_{(rs)i,j} C_{ijkl} \chi_{(rs)k,l} d\Omega = \sum_{p=2}^m \int_{\Gamma_p} \delta \chi_{(rs)i} [F_{(rs)i}]_{\Gamma_p} d\Gamma \quad (\text{no sum on } r,s) \quad (2.164)$$

Furthermore, let us define the composite global stiffness matrix as

$$K_{\alpha\beta} = \sum_{e=1}^E K_{\alpha\beta}^{(e)} = \sum_{e=1}^E \int_{\Omega_e} C_{ijkl} B_{ij\alpha} B_{kl\beta} d\Omega \quad (2.165)$$

Using this notation in (2.164) and minimising the variational statement with respect to the generalised coordinates we arrive at

$$K_{\alpha\beta} q_{(rs)\alpha} = Q_{(rs)\alpha} \quad (2.166)$$

with $Q_{(rs)\alpha}$ being the external load vector containing the boundary forces given by (2.155) – (2.156), which is employed to determine the homogenisation function $\chi_{(rs)i}$ in three numerical tests for $r,s=1,2$. To ensure the symmetry conditions on a periodicity cell, the orthogonal displacements and rotations for every nodal point belonging to the external boundaries of Ω are fixed. For the functions $\chi_{(rs)i}$ so defined we compute the stresses $\sigma_{ij}(\chi_{(rs)})$ and average this tensor numerically over the region Ω according to the formula (2.136).

The fibre–reinforced glass–epoxy composite example with an interphase between the fibre and the matrix is analysed in computational experiments [163]. The microgeometry of the periodicity cell is shown in Figure 2.66, while material characteristics of the constituents are collected in Table 2.11.

The weaker interphase in our tests may simulate any boundary defects appearing in fibre–reinforced composites that are caused by the difference in thermal stresses during the fabrication process in metal matrix composites (MMC) for instance. On the other hand, a stronger interphase model homogenised numerically is equivalent to the case when some layer between the fibre and matrix is introduced to enforce component interface bonding strength.

Generally, 11 groups of computational experiments are performed to compute the effective elastic and thermal characteristics for the composite considered. Material properties are increased in the interphase starting from 50% of additional matrix characteristics with increments equal to 10% for each of the next test group. Thus for the 6th group the interphase equivalent to the matrix is obtained and for the 11th the material properties of the interphase are equal to 150% of the matrix parameters; the results of this analysis are presented in Table 2.12.

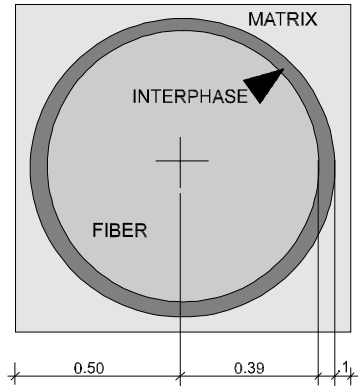


Figure 2.66. Microgeometry of the periodicity cell

Table 2.11. Material data for composite components

Material	\mathbf{e}	\mathbf{v}
Glass fibres	72.38	0.200
Epoxy matrix	2.75	0.350

Table 2.12. Effective elastic and thermal parameters

Test no	$C_{1111}^{(eff)}$	$C_{1122}^{(eff)}$	$C_{1212}^{(eff)}$
1	8.566	3.122	14.577
2	8.815	3.209	14.580
3	9.020	3.278	14.582
4	9.197	3.337	14.584
5	9.338	3.391	14.586
6	9.474	3.445	14.588
7	9.610	3.503	14.589
8	9.761	3.572	14.591
9	9.949	3.681	14.593
10	10.619	4.218	14.594
11	11.399	4.940	14.596

Analysing these results it can be concluded that all effective parameters show some sensitivity to the improved interphase and its material parameters. The greatest sensitivity is obtained for $C_{1122}^{(eff)}$ and $C_{1111}^{(eff)}$ components, while the smallest for $C_{1212}^{(eff)}$. To obtain more realistic results it will be valuable to introduce anisotropy in the equivalent parameters of the interphase; in that case the sensitivity of the $C_{1212}^{(eff)}$ component increases significantly. However, neglecting these disproportions the results computed lead us to the conclusion that the improved homogenisation method confirms the crucial role of the interphase on the overall characteristics of the composite structure, which is observed in engineering practice. Moreover, the variability resulting from computational experiments confirms generally the usefulness of the homogenisation method proposed. Other

series of computational tests are done to the visualisation of the homogenisation functions as well as the resulting stresses and various numerical error estimators.

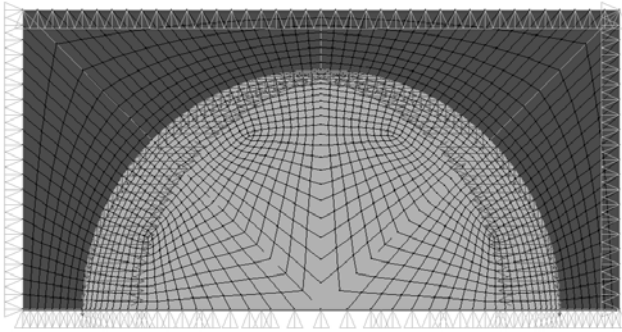


Figure 2.67. Boundary conditions for homogenisation problems χ^{11}

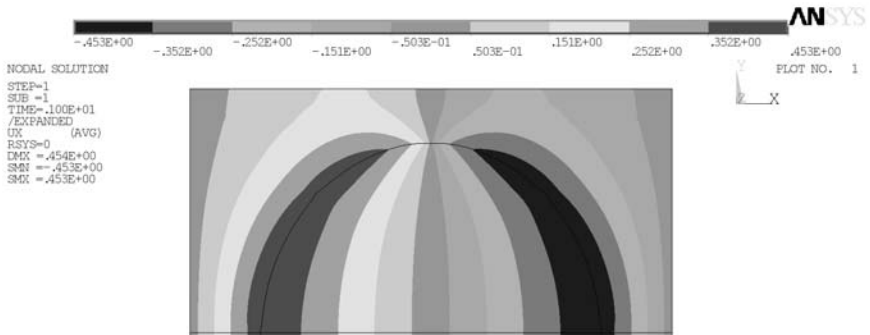


Figure 2.68. Horizontal components of the homogenisation function χ^{11}

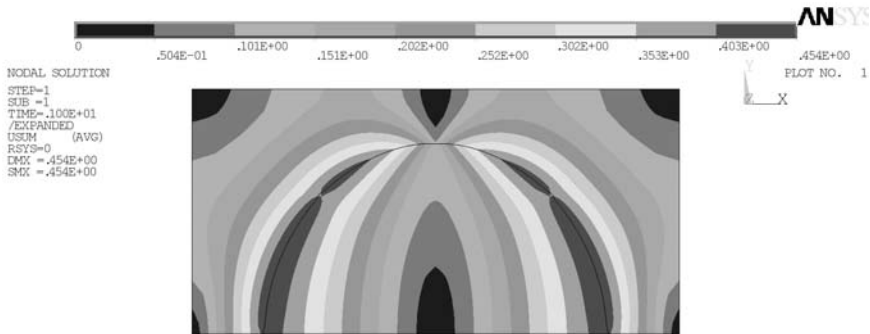


Figure 2.69. Vertical components of the homogenisation function χ^{11}



Figure 2.70. Horizontal stresses in the homogenisation problem χ^{11}

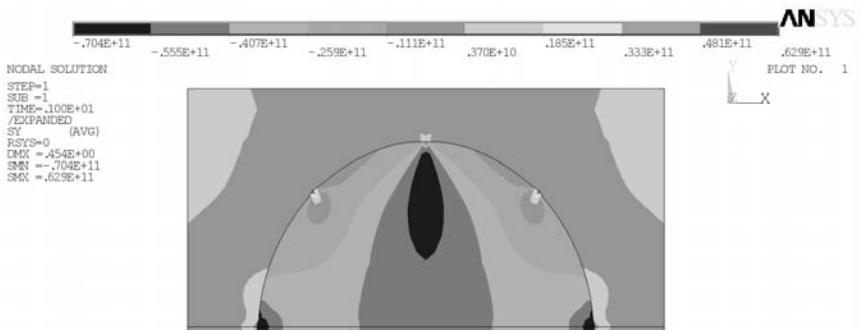


Figure 2.71. Vertical stresses in the homogenisation problem χ^{11}

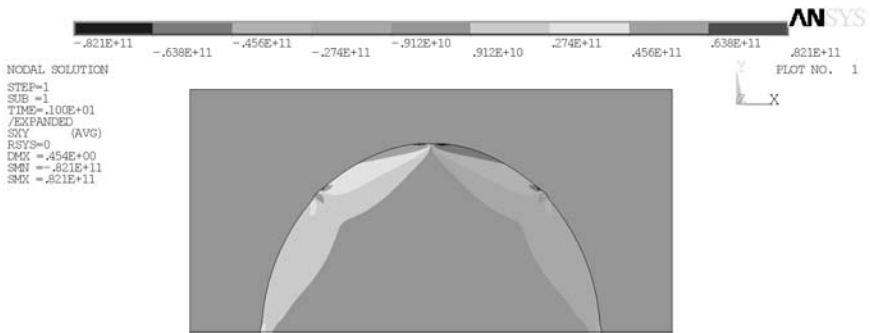


Figure 2.72. Shear stresses in the homogenisation problem χ^{11}

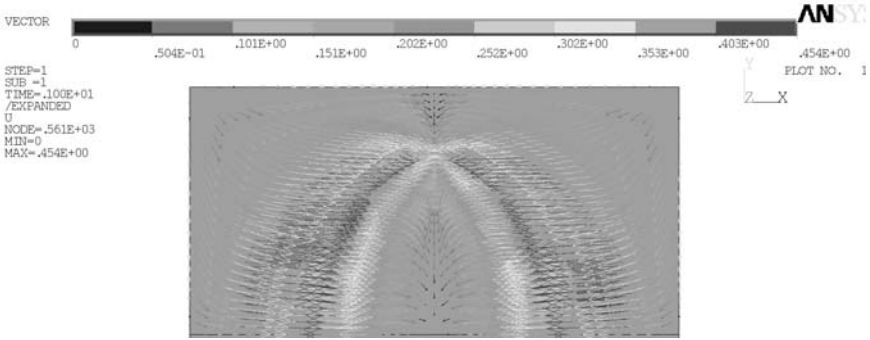


Figure 2.73. Vortex visualization of the homogenisation function χ^{II}

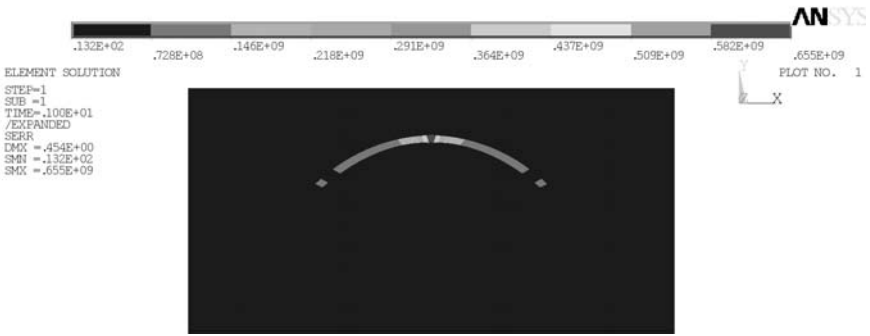


Figure 2.74. Relative error of the stresses determination in the problem χ^{II}

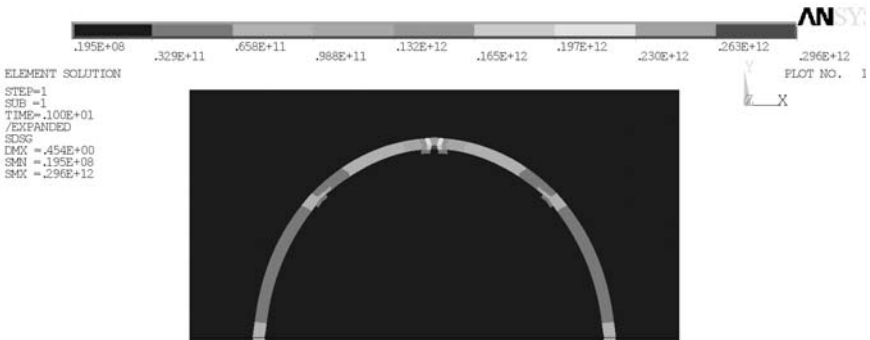


Figure 2.75. Relative error for strain determination in the homogenisation problem χ^{II}

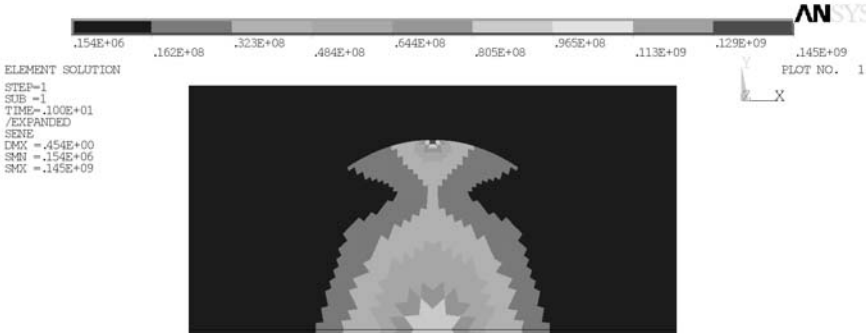


Figure 2.76. Relative error of the strain energy determination χ^{11}

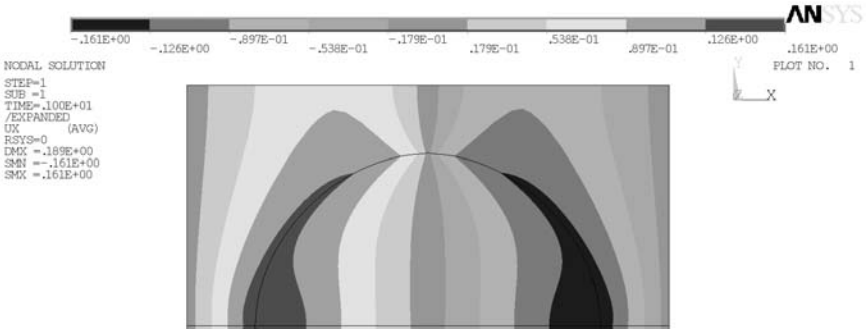


Figure 2.77. Horizontal components of the homogenisation function χ^{12}

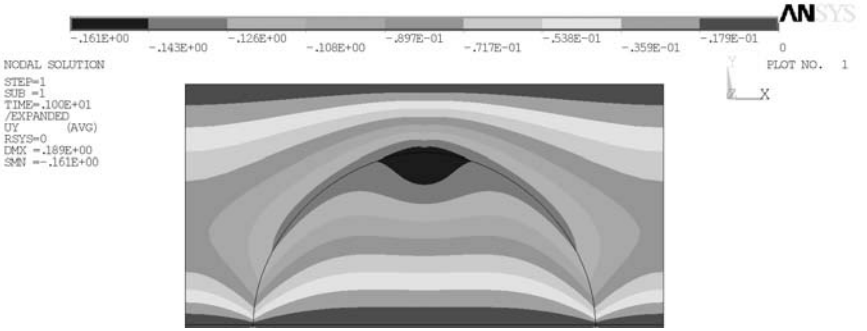


Figure 2.78. Vertical components of the homogenisation function χ^{12}

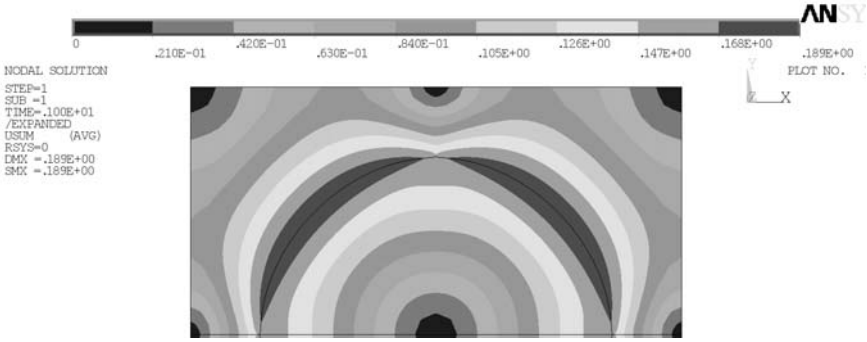


Figure 2.79. Total values of the homogenisation function χ^{12}



Figure 2.80. Horizontal stresses in the homogenisation problem χ^{12}

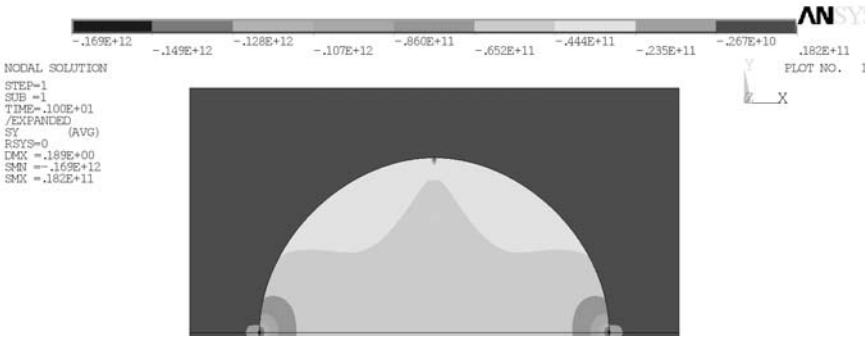


Figure 2.81. Vertical stresses in the homogenisation problem χ^{12}



Figure 2.82. Shear stresses in the homogenisation problem χ^{12}



Figure 2.83. Equivalent von Mises stresses in the homogenisation problem χ^{12}

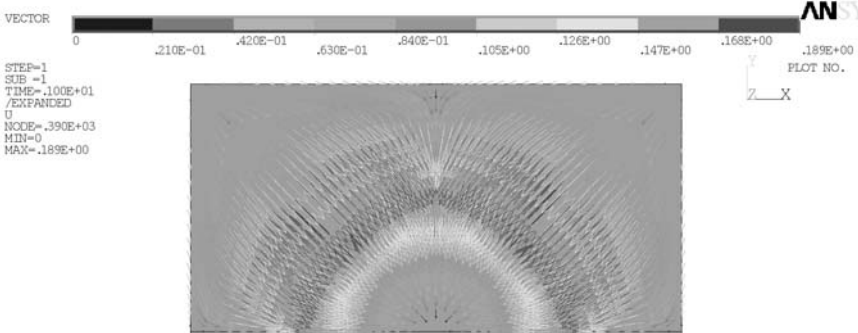


Figure 2.84. Vortex visualization of the homogenisation function χ^{12}



Figure 2.85. Relative error of the stresses determination in the problem χ^{12}

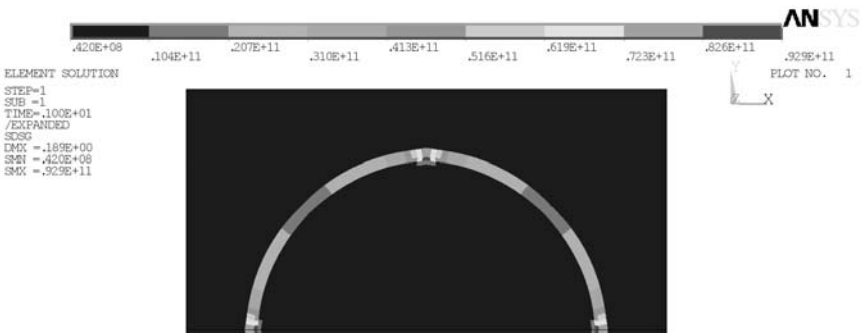


Figure 2.86. Relative error of the strain determination in the problem χ^{12}



Figure 2.87. Relative error of the strain energy determination χ^{12}

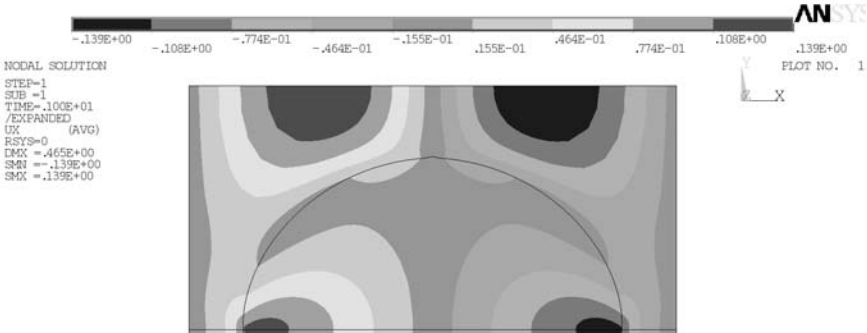


Figure 2.88. Horizontal components of the homogenisation function χ^{22}

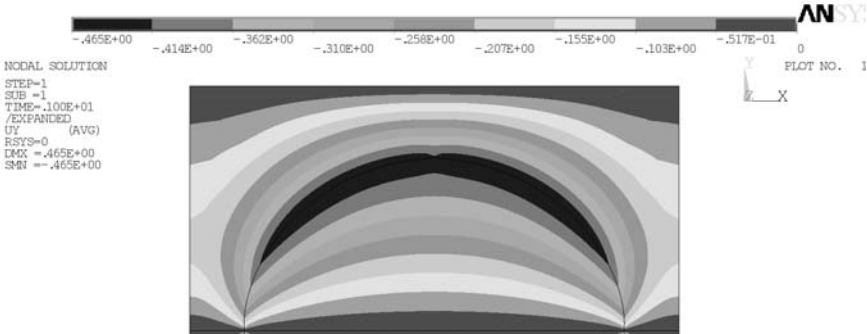


Figure 2.89. Vertical components of the homogenisation function χ^{22}

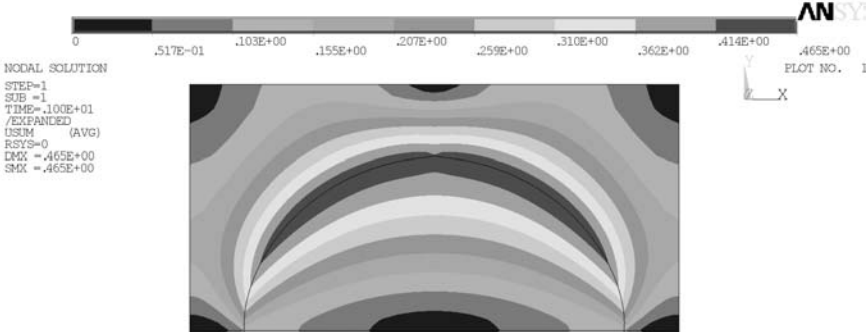


Figure 2.90. Total values of the homogenisation function χ^{22}

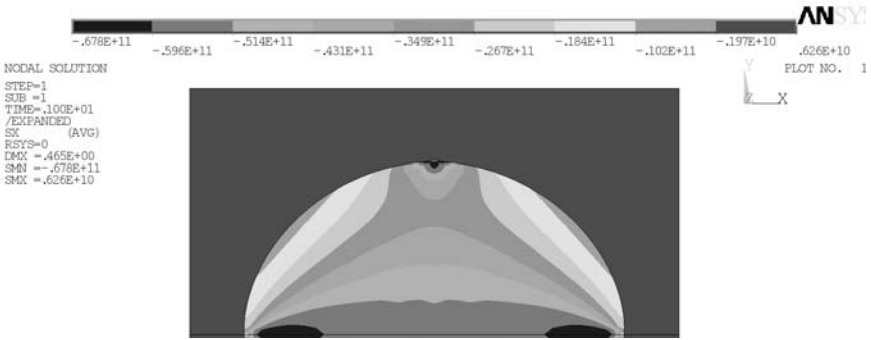


Figure 2.91. Horizontal stresses in the homogenisation problem χ^{22}

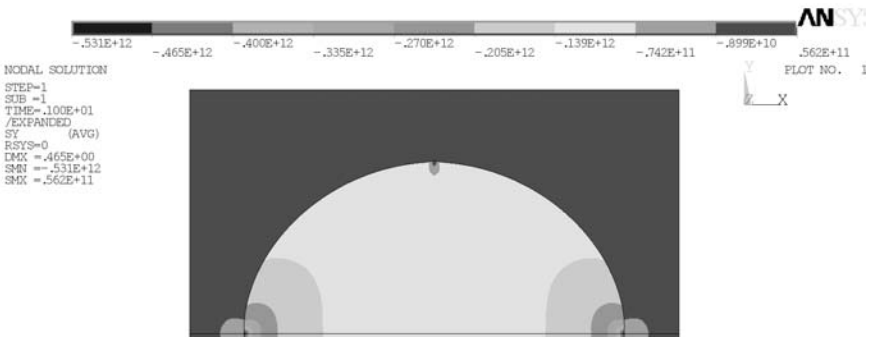


Figure 2.92. Vertical stresses in the homogenisation problem χ^{22}

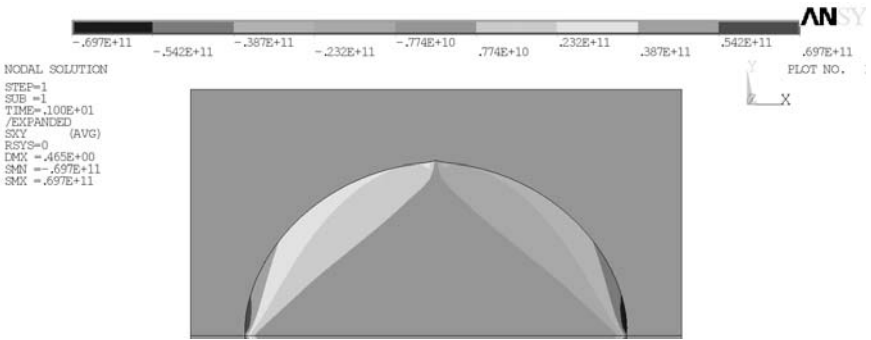


Figure 2.93. Shear stresses in the homogenisation problem χ^{22}

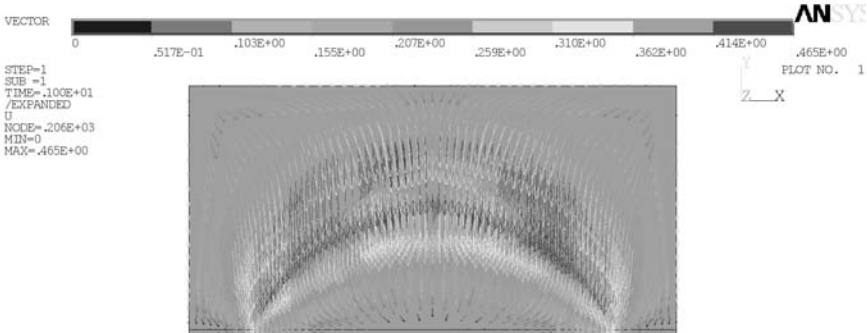


Figure 2.94. Vortex visualization of the homogenisation function χ^{22}



Figure 2.95. Relative error of the stresses determination in the problem χ^{22}



Figure 2.96. Relative error of the strain determination in the problem χ^{22}



Figure 2.97. Relative error of the strain energy determination χ ²²

The results of the computational analysis carried out in this section show that the effective properties of the composite and, at the same time, the overall behaviour of the composite, in the context of the homogenisation method, are sensitive to the interphase between the constituents and its material parameters. It should be underlined that the interphase, improved in the example presented above, has small total area in the comparison to the fibre and matrix. It can be expected that the previous, simplified approach (upper and lower bounds or direct approximations of effective properties cited above) do not enable us to arrive at such effects.

Considering the assumption that the scale factor between the RVE and the whole composite structure tends to 0 in our analysis and, on the other hand, that this quantity in real composites is small but differs from 0, the sensitivity of the effective characteristics to this parameter are to be calculated in the next analyses based on this approach. To carry out such studies, the scale parameter has to be introduced in the equations describing effective properties and next, due to the well-known sensitivity analysis methods, the influence of the scale parameter ϵ relating composite micro- and macrostructure may be shown. In the analogous way we can study the sensitivity of the effective characteristics of the composite to the component material parameters but there is no need in this case to introduce any extra components into the equations cited above.

Further mathematical and computational extensions of the model presented should be provided to include in the constitutive tensor the components responsible for the thermal expansion [228,311]. Having computed the effective characteristics on the basis of Young moduli, Poisson ratios, coefficient of thermal expansion and heat conduction coefficient [106,163,347] it will be possible to provide the coupled temperature–displacement FE analyses of periodic composite materials. At the same time it will be valuable to work out the problem presented in the context of viscoelastic or elastoviscoplastic material models of the composite constituents [74,368]. It will enable us to approximate computationally the fracture and failure phenomena in composites resulting from the interface defects or partial debonding using the homogenisation approach.

2.3.3.2.2 Monte Carlo Simulation Analysis

Starting from the formula describing the effective elasticity tensor components, their expected values are derived using the basic theorems on the random variables as follows [191]:

$$E[C_{ijkl}^{(eff)}(x; \omega)] = E\left[\left\langle \sigma_{kl}(\chi^{ij}(x; \omega)) \right\rangle_{\Omega}\right] + E\left[\left\langle C_{ijkl}(x; \omega) \right\rangle_{\Omega}\right] \quad (2.167)$$

The expressions for the variances (and generally covariances) have a more complicated form than the expectations because the averaged stresses and elasticity tensor are correlated variables. Therefore

$$\begin{aligned} Var(C_{ijkl}^{(eff)}(x; \omega)) &= Var\left(\left\langle \sigma_{kl}(\chi^{ij}(x; \omega)) \right\rangle_{\Omega}\right) \\ &+ 2Cov\left(\left\langle \sigma_{kl}(\chi^{ij}(x; \omega)) \right\rangle_{\Omega}, \left\langle C_{ijkl}(x; \omega) \right\rangle_{\Omega}\right) + Var\left(\left\langle C_{ijkl}(x; \omega) \right\rangle_{\Omega}\right) \end{aligned} \quad (2.168)$$

The random homogenisation fields $\chi^{ij}(x, \omega)$ for general composites, similar to the deterministic ones, are calculated only numerically. The following probabilistic stress boundary conditions are imposed on the boundary $\Gamma_{(a-1, a)}$ to find the homogenisation functions:

$$\begin{aligned} &E\left[F_{(pq)i}(\omega)\Big|_{\Gamma_{(a-1, a)}}\right] \\ &= E\left[\lambda(\omega)\Big|_{\Gamma_{(a-1, a)}} \delta_{pq} n_i\right] + E\left[\mu(\omega)\Big|_{\Gamma_{(a-1, a)}} (n_p \delta_{qi} + n_q \delta_{pi})\right] \end{aligned} \quad (2.169)$$

$$\begin{aligned} &Var\left(F_{(pq)i}(\omega)\Big|_{\Gamma_{(a-1, a)}}\right) \\ &= Var\left(\lambda(\omega)\Big|_{\Gamma_{(a-1, a)}} \delta_{pq} n_i\right) + Var\left(\mu(\omega)\Big|_{\Gamma_{(a-1, a)}} (n_p \delta_{qi} + n_q \delta_{pi})\right) \end{aligned} \quad (2.170)$$

where $\lambda(\omega)$ and $\mu(\omega)$ are the Lamé constants. If Young moduli of composite components are considered as input random variables then the expected values and variances of boundary forces are obtained by separating the RHS into those components corresponding to Ω_{a-1} and Ω_a , respectively. After some algebraic transformations there holds

$$E[F_{(pq)i}(x; \omega)] = B_{pqi}(v_a) \cdot E[e_a] - B_{pqi}(v_{a-1}) \cdot E[e_{a-1}] \quad (2.171)$$

where the operator $B_{pqi}(v(\mathbf{x}))$ similar to the tensor A_{ijkl} introduced by eqn (2.14) is defined as

$$B_{pqi}(v(\mathbf{x})) = \delta_{pq} n_i \frac{v(\mathbf{x})}{(1+v(\mathbf{x}))(1-2v(\mathbf{x}))} + (n_p \delta_{qi} + n_q \delta_{pi}) \frac{1}{2(1+v(\mathbf{x}))} \quad (2.172)$$

and their variances are equal to

$$Var(F_{(pq)i}(\mathbf{x}; \omega)) = \{B_{pqi}(v_a)\}^2 \cdot Var(e_a) + \{B_{pqi}(v_{a-1})\}^2 \cdot Var(e_{a-1}) \quad (2.173)$$

(no sum on p, q, i)

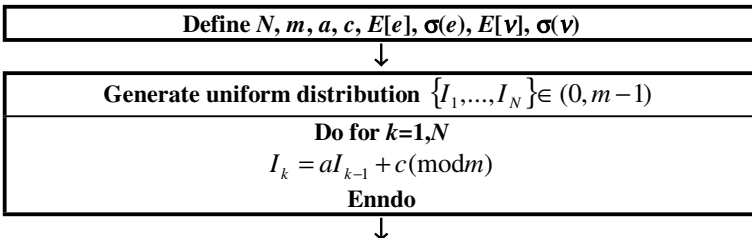
Finally, probabilistic moments of the effective characteristics are derived using statistical estimation methods, according to which the expected values and the relevant covariances (computed using the unbiased estimator) of the effective elasticity tensor components are obtained as

$$E[C_{ijpq}^{(eff)j}] = \frac{1}{M} \sum_{j=1}^M C_{ijpq}^{(eff)j} \quad (2.174)$$

$$Cov(C_{ijpq}^{(eff)j}(\omega), C_{rsuv}^{(eff)j}(\omega)) = \frac{1}{M} \sum_{j=1}^M (C_{ijpq}^{(eff)j} - E[C_{ijpq}^{(eff)j}])(C_{rsuv}^{(eff)j} - E[C_{rsuv}^{(eff)j}]) \quad (2.175)$$

where $C_{ijpq}^{(eff)j}(\omega)$, $j = 1, \dots, M$ are random series of the tensor components obtained as a result of the generation of numerical random values.

The homogenisation problem presented is implemented into the program MCCEFF, which is based on the Monte Carlo simulation technique. The implementation of the MCS has been selected from among many other probabilistic methods, because this method consists of computer generation of random variables in the mechanical problem (cf. Figure 2.98) and computing the sequence of deterministic solutions associated with each variable generated; similar engineering software is also available [47]. Considering the fact that a composite structure has a relatively small number of degrees of freedom, a crude random sampling method is used in the computations (contrary to the Random Importance or Stratified Sampling methods) [73,125,139].



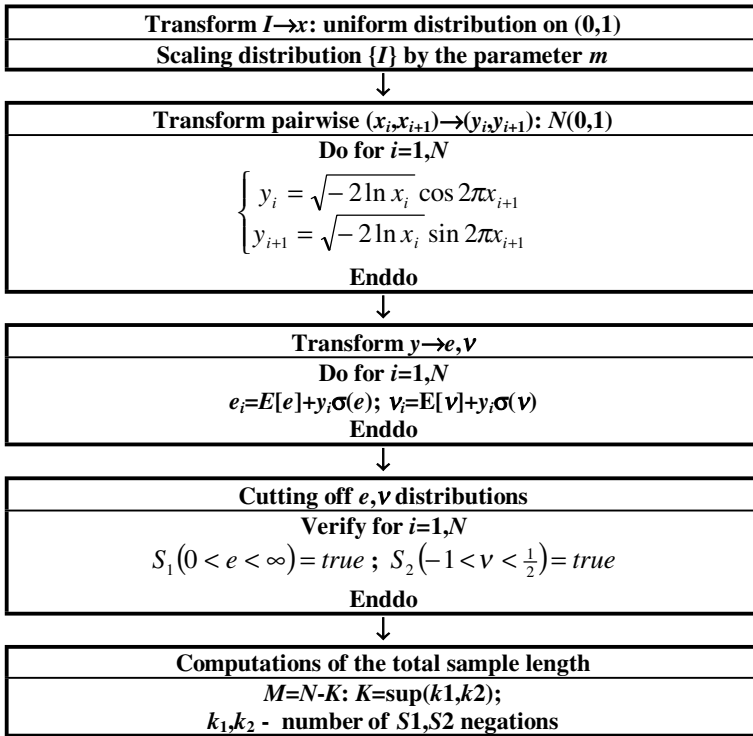
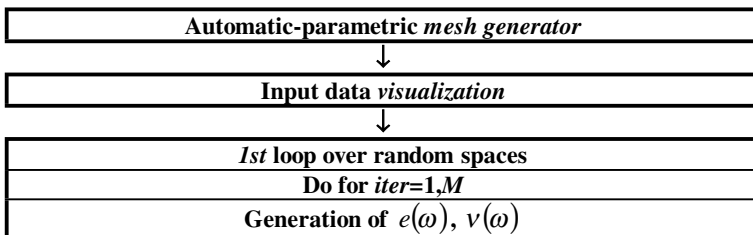


Figure 2.98. Algorithm for random numbers generation

However, the most important reason for the MCS application is that the accuracy of the output variable probabilistic moments estimation does not depend on the input variable coefficient of variation (as for the SFEM), but on the total number of iterations performed. Taking into account the estimator convergence studies and some theoretical considerations, the total number of random trials M has been taken as equal to 1,000. The flowchart of the program used for probabilistic homogenisation is shown in Figure 2.99. As presented, the program makes it possible to discretise automatically the RVE on the basis of the main cell geometrical parameters, visualisation of the mesh introduced, random generation of the input random variables and iterative computations of the homogenisation functions as well as statistical estimators of either upper and lower bounds or direct effective characteristics of the elasticity tensor components.



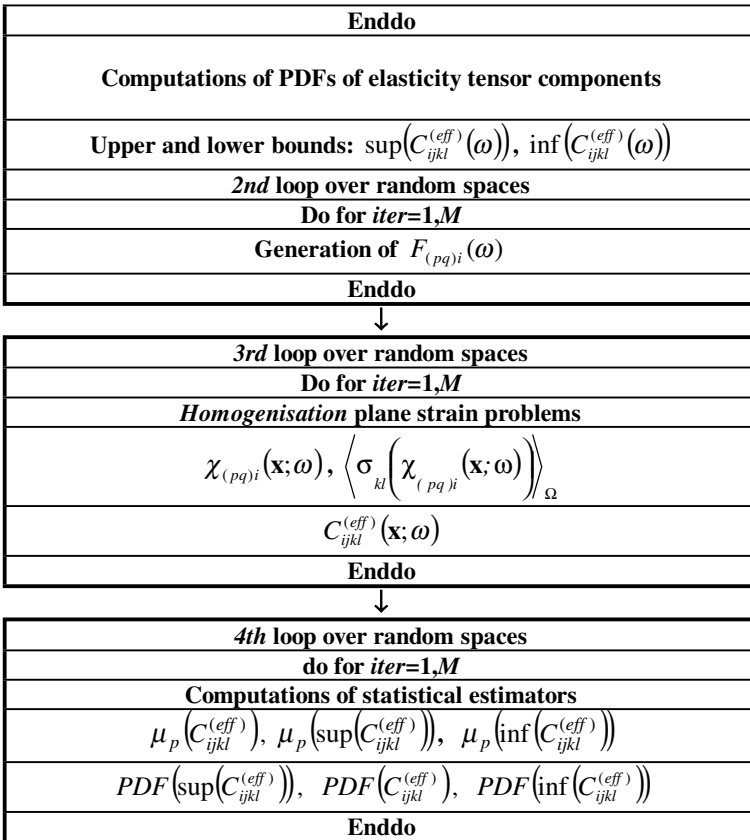


Figure 2.99. Algorithm for the MCS simulation of homogenisation procedure

Numerical analysis of probabilistic homogenisation of the fibre composite with stochastic interface defects has been performed using the MCCEFF system described above. Internal automatic generator for the square RVE with a centrally located round fibre occupying about 50% of the RVE with interface defects has been used (the influence of fibre radius variation on the stochastic displacements and stress fields has been discussed previously). Considering greater composite sensitivity to the matrix defects (bubbles), only composites having such discontinuities have been homogenised. The elastic constants for the fibre material have been taken as follows: $E[e_1]=84$ GPa, $\nu_1=0.22$ and the coefficient of Young modulus variation $\alpha(e_1)=0.1$, and for matrix: $E[e_2]=4$ GPa, $\nu_2=0.34$. Interface defect parameters have been taken in such a way that the coefficients of variation of these parameters were equal to 0.1 in all tests: $\sigma(r)=0.1 \cdot E[r]$ and $\sigma(n)=0.1 \cdot E[n]$.

The main aim of the numerical experiments performed was a numerical verification of the presented mathematical approach to homogenisation of composites with stochastic interface defects. Considering large number of

parameters in this approach it was necessary to analyse the probabilistic sensitivity of the effective elasticity tensor components. It was done with respect to the expected values of the interface defect number and volume and the coefficient of matrix Young moduli variation as design parameters. Finally, 132 simulations have been performed (with 1000 iterations each) with the following remaining input values: $E[r]=R\{0.03,0.04,0.05\}$ and $E[n]$ has been assumed as equivalent to the percentage ratio of the boundary where the defects are located to the total interface length from 10% to 60% every 5%. The coefficient of matrix Young modulus variation for tests No 1–4 has been taken as 0.100, 0.075, 0.050, 0.025, respectively.

Probabilistic moments of the effective elasticity tensor obtained as a result of the simulations are compared in Figures 2.100–2.119. The expected values of $C_{1111}^{(eff)}(\omega)$ are shown in such a way that the test results are presented in increasing order in the relevant figures. The coefficients of variation of $C_{1212}^{(eff)}(\omega)$ are neglected in the sensitivity analysis because this random variable is a function of random fluctuations of the fibre Young modulus. In all the collected figures the ratio of interface discontinuities (DB) to the entire boundary is marked on the horizontal axes, while the expected values $E[C_{ijkl}^{(eff)}(\omega)]$ or the coefficients of variation $\alpha(C_{ijkl}^{(eff)}(\omega))$ are displayed on the vertical axes, respectively.

A decrease of the expected values of $C_{ijkl}^{(eff)}(\omega)$ with an increase of the interface defects number is observed with generally small differences in comparison with the composite with perfect interface. For an increase of the parameter DB from 10% to 60%, the decrease considered is about 10% for $E[C_{1111}^{(eff)}(\omega)]$ and $E[C_{1122}^{(eff)}(\omega)]$ components, while for $E[C_{1212}^{(eff)}(\omega)]$ it is only 1%. The low sensitivity of the values for $E[C_{ijkl}^{(eff)}(\omega)]$ obtained with respect to the coefficient of the matrix Young modulus variation seems to be very important, as well. Moreover, it can be noted that for an increase of the expected values of the interface defects, the values of $E[C_{1111}^{(eff)}(\omega)]$ and $E[C_{1122}^{(eff)}(\omega)]$ increase too, and $E[C_{1212}^{(eff)}(\omega)]$ – decreases. Finally, the increasing DB implies a decrease in the differences of $E[C_{1111}^{(eff)}(\omega)]$ and $E[C_{1122}^{(eff)}(\omega)]$ obtained for different defects values, while for $E[C_{1212}^{(eff)}(\omega)]$ these differences increase with the increasing total number of the defects.

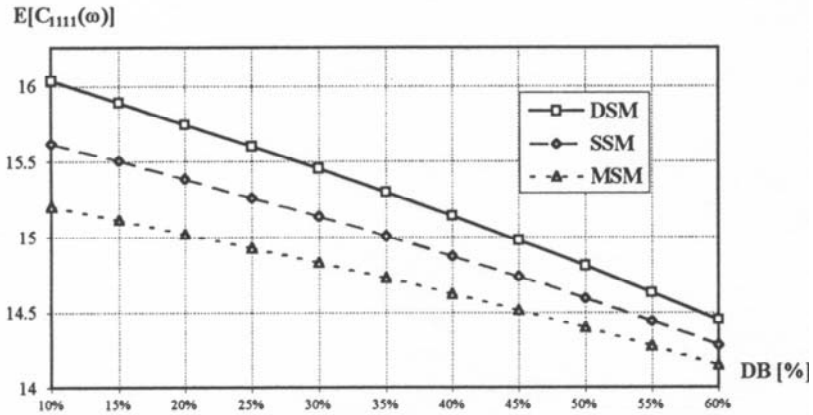


Figure 2.100. Expected values $E[C_{1111}^{(eff)}(\omega)]$ in test 1

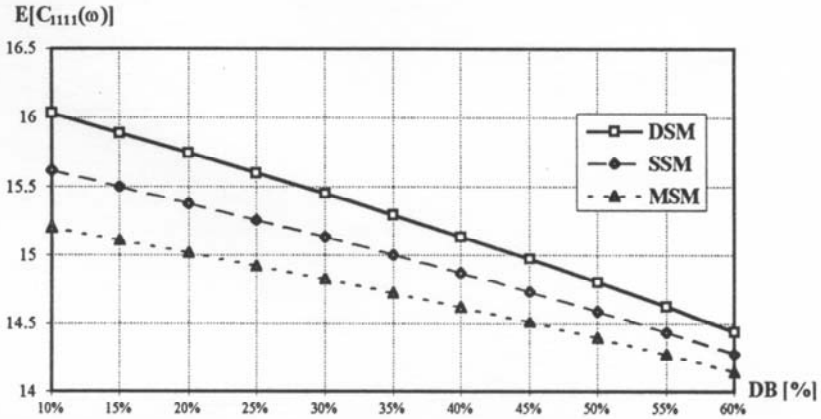


Figure 2.101. Expected values $E[C_{1111}^{(eff)}(\omega)]$ in test 2

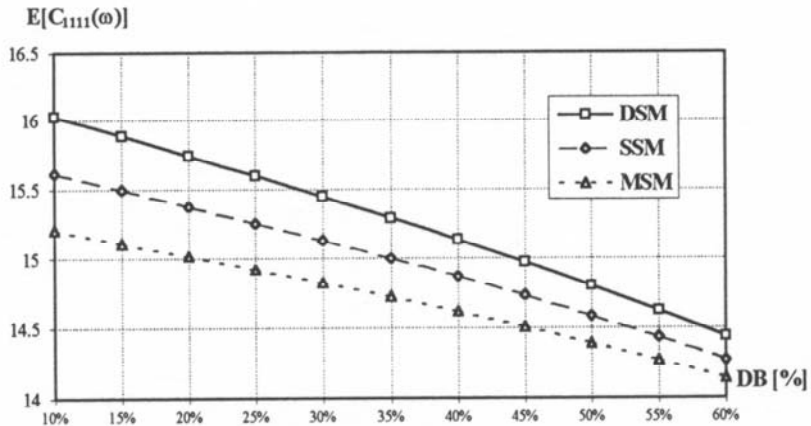


Figure 2.102. Expected values $E[C_{1111}^{(eff)}(\omega)]$ in test 3

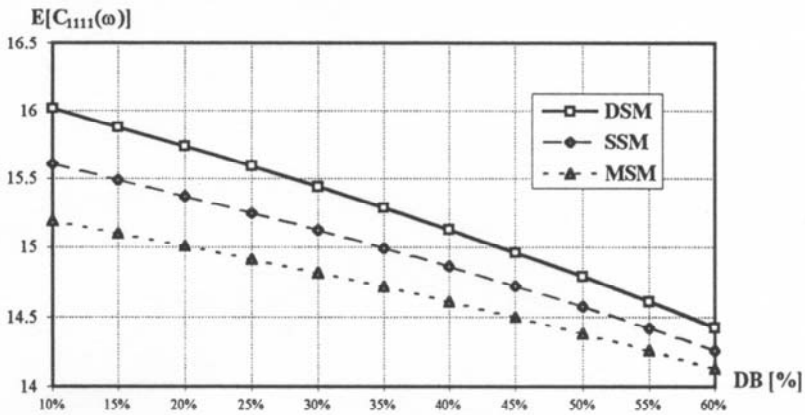


Figure 2.103. Expected values $E[C_{1111}^{(eff)}(\omega)]$ in test 4

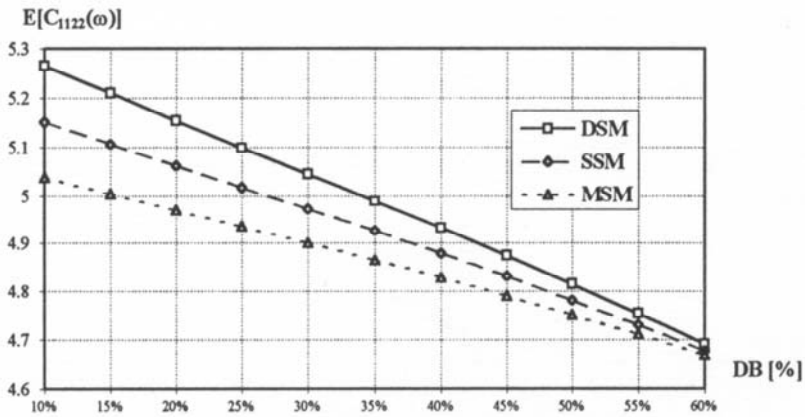


Figure 2.104. Expected values $E[C_{1122}^{(eff)}(\omega)]$ in test 1

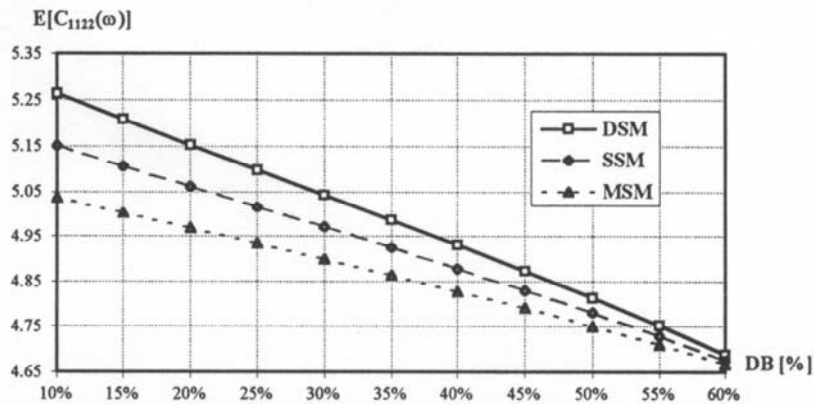


Figure 2.105. Expected values $E[C_{1122}^{(eff)}(\omega)]$ in test 2

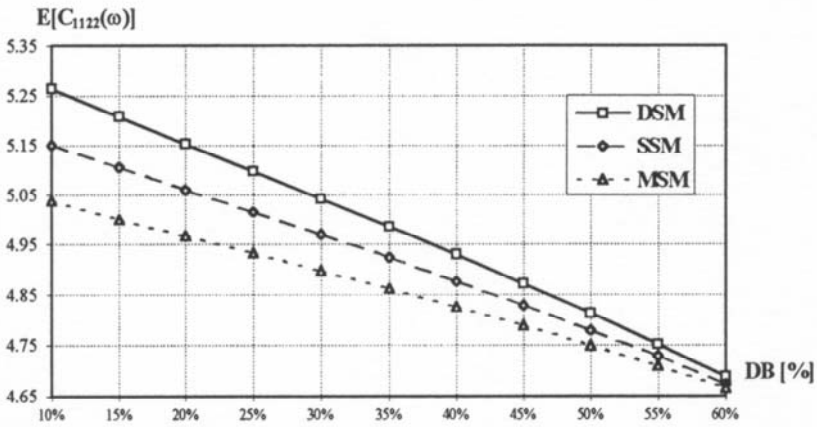


Figure 2.106. Expected values $E[C_{1122}(\omega)]$ in test 3

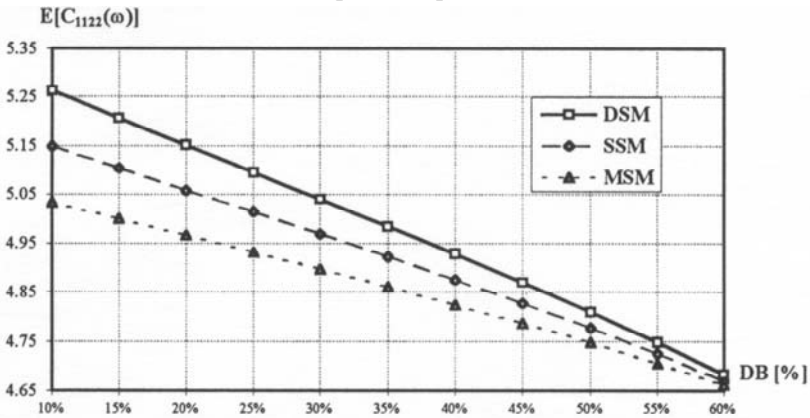


Figure 2.107. Expected values $E[C_{1122}(\omega)]$ in test 4

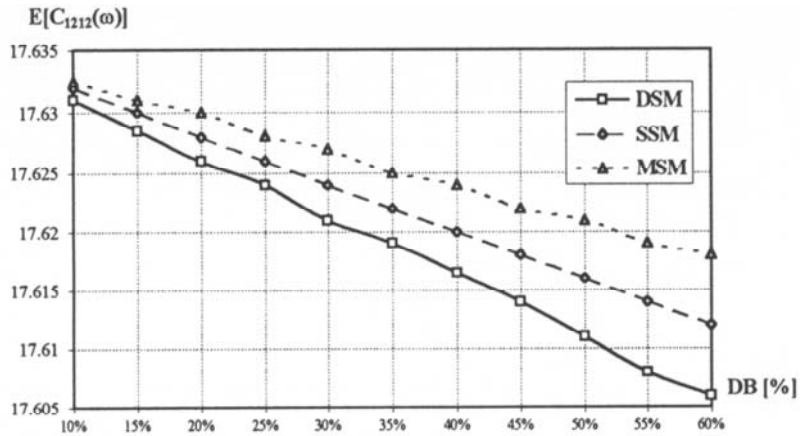


Figure 2.108. Expected values $E[C_{1212}(\omega)]$ in test 1

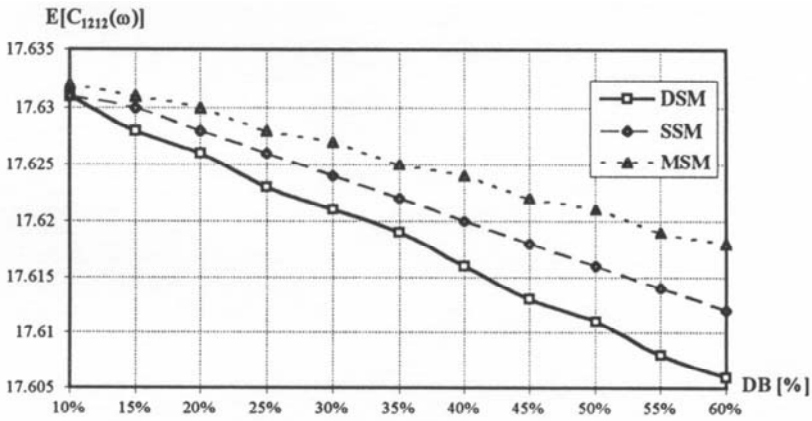


Figure 2.109. Expected values $E[C_{1212}^{(eff)}(\omega)]$ in test 2

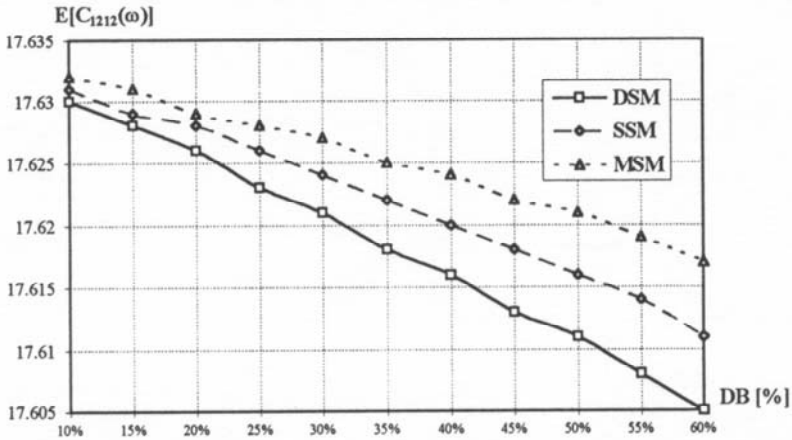


Figure 2.110. Expected values $E[C_{1212}^{(eff)}(\omega)]$ in test 3

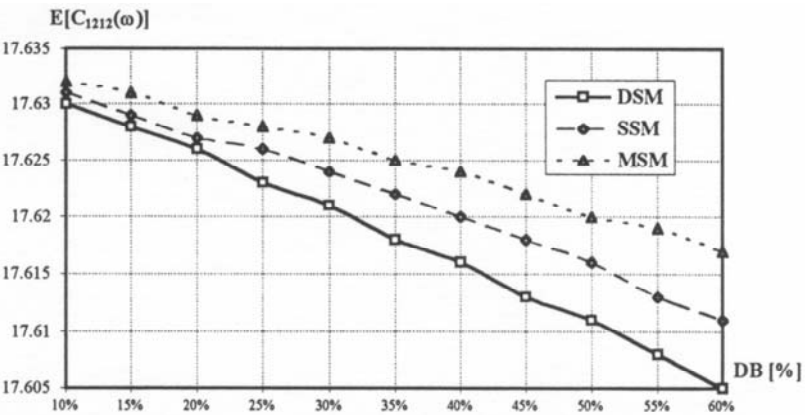


Figure 2.111. Expected values $E[C_{1212}^{(eff)}(\omega)]$ in test 4

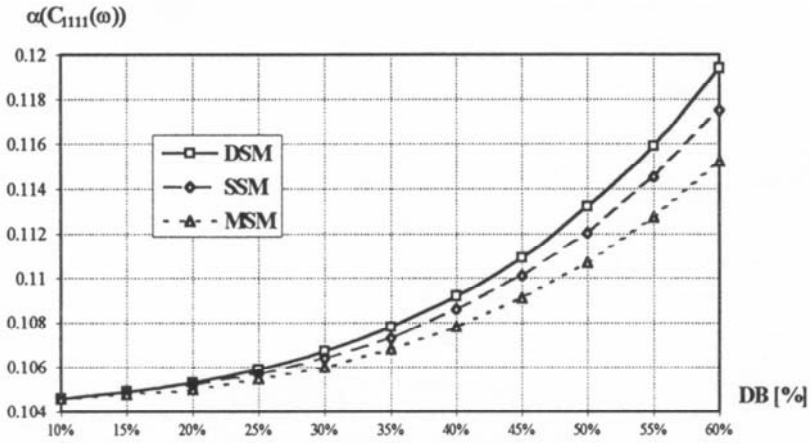


Figure 2.112. Coefficients of variation $\alpha(C_{1111}^{(eff)}(\omega))$ in test 1

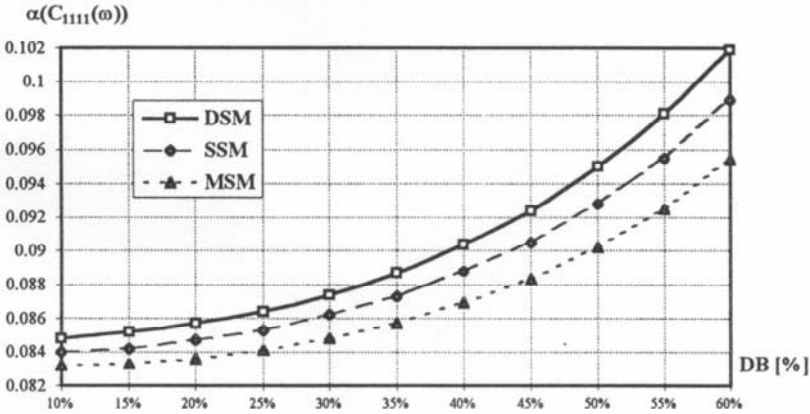


Figure 2.113. Coefficients of variation $\alpha(C_{1111}^{(eff)}(\omega))$ in test 2

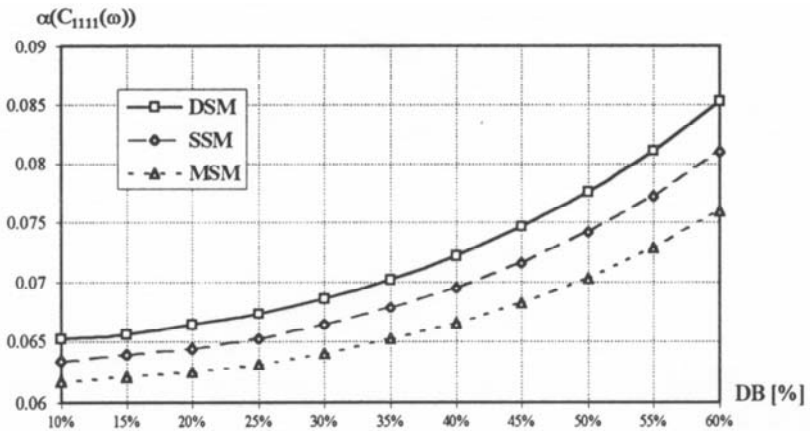


Figure 2.114. Coefficients of variation $\alpha(C_{1111}^{(eff)}(\omega))$ in test 3

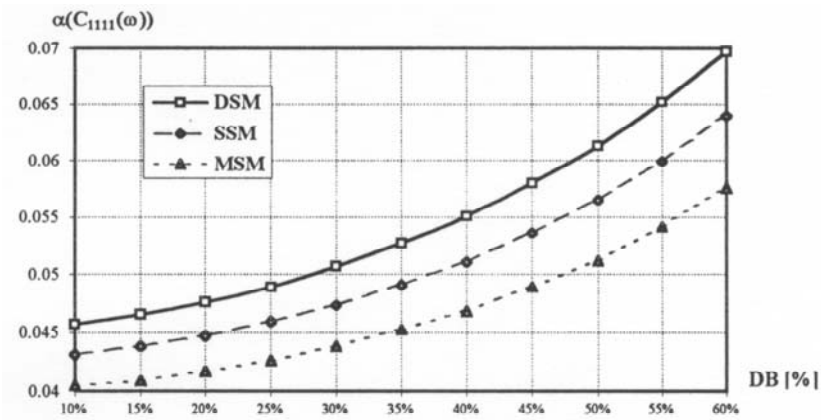


Figure 2.115. Coefficients of variation $\alpha(C_{1111}^{(eff)}(\omega))$ in test 4

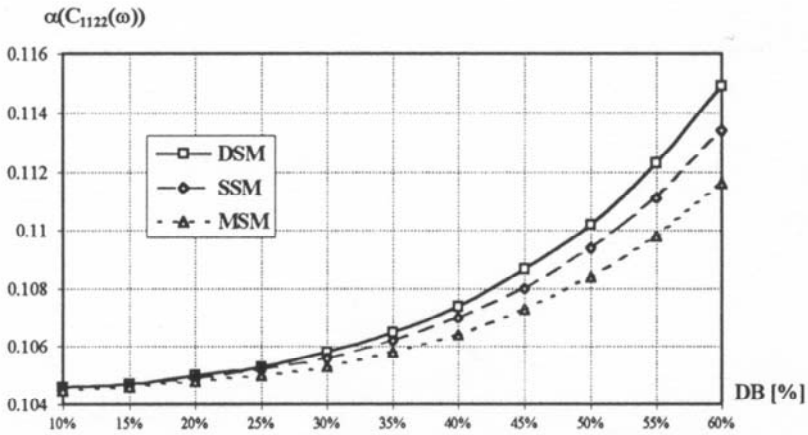


Figure 2.116. Coefficients of variation $\alpha(C_{1122}^{(eff)}(\omega))$ in test 1

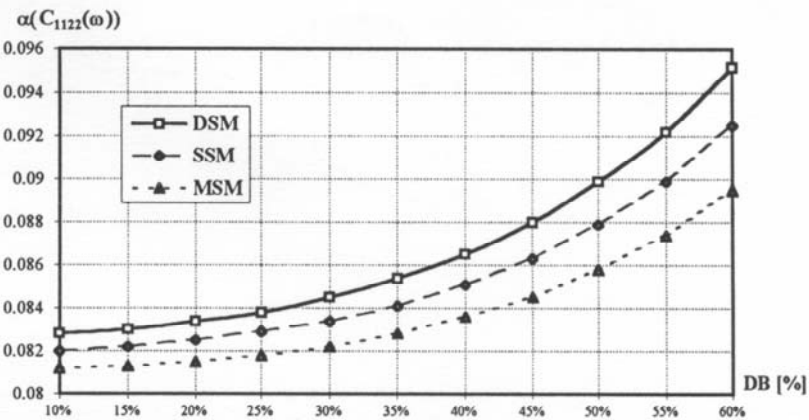


Figure 2.117. Coefficients of variation $\alpha(C_{1122}^{(eff)}(\omega))$ in test 2

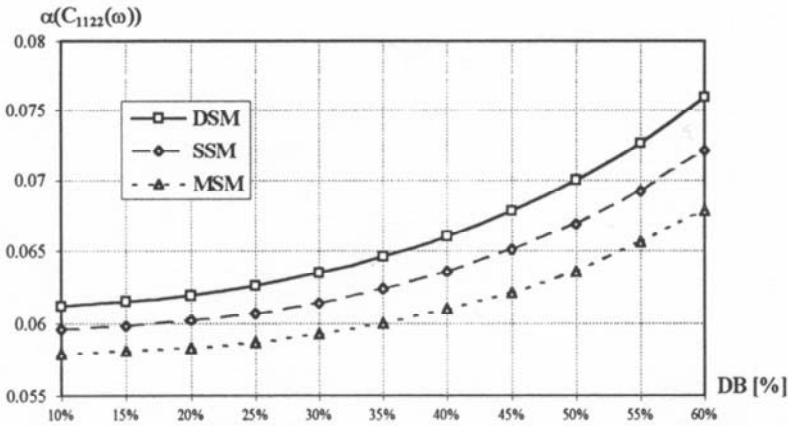


Figure 2.118. Coefficients of variation $\alpha(C_{1122}^{(eff)}(\omega))$ in test 3

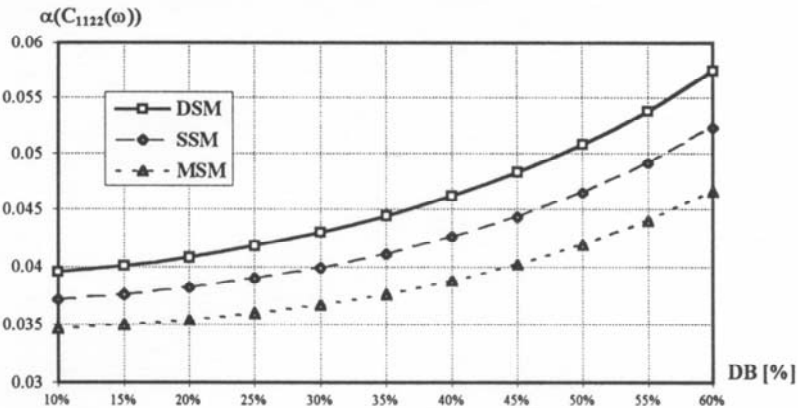


Figure 2.119. Coefficients of variation $\alpha(C_{1122}^{(eff)}(\omega))$ in test 4

Analysing the coefficients of variation $\alpha(C_{ijkl}^{(eff)}(\omega))$, a nonlinear increase of these coefficients with a DB increase can be observed in all tests. This dependence has a character similar to the behaviour of the coefficient of variation of the Young modulus obtained during the interphase probabilistic averaging. Moreover, all results are in the range of [0.00,0.12] for all the numerical tests, being negligibly greater than the maximum value of the input parameter $\alpha(e_2)$. Furthermore, the correlation of interface defect value increases and an $\alpha(C_{ijkl}^{(eff)}(\omega))$ increase is observed, and in opposition to the expected values, the coefficients of the $C_{ijkl}^{(eff)}(\omega)$ tensor variation are sensitive to $\alpha(e_2)$ changes. Together with the decreasing coefficients of the matrix Young modulus variation the following changes are observed:

- decrease of $\alpha(C_{1111}^{(eff)}(\omega))$ and $\alpha(C_{1122}^{(eff)}(\omega))$;

- increase of differences between these coefficients obtained for particular values of interface defects;
- significantly faster increase of $\alpha(C_{ijkl}^{(eff)}(\omega))$ (from 10% in test no 1 to about 30% in test no 4).

The coefficients $\alpha(C_{1212}^{(eff)}(\omega))$ (not considered in the analysis) show total non-sensitivity to analysed parameters.

Further, taking into account that all the results obtained from the Monte Carlo simulations, e.g. the first two probabilistic moments of the effective elasticity tensor, are only statistical estimators of the real values of these parameters, the numerical sensitivity of these estimators to the number of iterations should be analysed. Such an analysis is performed on the periodicity cell taking the total number of random trials as $N=5, 10, 25, 50, 100, 250, 500, 1000, 2500, 5000$ and 10000, respectively.

Only the probabilistic parameters of $C_{1111}^{(eff)}(\omega)$ are shown, because variations of the other component moments of $C_{ijkl}^{(eff)}(\omega)$ are quite similar to those presented. The total numbers of random number sampling are marked on the horizontal axes, while the analysed values of $C_{ijkl}^{(eff)}(\omega)$ are on the vertical axes. The functions describing convergence of particular estimators obtained in the numerical experiments enable us to verify the correctness of the simulations performed and come up with an optimum number of the samples for estimation of any probabilistic coefficient and/or moment for the tensor $C_{ijkl}^{(eff)}(\omega)$.

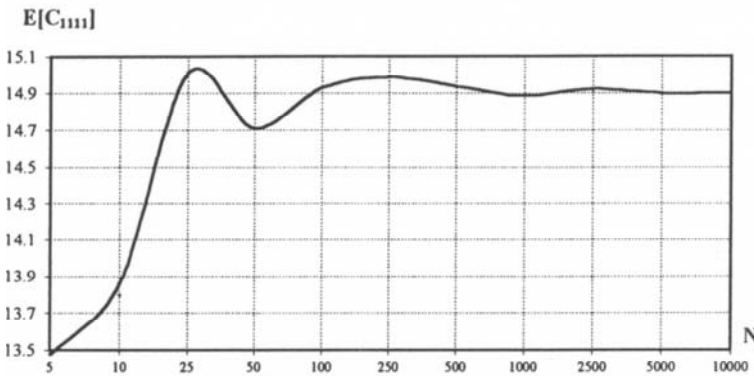


Figure 2.120. Statistical convergence of the expected value $E[C_{1111}^{(eff)}(\omega)]$

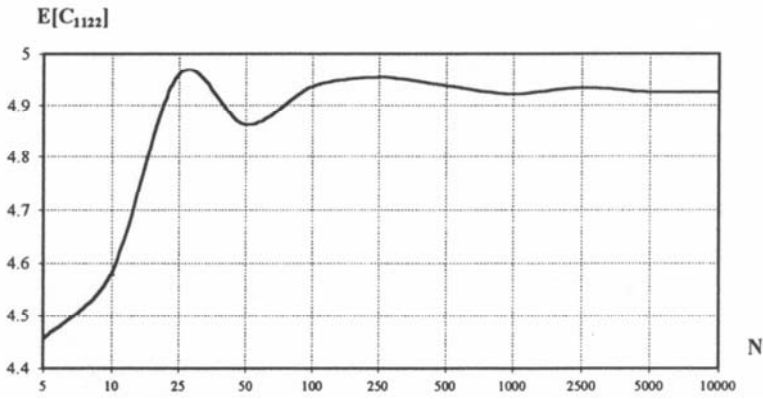


Figure 2.121. Statistical convergence of the expected value $E[C_{1122}^{(eff)}(\omega)]$

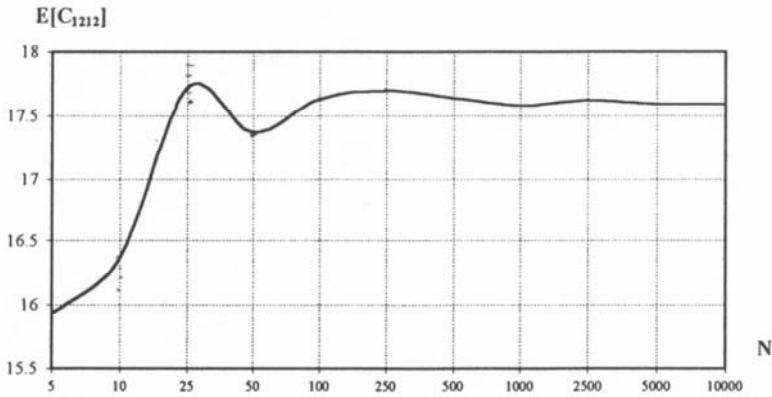


Figure 2.122. Statistical convergence of the expected value $E[C_{1212}^{(eff)}(\omega)]$

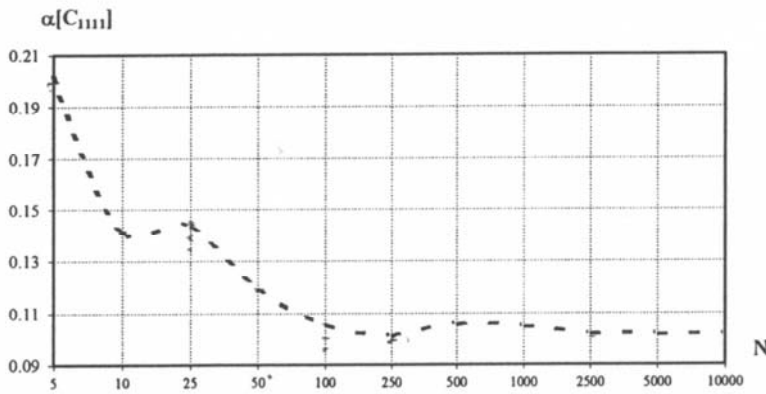


Figure 2.123. Statistical convergence of coefficient of variation $\alpha(C_{1111}^{(eff)}(\omega))$

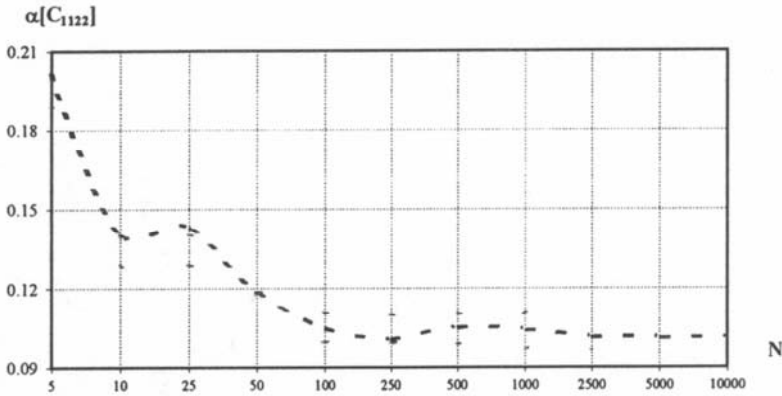


Figure 2.124. Statistical convergence of coefficient of variation $\alpha(C_{1122}^{(eff)}(\omega))$

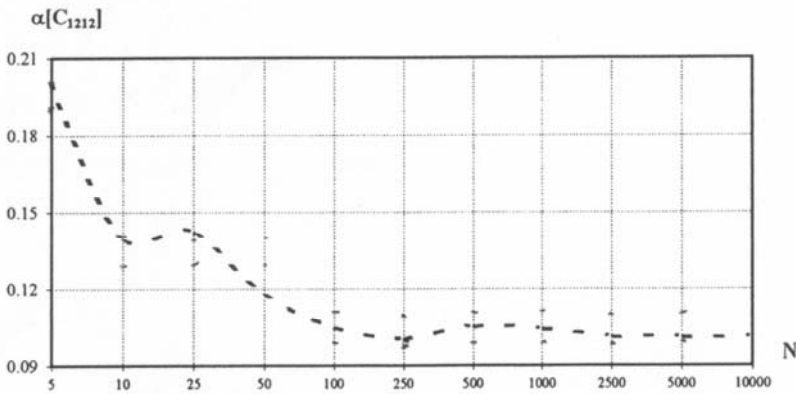


Figure 2.125. Statistical convergence of coefficient of variation $\alpha(C_{1212}^{(eff)}(\omega))$

It is seen from the analysis of the expected values of $C_{ijkl}^{(eff)}(\omega)$ that the estimator convergence character is described by a curve of similar shape in all the tests. This curve gradually increases from a minimum at $N=5$ to a maximum at about $N=30$ to oscillate with asymptotic convergence to the value approximated. It is important that in practice for $N=100$ estimator gives quite a good estimation with satisfactory accuracy. Taking for example $N=1000$, computational error resulting from statistical estimation is negligibly small in comparison with the estimated value.

Convergence of $\alpha(C_{ijkl}^{(eff)}(\omega))$ estimators has quite a different character than for $E[C_{ijkl}^{(eff)}(\omega)]$ estimators described above. From the maximum obtained for $N=5$ the curve describing the estimator as a function of the total number of iterations decreases between two inflection points for about $N=10$ and $N=30$, then for about $N=100$ it starts to converge asymptotically to the approximated quantity. Analogous to the expected values the shape of the analysed curves is quite similar

each time for different tests and different effective elasticity tensor components. Finally, a good approximation is obtained for $N=100$, while for $N=1000$ the computational error is negligibly small.

As can be seen in Figures 2.126 and 2.127, the total number of random trials necessary in the simulation for precise enough determination of the PDF for $C_{1111}^{(eff)}(\omega)$ is even greater than, for example 5,000–10,000.

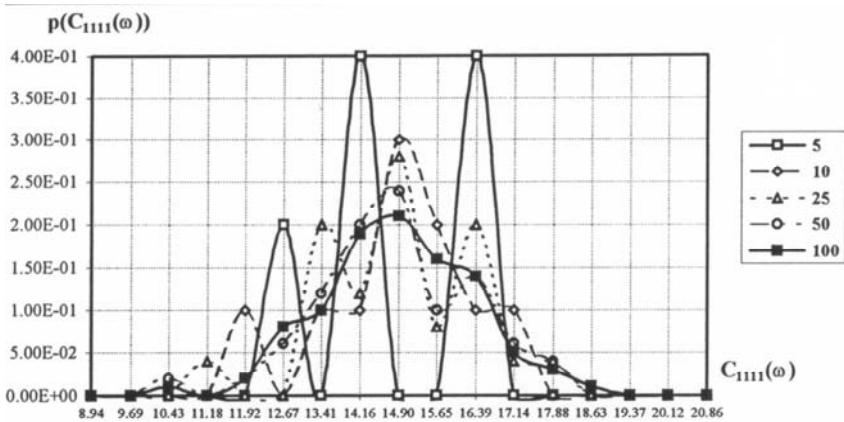


Figure 2.126. Statistical convergence of PDF of $C_{1111}^{(eff)}(\omega)$

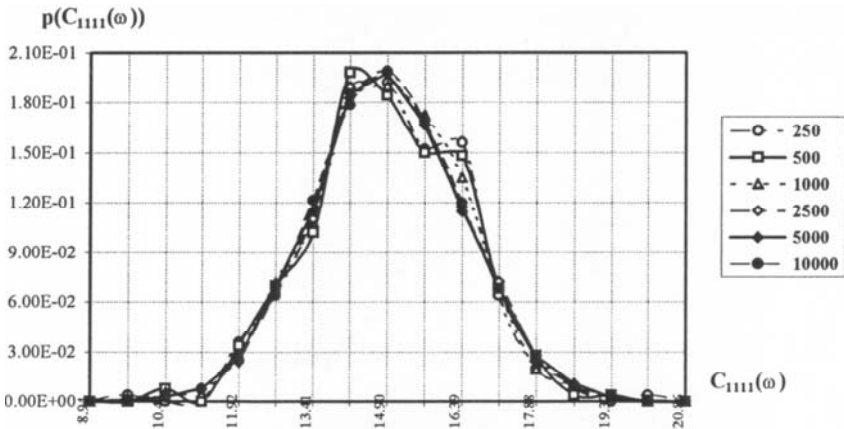


Figure 2.127. Statistical convergence of PDF of $C_{1111}^{(eff)}(\omega)$

The main idea behind performing further numerical experiments is to compute the expected values and variances (or the coefficients of variation) of the effective elasticity tensor components for the RVE of the superconducting coil cable [199,221]. Next aim is to check the variability of the effective characteristic probabilistic moments with respect to the moments of the input random variables.

Probabilistic effective characteristics are compared with the appropriate upper and lower bounds probabilistic moments for the same composite specimen.

Due to the internal horizontal and vertical symmetry of the RVE, only a simple quarter of the periodicity cell has been analysed in the homogenisation procedure for the discretisation of this cell shown before.

Elastic characteristics and their probabilistic moments of the RVE components in the form of the expected values and the standard deviations of Young moduli and Poisson ratios as well as of the Kirchhoff moduli are collected in Table 2.14.

Table 2.14. Probabilistic moments of the elastic characteristics of the superconductor

Material	$E[e]$ [GPa]	$\sigma(e)$ [GPa]	$E[v]$	$\sigma(v)$	$E[G]$ [GPa]	$\sigma(G)$ [GPa]
Tube	205.0	8.0	0.265	0.010	81.0	2.0
Superconductor (test 1)	130.0	0.0	0.340	0.000	70.0	0.0
Superconductor (test 2)	46.8	0.0	0.122	0.000	25.2	0.0
Jacket	126.0	12.0	0.311	0.012	48.0	6.0
Insulation	36.0	0.0	0.210	0.000	11.0	0.0

Three groups of computational experiments have been performed. It is assumed that all elastic characteristics are equal to those specified in Table 2.14 in the first and second groups of computations (tests 1 and 2), while the elastic parameters of the superconducting strands are omitted in the last test. The strand volume fraction in the plane considered is assumed in test 1 as equal to 100%, while in the test 2 it is assumed equal to 36% (approximately the real value). The elastic characteristics of the strands for the second case are calculated using of spatial averaging only. These characteristics can be derived by some homogenisation approach (Mori–Tanaka or self-consistent, for instance) if only the longitudinal elastic modulae are measured statistically.

The results of numerical analyses are presented in Tables 2.15–2.20. Upper and lower bounds as well as the effective elastic properties for test 1 are collected in Tables 2.15 and 2.16, respectively, for test 2 they are outlined in Tables 2.17 and 2.18, while for test 3 they are outlined in Tables 2.19–2.20. Deterministic values of the effective elasticity tensor and their up to fourth order probabilistic characteristics (expected values, coefficients of variation, asymmetry and concentration) are shown for all these tests.

Table 2.15. Effective elasticity tensor components [GPa] in test 1

Effective characteristics	$C_{1111}^{(eff)}$	$C_{1212}^{(eff)}$	$C_{1122}^{(eff)}$
Deterministic values	154.94	68.85	43.67
$E[C]$	154.27	68.52	43.94
$\alpha(C)$	5.56e-2	5.44e-2	5.76e-2
$\beta(C)$	-2.06e-1	-2.41e-1	9.98e-2
$\gamma(C)$	3.27	3.29	3.15

Table 2.16. Upper and lower bounds for effective elasticity tensor [GPa] in test 1

Effective characteristics	$C_{1111}^{(eff)}$		$C_{1212}^{(eff)}$		$C_{1122}^{(eff)}$	
Upper and lower bounds presented						
	sup(C)	inf(C)	sup(C)	inf(C)	Sup(C)	inf(C)
Deterministic values	163.49	146.47	75.56	63.27	43.97	41.60
E[C]	163.60	146.18	75.81	63.16	43.89	41.51
$\alpha(C)$	6.89e-2	5.76e-2	9.78e-2	8.14e-2	4.42e-2	3.95e-2
$\beta(C)$	1.79e-7	-1.04e-7	3.32e-7	-1.12e-8	-1.15e-7	-2.51e-7
$\gamma(C)$	3.09	3.06	3.20	3.02	3.07	3.17
Voigt-Reuss bounds						
Deterministic values	171.49	130.33	80.95	52.63	45.27	38.85
E[C]	171.88	129.97	81.43	52.46	45.23	38.76
$\alpha(C)$	6.78e-2	4.72e-2	9.29e-2	6.60e-2	4.54e-2	3.45e-2
$\beta(C)$	3.23e-7	-2.51e-7	5.15e-7	-1.75e-7	-2.30e-8	-2.50e-7
$\gamma(C)$	3.26	3.17	3.54	3.09	3.03	3.30

Table 2.17. Effective elasticity tensor components [GPa] in test 2

Effective characteristics	$C_{1111}^{(eff)}$	$C_{1212}^{(eff)}$	$C_{1122}^{(eff)}$
Deterministic values	102.33	36.47	33.69
E[C]	102.50	36.69	33.49
$\alpha(C)$	5.83e-2	5.90e-2	6.38e-2
$\beta(C)$	-1.86e-1	-1.92e-1	-9.96e-2
$\gamma(C)$	3.23	3.25	3.15

Table 2.18. Upper and lower bounds for effective elasticity tensor [GPa] in test 2

Effective characteristics	$C_{1111}^{(eff)}$		$C_{1212}^{(eff)}$		$C_{1122}^{(eff)}$	
Upper and lower bounds presented						
	sup(C)	inf(C)	sup(C)	inf(C)	sup(C)	inf(C)
Deterministic values	100.24	82.24	35.21	22.74	32.52	29.75
E[C]	100.37	82.05	35.45	22.68	32.46	29.69
$\alpha(C)$	8.18e-2	4.11e-2	1.40e-1	5.84e-2	4.99e-2	3.46e-2
$\beta(C)$	2.12e-7	-2.38e-7	4.16e-7	-1.58e-7	-9.73e-8	-2.89e-7
$\gamma(C)$	3.16	3.15	3.38	3.08	3.06	3.21
Voigt-Reuss bounds						
Deterministic values	113.11	71.80	43.86	16.64	34.63	27.58
E[C]	113.50	71.65	44.34	16.61	34.58	27.52
$\alpha(C)$	1.03e-2	2.48e-2	1.71e-1	2.57e-2	5.94e-2	2.46e-2
$\beta(C)$	3.23e-7	-4.13e-7	5.15e-7	-4.02e-7	-2.30e-8	-4.17e-7
$\gamma(C)$	3.26	3.40	3.54	3.38	3.03	3.41

Table 2.19. Effective elasticity tensor components [GPa] in test 3

Effective Characteristics	$C_{1111}^{(eff)}$	$C_{1212}^{(eff)}$	$C_{1122}^{(eff)}$
Deterministic values	75.07	30.15	25.89
$E[C]$	75.09	30.29	25.38
$\alpha(C)$	9.29e-2	1.06e-1	6.94e-2
$\beta(C)$	-1.14e-1	-6.40e-2	-9.97e-2
$\gamma(C)$	3.16	3.15	3.17

Tab. 2.20. Upper and lower bounds for effective elasticity tensor [GPa] in test 3

Effective characteristics	$C_{1111}^{(eff)}$		$C_{1212}^{(eff)}$		$C_{1122}^{(eff)}$	
Upper and lower bounds presented						
	sup(C)	inf(C)	sup(C)	inf(C)	sup(C)	inf(C)
Deterministic values	73.50	4.02	30.47	4.64e-2	21.51	1.984
$E[C]$	73.34	4.02	30.37	4.64e-2	21.49	1.98
$\alpha(C)$	1.03e-1	2.34e-3	1.57e-1	3.34e-2	6.56e-3	2.75e-3
$\beta(C)$	2.42e-7	-5.64e-7	4.30e-7	5.57e-7	-7.35e-8	-5.67e-7
$\gamma(C)$	3.182	3.730	3.398	3.704	3.049	3.729
Voigt-Reuss bounds						
Deterministic values	94.84	2.55	41.27	1.23e-2	26.79	1.27
$E[C]$	95.23	2.55	41.74	1.23e-2	26.74	1.27
$\alpha(C)$	1.22e-1	9.72e-4	1.81e-1	3.55e-2	7.67e-2	1.15e-3
$\beta(C)$	3.23e-7	-5.80e-7	5.15e-7	5.79e-7	-2.30e-8	-5.89e-7
$\gamma(C)$	3.26	3.77	3.54	3.76	3.03	3.77

First a general observation, which agrees with engineering intuition, is that the deterministic quantities and expected values for upper and lower bounds and effective elasticity tensor components are greater for test 1 (composite including superconductor) than for test 2 (the cell without superconducting strands). Further, it is seen that the results of deterministic analyses approximate very well the expected values obtained in probabilistic simulations and that deterministic results are generally lower than the approximated expectations.

Analysing the coefficients of variation of all variables computed it is characteristic that the results of test 1 are significantly smaller than the input coefficients and the coefficients resulting from test 2. It is caused mainly by the fact that some of the input elastic characteristics including superconductor have the coefficients of variation equal to 0. Considering that the superconductor occupies a significant part of the periodicity cell, the coefficients α resulting from test 2 are in the range of those characterising the elastic properties of composite components. It should be outlined at the moment that probabilistic moments of effective characteristics of order higher than the second are in general in the range of the corresponding characteristics of the input elastic parameters in the probabilistic homogenisation of elastostatic problems.

Observing characteristics of the third and fourth order it may be concluded that the upper and lower bounds of the effective tensor in both tests have symmetric probability density functions, while the effective characteristics PDFs show some

asymmetry. Finally, it can be observed that the coefficients of concentration are approximately equal to the value corresponding to the Gaussian variable probability distribution function.

Considering these observations we can treat the probability density functions of the effective elastic characteristics as Gaussian, which enables us to characterise uniquely these distributions using only their first two probabilistic moments. This conclusion is very important in the context of the SFEM implementation of the problem where only the first two moments of the state functions can be computed and, furthermore, all odd moments are equal to 0.

2.3.2.2.3 Stochastic Perturbation Approach to the Homogenisation

The homogenisation technique presented in the preceding sections is combined now with the stochastic second order perturbation second central probabilistic moment method. To rewrite the stochastic version of the variational formulation of the homogenisation problem, the interface forces equivalent to the stress interface conditions should be stochastically perturbed first. It is known from the classical theory of homogenisation that in case of ideal bonds between the fibre and matrix, the interface load components are obtained in the form of the following difference, cf. (2.155)

$$F_{(pq)i} = F_{(pq)i}^{(2)} - F_{(pq)i}^{(1)} \quad (2.176)$$

Taking into account the general Taylor series expansion it is found that

$$F_{(pq)i} = (F_{(pq)i})^0 + \theta (F_{(pq)i})^{,r} \Delta b^r + \frac{1}{2} \theta^2 (F_{(pq)i})^{,rs} \Delta b^r \Delta b^s \quad (2.177)$$

Rewriting the forces $F_{(pq)i}^{(t)}$ for $t=0,1,2$, comparing the respective terms of zeroth, first and second order, it is obtained after some additional algebra that

$$(F_{(pq)i})^0 = (F_{(pq)i}^{(2)})^0 - (F_{(pq)i}^{(1)})^0 \quad (2.178)$$

$$(F_{(pq)i})^{,r} = (F_{(pq)i}^{(2)})^{,r} - (F_{(pq)i}^{(1)})^{,r} \quad (2.179)$$

$$(F_{(pq)i})^{,rs} = (F_{(pq)i}^{(2)})^{,rs} - (F_{(pq)i}^{(1)})^{,rs} \quad (2.180)$$

Thus, the stochastic version of minimum potential energy principle for the homogenisation problem has the following form:

- a single zeroth order equation:

$$\sum_{a=1,2} \int_{\Omega_a} \delta v_{i,j} C_{ijkl}^0 (\chi_{(pq)k,l})^0 d\Omega = - \int_{\partial\Omega_{12}} \delta v_i (F_{(pq)i})^0 d(\partial\Omega) \quad (2.181)$$

- R first order equations:

$$\begin{aligned} & \sum_{a=1,2} \int_{\Omega_a} \delta v_{i,j} C_{ijkl}^0 (\chi_{(pq)k,l})^r d\Omega \\ &= - \int_{\partial\Omega_{12}} \delta v_i (F_{(pq)i})^r d(\partial\Omega) - \sum_{a=1,2} \int_{\Omega_a} \delta v_{i,j} C_{ijkl}^r (\chi_{(pq)k,l})^0 d\Omega \end{aligned} \quad (2.182)$$

- a single second order equation:

$$\begin{aligned} & \left(\sum_{a=1,2} \int_{\Omega_a} \delta v_{i,j} C_{ijkl}^0 (\chi_{(pq)k,l})^{rs} d\Omega \right) Cov(b^r, b^s) \\ &= - \left(\int_{\partial\Omega_{12}} \delta v_i (F_{(pq)i})^{rs} d(\partial\Omega) \right) Cov(b^r, b^s) \\ &- \left(2 \sum_{a=1,2} \int_{\Omega_a} \delta v_{i,j} C_{ijkl}^r (\chi_{(pq)k,l})^{rs} d\Omega + \sum_{a=1,2} \int_{\Omega_a} \delta v_{i,j} C_{ijkl}^{rs} (\chi_{(pq)k,l})^0 d\Omega \right) \\ &\times Cov(b^r, b^s) \end{aligned} \quad (2.183)$$

If the Young moduli of fibre and matrix are the components of the input random variable vector then there holds

$$\frac{\partial (C_{ijkl}(e(\mathbf{x}; \omega); \mathbf{x}))}{\partial e_a} = \Psi^{(a)} A_{ijkl}^{(a)}(x), \quad \text{for } a=1,2 \quad (2.184)$$

where $A_{ijkl}^{(a)}$ is the tensor given by (2.14) and calculated for the elastic characteristics of the respective material indexed by a , whereas $\Psi^{(a)}$ is the characteristic function. Thus, the first order derivatives of the elasticity tensor with respect to the input random variable vector are obtained as

$$\frac{\partial (C_{ijkl}(e(\mathbf{x}; \omega); \mathbf{x}))}{\partial e_a} = \left\{ \Psi^{(1)} A_{ijkl}^{(1)}, \Psi^{(2)} A_{ijkl}^{(2)} \right\} \quad (2.185)$$

Hence, the second order derivatives have the form

$$\frac{\partial^2 (C_{ijkl}(e(\mathbf{x}; \omega), \mathbf{x}))}{\partial e_a^2} = \psi^{(a)} \frac{\partial A_{ijkl}^{(a)}(x)}{\partial e_a} = 0, \quad \text{for } a=1,2 \quad (2.186)$$

while mixed second order derivatives can be written as

$$\frac{\partial^2 (C_{ijkl}(e(\mathbf{x}; \omega), \mathbf{x}))}{\partial e_1 \partial e_2} = \psi^{(1)} \frac{\partial A_{ijkl}^{(1)}(\mathbf{x})}{\partial e_2} = \psi^{(2)} \frac{\partial A_{ijkl}^{(2)}(\mathbf{x})}{\partial e_1} = 0 \quad (2.187)$$

Considering the above, all components of the second order derivatives of the stiffness matrixes $K_{\alpha\beta}^{(pq)}$ in this problem are equal to 0. Moreover, since the assumption of the uncorrelation of input random variables

$$\text{Cov}(e_1; e_2) = \begin{bmatrix} \text{Vare}_1 & 0 \\ 0 & \text{Vare}_2 \end{bmatrix} \quad (2.188)$$

thus, the first and second partial derivatives of the vectors $F_{(pq)i}^{(a)}$ with respect to the random variables vector are calculated as

$$\frac{\partial F_{(pq)i}^{(a)}}{\partial e_a} = \frac{\partial C_{ijpq}^{(a)}}{\partial e_a} n_j = A_{ijpq}^{(a)} n_j, \quad \mathbf{x} \in \partial \Omega_a, \quad a=1,2 \quad (2.189)$$

and

$$\frac{\partial^2 F_{(pq)i}^{(a)}}{\partial e_a^2} = \frac{\partial^2 C_{ijpq}^{(a)}}{\partial e_a^2} n_j = \frac{\partial A_{ijpq}^{(a)}}{\partial e_a} n_j = 0, \quad \mathbf{x} \in \partial \Omega_a, \quad a=1,2 \quad (2.190)$$

After all these simplifications, the set of equations (2.181) – (2.183) can be written in the following form:

- a single zeroth order equation:

$$\sum_{a=1,2} \int_{\Omega_a} \delta v_{i,j} C_{ijkl}^0 (\chi_{(pq)k,l})^0 d\Omega = - \int_{\partial\Omega_{12}} \delta v_i (F_{(pq)i})^0 d(\partial\Omega) \quad (2.191)$$

- R first order equations:

$$\begin{aligned} \sum_{a=1,2} \int_{\Omega_a} \delta v_{i,j} C_{ijkl}^0 (\chi_{(pq)k,l})^r d\Omega &= - \int_{\partial\Omega_{12}} \delta v_i [A_{pqij}] n_j d(\partial\Omega) \\ - \sum_{a=1,2} \int_{\Omega_a} \delta v_{i,j} A_{ijkl}^{(a)} (\chi_{(pq)k,l})^0 d\Omega & \end{aligned} \quad (2.192)$$

- a single second order equation:

$$\begin{aligned} & \sum_{a=1,2} \int_{\Omega_a} \delta v_{i,j} C_{ijkl}^0 (\chi_{(pq)k,l})^2 d\Omega \\ & = - \sum_{a=1,2} \int_{\Omega_a} \delta v_{i,j} C_{ijkl}^r (\chi_{(pq)k,l})^{,s} d\Omega \text{Cov}(b^r, b^s) \end{aligned} \quad (2.193)$$

where

$$(\chi_{(pq)k,l})^{(2)} = -\frac{1}{2} (\chi_{(pq)k,l})^{,rs} \text{Cov}(b^r, b^s) \quad (2.194)$$

It should be noted that (2.191) – (2.194) give the set of fundamental variational equations of the homogenisation problem due to the second order stochastic perturbation method. Next, these equations will be discretised by the use of classical finite element technique and, as a result, the zeroth, first and second order algebraic equations are derived. Further, let us introduce the following discretisation of the homogenisation function and its derivatives with respect to the random variables using the classical shape functions $\varphi_{i\alpha}(\mathbf{x})$:

$$(\chi_{(pv)i}(\mathbf{x}))^0 = \varphi_{i\alpha}(\mathbf{x}) \cdot (q_{(pv)\alpha})^0, \quad \mathbf{x} \in \Omega, \quad p, v=1,2 \quad (2.195)$$

$$(\chi_{(pv)i}(\mathbf{x}))^{,r} = \varphi_{i\alpha}(\mathbf{x}) \cdot (q_{(pv)\alpha})^{,r}, \quad \mathbf{x} \in \Omega, \quad p, v=1,2 \quad (2.196)$$

$$(\chi_{(pv)i}(\mathbf{x}))^{,rs} = \varphi_{i\alpha}(\mathbf{x}) \cdot (q_{(pv)\alpha})^{,rs}, \quad \mathbf{x} \in \Omega, \quad p, v=1,2 \quad (2.197)$$

where $i=1,2$; $r, s=1, \dots, R$; $\alpha=1, \dots, N$ (N is the total number of degrees of freedom employed in the region Ω). In an analogous way, the approximation of the strain tensor components is introduced as

$$\varepsilon_{ij}^0(\chi_{(pv)}(\mathbf{x})) = B_{ij\alpha}(\mathbf{x}) (q_{(pv)\alpha})^0, \quad \mathbf{x} \in \Omega \quad (2.198)$$

$$\varepsilon_{ij}^{,r}(\chi_{(pv)}(\mathbf{x})) = B_{ij\alpha}(\mathbf{x}) (q_{(pv)\alpha})^{,r}, \quad \mathbf{x} \in \Omega \quad (2.199)$$

$$\varepsilon_{ij}^{,rs}(\chi_{(pv)}(\mathbf{x})) = B_{ij\alpha}(\mathbf{x}) (q_{(pv)\alpha})^{,rs}, \quad \mathbf{x} \in \Omega \quad (2.200)$$

where $B_{ij\alpha}(\mathbf{x})$ is the typical FEM shape functions derivatives

$$B_{ij\alpha}(\mathbf{x}) = \frac{1}{2} [\varphi_{i\alpha,j}(\mathbf{x}) + \varphi_{j\alpha,i}(\mathbf{x})], \quad \mathbf{x} \in \Omega \quad (2.201)$$

Introducing equations stated above to the zeroth, first and second order statements of the homogenisation problem represented by (2.191) – (2.194), the stochastic formulation of the problem can be discretised through the following set of algebraic linear (in fact deterministic) equations:

$$K^0 q_{(pv)}^0 = Q_{(pv)}^0 \quad (2.202)$$

$$K^0 q_{(pv)}^{,r} = Q_{(pv)}^0 - K^{,r} q_{(pv)}^0 \quad (2.203)$$

$$K^0 q_{(pv)}^{(2)} = -K^{,r} q_{(pv)}^{,s} Cov(b^r, b^s) \quad (2.204)$$

where

$$q_{(pv)}^{(2)} = \frac{1}{2} q_{(pv)}^{,rs} Cov(b^r, b^s) \quad (2.205)$$

and \mathbf{K} , $\mathbf{q}_{(pv)}$, $\mathbf{Q}_{(pv)}$ denote the global stiffness matrix, generalised coordinates vectors of the homogenisation functions and external load vectors, correspondingly. Considering the plane strain nature of the homogenisation problem, the global stiffness matrix and its partial derivatives with respect to the random variables of the problem can be rewritten as follows:

$$K_{\alpha\beta}^0 = \sum_{e=1}^E \int_{\Omega_e} C_{ijkl}^0 B_{ij\alpha} B_{kl\beta} d\Omega \quad (2.206)$$

$$= \sum_{e=1}^E \frac{e(1-\nu)}{(1+\nu)(1-2\nu)} \int_{\Omega_e} \begin{bmatrix} 1 & \frac{\nu}{1-\nu} & 0 \\ & 1 & 0 \\ \text{symm} & & \frac{1-2\nu}{2(1-\nu)} \end{bmatrix} B_{ij\alpha} B_{kl\beta} d\Omega$$

$$K_{\alpha\beta}^{,r} = \sum_{e=1}^E \int_{\Omega_e} C_{ijkl}^{,r} B_{ij\alpha} B_{kl\beta} d\Omega \quad (2.207)$$

$$= \sum_{e=1}^E \frac{(1-\nu)}{(1+\nu)(1-2\nu)} \int_{\Omega_e} \begin{bmatrix} 1 & \frac{\nu}{1-\nu} & 0 \\ & 1 & 0 \\ \text{symm} & & \frac{1-2\nu}{2(1-\nu)} \end{bmatrix} B_{ij\alpha} B_{kl\beta} d\Omega$$

$$K_{\alpha\beta}^{,rs} = \sum_{e=1}^E \int_{\Omega_e} C_{ijkl}^{,rs} B_{ij\alpha} B_{kl\beta} d\Omega \quad (2.208)$$

as far as Young moduli are randomised only. Computing from the above equations successively the zeroth order displacement vector $q_{(pv)}^{(0)}$ from (2.202), first order displacement vector $q_{(pv)}^{,r}$ from (2.203) and the second order displacement vector $q_{(pv)}^{(2)}$ from (2.204) – (2.205), the expected values of the homogenisation function can be derived as

$$E[q_{(pv)}] = q_{(pv)}^0 + \frac{1}{2} q_{(pv)}^{,rs} Cov(b^r, b^s) \quad (2.209)$$

Their covariance matrix can be determined in the form

$$Cov(q_{(pv)r}, q_{(pv)s}) = q_{(pv)r}^r q_{(pv)s}^s Cov(b^r, b^s) \quad (2.210)$$

where α, β are indexing all the degrees of freedom of the RVE. Then, the expected values of the stress tensor components can be expressed as

$$E[\sigma_{ij}^{(e)}] = \left\{ C_{ijkl}^{(e)0} (q_{(pv)}^0 + \frac{1}{2} q_{(pv)}^{rs}) + C_{ijkl}^{(e),r} q_{(pv)}^{r,s} \right\} B_{kl}^{(e)} Cov(b^r, b^s) \quad (2.211)$$

while its covariances – from the following equation:

$$\begin{aligned} Cov(\sigma_{ij}^{(e)}, \sigma_{ij}^{(f)}) &= B_{kl}^{(e)} B_{mn}^{(f)} Cov(b^r, b^s) \\ &\left\{ C_{ijkl}^{(e)0} C_{ijmn}^{(f)0} q_{(pv)}^{r,s} q_{(pv)}^{r,s} + C_{ijkl}^{(e),r} C_{ijmn}^{(f),s} q_{(pv)}^0 q_{(pv)}^0 \right. \\ &\left. + C_{ijkl}^{(e),r} C_{ijmn}^{(f)0} q_{(pv)}^{r,s} q_{(pv)}^0 + C_{ijkl}^{(e)0} C_{ijmn}^{(f),r} q_{(pv)}^0 q_{(pv)}^{r,s} \right\} \end{aligned} \quad (2.212)$$

where $i, j, k, l, g, h, p, v = 1, 2$; $1 \leq d, f \leq E$ standing for the finite elements numbers in the cell mesh. In accordance with the probabilistic homogenisation methodology, the expected values of the elasticity tensor components can be found starting from (2.136) as

$$E[C_{ijpq}^{(eff)}] = \frac{1}{|\Omega|} \int_{\Omega} \left(E[C_{ijpq}] + E[C_{ijkl} \varepsilon_{kl}(\chi_{(pq)})] \right) d\Omega \quad (2.213)$$

The second term in this integral can be extended using second order perturbation method as follows:

$$\begin{aligned} &E[C_{ijkl} \varepsilon_{kl}(\chi_{(pq)})] \\ &= \int_{-\infty}^{+\infty} \left(C_{ijkl}^0 + \Delta b^r C_{ijkl}^{,r} + \frac{1}{2} \Delta b^r \Delta b^s C_{ijkl}^{,rs} \right) p_R(\mathbf{b}(x)) d\mathbf{b} \\ &\times \int_{-\infty}^{+\infty} \left((\chi_{(pq)k,l})^0 + \Delta b^u (\chi_{(pq)k,l})^{,u} + \frac{1}{2} \Delta b^u \Delta b^v (\chi_{(pq)k,l})^{,uv} \right) p_R(\mathbf{b}(x)) d\mathbf{b} \end{aligned} \quad (2.214)$$

There holds

$$\begin{aligned}
 E[C_{ijkl}\varepsilon_{kl}(\chi_{(pq)})] &= \int_{-\infty}^{+\infty} C_{ijkl}^0(\chi_{(pq)k,l})^0 p_R(\mathbf{b}(x)) d\mathbf{b} \\
 &+ \int_{-\infty}^{+\infty} \Delta b^r C_{ijkl}^{,r} \Delta b^u(\chi_{(pq)k,l})^{,u} p_R(\mathbf{b}(x)) d\mathbf{b} \\
 &+ \frac{1}{2} \int_{-\infty}^{+\infty} C_{ijkl}^0 \Delta b^u \Delta b^r(\chi_{(pq)k,l})^{,uv} p_R(\mathbf{b}(x)) d\mathbf{b} \\
 &= C_{ijkl}^0(\chi_{(pq)k,l})^0 + \left\{ C_{ijkl}^{,r}(\chi_{(pq)k,l})^{,s} + \frac{1}{2} C_{ijkl}^0(\chi_{(pq)k,l})^{,rs} \right\} Cov(b^r, b^s)
 \end{aligned} \tag{2.215}$$

Averaging both sides of this equation over the region Ω and including in the relation (2.213) together with spatially averaged expected values of the original elasticity tensor, the expected values of the homogenised elasticity tensor are obtained. Next, the covariances of the effective elasticity tensor components can be derived similarly as

$$\begin{aligned}
 Cov(C_{ijkl}^{(eff)}; C_{mnpq}^{(eff)}) &= Cov(C_{ijkl}, C_{mnpq}) + Cov(C_{ijkl}, C_{mnuv}\chi_{(pq)u,v}) \\
 &+ Cov(C_{ijrs}\chi_{(kl)r,s}, C_{mnpq}) + Cov(C_{ijrs}\chi_{(kl)r,s}, C_{mnuv}\chi_{(pq)u,v})
 \end{aligned} \tag{2.216}$$

Finally, the covariances of the effective elasticity tensor components are calculated below. Covariance of the first component in (2.216) is derived as

$$\begin{aligned}
 Cov(C_{ijkl}; C_{mnpq}) &= \int_{-\infty}^{+\infty} (C_{ijkl} - E[C_{ijkl}]) (C_{mnpq} - E[C_{mnpq}]) p_R(\mathbf{b}(x)) d\mathbf{b} \\
 &= \int_{-\infty}^{+\infty} (C_{ijkl}^0 + \Delta b_r C_{ijkl}^{,r} - C_{ijkl}^0) (C_{mnpq}^0 + \Delta b_s C_{mnpq}^{,s} - C_{mnpq}^0) p_R(\mathbf{b}(x)) d\mathbf{b} \\
 &= C_{ijkl}^{,r} C_{mnpq}^{,s} \int_{-\infty}^{+\infty} \Delta b_r \Delta b_s p_R(\mathbf{b}(x)) d\mathbf{b} = C_{ijkl}^{,r} C_{mnpq}^{,s} Cov(b^r, b^s)
 \end{aligned} \tag{2.217}$$

Next, the cross-covariances of the second component are calculated and there holds

$$\begin{aligned}
 Cov(C_{ijtw}\chi_{(kl)t,w}; C_{mnuv}\chi_{(pq)u,v}) &= \int_{-\infty}^{+\infty} (C_{ijtw}\chi_{(kl)t,w} - E[C_{ijtw}\chi_{(kl)t,w}]) \\
 &\times (C_{mnuv}\chi_{(pq)u,v} - E[C_{mnuv}\chi_{(pq)u,v}]) p_R(\mathbf{b}(x)) d\mathbf{b}
 \end{aligned} \tag{2.218}$$

which, by introducing the simplifying notation, becomes

$$\begin{aligned}
& \int_{-\infty}^{+\infty} \left(\mathbf{C}^0 \chi^0 + \mathbf{C}^{,r} \Delta b_r \chi^0 + \mathbf{C}^0 \chi^{,u} \Delta b_u + \mathbf{C}^{,r} \Delta b_r \chi^{,u} \Delta b_u + \frac{1}{2} \mathbf{C}^0 \chi^{,uv} \Delta b_u \Delta b_v \right. \\
& \left. - \left\{ \mathbf{C}^0 \chi^0 + \left(\mathbf{C}^{,r} \chi^{,s} + \frac{1}{2} \mathbf{C}^0 \chi^{,rs} \right) \text{Cov}(b^r, b^s) \right\} \right) p_R(\mathbf{b}(x)) d\mathbf{b} \\
& \times \int_{-\infty}^{+\infty} \left(\mathbf{D}^0 \varphi^0 + \mathbf{D}^{,a} \Delta b_a \varphi^0 + \mathbf{D}^0 \varphi^{,c} \Delta b_c + \mathbf{D}^{,a} \Delta b_a \varphi^{,c} \Delta b_c + \frac{1}{2} \mathbf{D}^0 \varphi^{,cd} \Delta b_c \Delta b_d \right. \\
& \left. - \left\{ \mathbf{D}^0 \varphi^0 + \left(\mathbf{D}^{,a} \varphi^{,c} + \frac{1}{2} \mathbf{D}^0 \varphi^{,ac} \right) \text{Cov}(b^a, b^c) \right\} \right) p_R(\mathbf{b}(x)) d\mathbf{b}
\end{aligned} \tag{2.219}$$

Further, it is obtained that

$$\begin{aligned}
& \int_{-\infty}^{+\infty} \left(\mathbf{C}^0 \chi^0 + \mathbf{C}^{,r} \Delta b_r \chi^0 + \mathbf{C}^0 \chi^{,u} \Delta b_u + \mathbf{C}^{,r} \Delta b_r \chi^{,u} \Delta b_u + \frac{1}{2} \mathbf{C}^0 \chi^{,uv} \Delta b_u \Delta b_v \right. \\
& \left. - \left\{ \mathbf{C}^0 \chi^0 + \left(\mathbf{C}^{,r} \chi^{,s} + \frac{1}{2} \mathbf{C}^0 \chi^{,rs} \right) \text{Cov}(b^r, b^s) \right\} \right) p_R(\mathbf{b}(x)) d\mathbf{b} \\
& \times \int_{-\infty}^{+\infty} \left(\mathbf{D}^0 \varphi^0 + \mathbf{D}^{,a} \Delta b_a \varphi^0 + \mathbf{D}^0 \varphi^{,c} \Delta b_c + \mathbf{D}^{,a} \Delta b_a \varphi^{,c} \Delta b_c + \frac{1}{2} \mathbf{D}^0 \varphi^{,cd} \Delta b_c \Delta b_d \right. \\
& \left. - \left\{ \mathbf{D}^0 \varphi^0 + \left(\mathbf{D}^{,a} \varphi^{,c} + \frac{1}{2} \mathbf{D}^0 \varphi^{,ac} \right) \text{Cov}(b^a, b^c) \right\} \right) p_R(\mathbf{b}(x)) d\mathbf{b} \\
& = \int_{-\infty}^{+\infty} \mathbf{C}^{,r} \Delta b_r \chi^0 \mathbf{D}^{,a} \Delta b_a \varphi^0 p_R(\mathbf{b}(x)) d\mathbf{b} + \int_{-\infty}^{+\infty} \mathbf{C}^{,r} \Delta b_r \chi^0 \mathbf{D}^0 \varphi^{,c} \Delta b_c p_R(\mathbf{b}(x)) d\mathbf{b} \\
& + \int_{-\infty}^{+\infty} \mathbf{C}^0 \chi^{,u} \Delta b_u \mathbf{D}^{,a} \Delta b_a \varphi^0 p_R(\mathbf{b}(x)) d\mathbf{b} + \int_{-\infty}^{+\infty} \mathbf{C}^0 \chi^{,u} \Delta b_u \mathbf{D}^0 \varphi^{,c} \Delta b_c p_R(\mathbf{b}(x)) d\mathbf{b}
\end{aligned} \tag{2.220}$$

Integration over the probability domain gives

$$\begin{aligned}
& \int_{-\infty}^{+\infty} \mathbf{C}^{,r} \Delta b_r \chi^0 \mathbf{D}^{,a} \Delta b_a \varphi^0 p_R(\mathbf{b}(x)) d\mathbf{b} + \int_{-\infty}^{+\infty} \mathbf{C}^{,r} \Delta b_r \chi^0 \mathbf{D}^0 \varphi^{,c} \Delta b_c p_R(\mathbf{b}(x)) d\mathbf{b} \\
& + \int_{-\infty}^{+\infty} \mathbf{C}^0 \chi^{,u} \Delta b_u \mathbf{D}^{,a} \Delta b_a \varphi^0 p_R(\mathbf{b}(x)) d\mathbf{b} + \int_{-\infty}^{+\infty} \mathbf{C}^0 \chi^{,u} \Delta b_u \mathbf{D}^0 \varphi^{,c} \Delta b_c p_R(\mathbf{b}(x)) d\mathbf{b} \\
& = \left\{ \mathbf{C}^{,r} \mathbf{D}^{,s} \chi^0 \varphi^0 + \mathbf{C}^{,r} \chi^0 \mathbf{D}^0 \varphi^{,s} + \mathbf{C}^0 \chi^{,r} \mathbf{D}^{,s} \varphi^0 + \mathbf{C}^0 \chi^{,r} \mathbf{D}^0 \varphi^{,s} \right\} \text{Cov}(b^r, b^s)
\end{aligned} \tag{2.221}$$

or, in a more explicit way, that

$$\begin{aligned}
& Cov(C_{ijtw} \chi_{(kl)t,w}; C_{mnuv} \chi_{(pq)u,v}) \\
&= \left\{ C_{ijtw}^{,r} C_{mnuv}^{,s} (\chi_{(kl)t,w})^0 (\chi_{(pq)u,v})^0 + C_{ijtw}^{,r} C_{mnuv}^0 (\chi_{(kl)t,w})^0 (\chi_{(pq)u,v})^{,s} \right. \\
&+ \left. C_{ijtw}^0 C_{mnuv}^{,r} (\chi_{(kl)t,w})^{,s} (\chi_{(pq)u,v})^0 + C_{ijtw}^0 C_{mnuv}^0 (\chi_{(kl)t,w})^{,r} (\chi_{(pq)u,v})^{,s} \right\} \\
&\times Cov(b^r, b^s)
\end{aligned} \tag{2.222}$$

Now, the third component is transformed as follows:

$$\begin{aligned}
& Cov(C_{ijkl}; C_{mnuv} \chi_{(pq)u,v}) = Cov(\mathbf{C}; \mathbf{D}\chi) \\
&= \int_{-\infty}^{+\infty} (\mathbf{C}^0 + \mathbf{C}^{,r} \Delta b_r - \mathbf{C}^0) \cdot p_R(\mathbf{b}(x)) d\mathbf{b} \\
&\times \int_{-\infty}^{+\infty} (\mathbf{D}^0 \chi^0 + \mathbf{D}^{,a} \Delta b_a \chi^0 + \mathbf{D}^0 \chi^{,c} \Delta b_c + \mathbf{D}^{,a} \Delta b_a \chi^{,c} \Delta b_c + \frac{1}{2} \mathbf{D}^0 \chi^{,cd} \Delta b_c \Delta b_d \\
&- \left\{ \mathbf{D}^0 \chi^0 + \left(\mathbf{D}^{,a} \chi^{,c} + \frac{1}{2} \mathbf{D}^0 \chi^{,ac} \right) Cov(b^a, b^c) \right\}) p_R(\mathbf{b}(x)) d\mathbf{b} \\
&= \int_{-\infty}^{+\infty} \mathbf{C}^{,r} \Delta b_r \mathbf{D}^{,a} \Delta b_a \chi^0 p_R(\mathbf{b}(x)) d\mathbf{b} + \int_{-\infty}^{+\infty} \mathbf{C}^{,r} \Delta b_r \mathbf{D}^0 \chi^{,c} \Delta b_c p_R(\mathbf{b}(x)) d\mathbf{b} \\
&= \left\{ \mathbf{C}^{,r} \mathbf{D}^{,s} \chi^0 + \mathbf{C}^{,r} \mathbf{D}^0 \chi^{,s} \right\} Cov(b^r, b^s)
\end{aligned} \tag{2.223}$$

Introducing the symbolic summation notation for the tensor function considered above it can be written that

$$\begin{aligned}
& Cov(C_{ijkl}; C_{mnuv} \chi_{(pq)u,v}) \\
&= Cov(\mathbf{C}; \mathbf{D}\chi) = \left\{ \mathbf{C}^{,r} \mathbf{D}^{,s} \chi^0 + \mathbf{C}^{,r} \mathbf{D}^0 \chi^{,s} \right\} Cov(b^r, b^s) \\
&= \left\{ C_{ijkl}^{,r} C_{mnuv}^{,s} (\chi_{(pq)u,v})^0 + C_{ijkl}^{,r} C_{mnuv}^0 (\chi_{(pq)u,v})^{,s} \right\} Cov(b^r, b^s)
\end{aligned} \tag{2.224}$$

By the analogous way, it is obtained

$$\begin{aligned}
& Cov(C_{ijtw} \chi_{(kl)t,w}; C_{mnpq}) \\
&= Cov(\mathbf{C}\chi; \mathbf{D}) = \left\{ \mathbf{C}^{,r} \chi^0 \mathbf{D}^{,s} + \mathbf{C}^0 \chi^{,r} \mathbf{D}^{,s} \right\} Cov(b^r, b^s) \\
&= \left\{ C_{ijtw}^{,r} (\chi_{(kl)t,w})^0 C_{mnpq}^{,s} + C_{ijtw}^{,r} (\chi_{(kl)t,w})^{,s} C_{mnpq}^0 \right\} Cov(b^r, b^s)
\end{aligned} \tag{2.225}$$

The components of effective elasticity tensor covariances are found. Starting from the classical definition

$$\begin{aligned}
& Cov(C_{ijkl}^{(eff)}; C_{mnpq}^{(eff)}) \\
&= Cov(C_{ijkl} + C_{ijtw} \chi_{(kl)t,w} ; C_{mnpq} + C_{mnuv} \chi_{(pq)u,v}) \\
&= \int_{-\infty}^{+\infty} (C_{ijkl} + C_{ijtw} \chi_{(kl)t,w} - E[C_{ijkl}]) - E[C_{ijtw} \chi_{(kl)t,w}] \\
&\quad \times (C_{mnpq} + C_{mnuv} \chi_{(pq)u,v} - E[C_{mnpq}]) - E[C_{mnuv} \chi_{(pq)u,v}] p_R(\mathbf{b}(x)) d\mathbf{b}
\end{aligned} \tag{2.226}$$

Transforming the respective integrands and using Fubini theorem applied to the integrals of random functions we obtain further

$$\begin{aligned}
& \int_{-\infty}^{+\infty} (C_{ijkl} - E[C_{ijkl}]) (C_{mnpq} - E[C_{mnpq}]) p_R(\mathbf{b}(x)) d\mathbf{b} \\
& \times \int_{-\infty}^{+\infty} (C_{ijkl} - E[C_{ijkl}]) (C_{mnuv} \chi_{(pq)u,v} - E[C_{mnuv} \chi_{(pq)u,v}]) p_R(\mathbf{b}(x)) d\mathbf{b} \\
& \times \int_{-\infty}^{+\infty} (C_{ijtw} \chi_{(kl)t,w} - E[C_{ijtw} \chi_{(kl)t,w}]) (C_{mnpq} - E[C_{mnpq}]) p_R(\mathbf{b}(x)) d\mathbf{b} \\
& \times \int_{-\infty}^{+\infty} (C_{ijtw} \chi_{(kl)t,w} - E[C_{ijtw} \chi_{(kl)t,w}]) (C_{mnuv} \chi_{(pq)u,v} - E[C_{mnuv} \chi_{(pq)u,v}]) p_R(\mathbf{b}(x)) d\mathbf{b}
\end{aligned} \tag{2.227}$$

which, using the classical definition of the covariance, is equal to

$$\begin{aligned}
& Cov(C_{ijkl}, C_{mnpq}) + Cov(C_{ijkl}, C_{mnuv} \chi_{(pq)u,v}) + \\
& + Cov(C_{ijtw} \chi_{(kl)t,w}, C_{mnpq}) + Cov(C_{ijtw} \chi_{(kl)t,w}, C_{mnuv} \chi_{(pq)u,v})
\end{aligned} \tag{2.228}$$

Introducing all the statements into the last one it can finally be written that

$$\begin{aligned}
& Cov(C_{ijkl}^{(eff)}; C_{mnpq}^{(eff)}) \\
&= \left\{ C_{ijkl}^{,r} C_{mnpq}^{,s} + C_{ijtw}^{,r} (\chi_{(kl)t,w})^0 C_{mnpq}^{,s} + C_{ijtw}^{,r} (\chi_{(kl)t,w})^{,s} C_{mnpq}^0 \right. \\
& + C_{ijkl}^{,r} C_{mnuv}^{,s} (\chi_{(pq)u,v})^0 + C_{ijkl}^{,r} C_{mnuv}^0 (\chi_{(pq)u,v})^{,s} \\
& + C_{ijtw}^{,r} C_{mnuv}^{,s} (\chi_{(kl)t,w})^0 (\chi_{(pq)u,v})^0 + C_{ijtw}^{,r} C_{mnuv}^0 (\chi_{(kl)t,w})^0 (\chi_{(pq)u,v})^{,s} \\
& \left. + C_{ijtw}^0 C_{mnuv}^{,r} (\chi_{(kl)t,w})^{,s} (\chi_{(pq)u,v})^0 + C_{ijtw}^0 C_{mnuv}^0 (\chi_{(kl)t,w})^{,r} (\chi_{(pq)u,v})^{,s} \right\} \\
& \times Cov(b^r, b^s)
\end{aligned} \tag{2.229}$$

It should be underlined here that the above equations give complete a description of the effective elasticity tensor components in the stochastic second moment and second order perturbation approach. Finally, let us note that many simplifications

resulted here thanks to the assumption that the input random variables of the homogenisation problem are just the Young moduli of the fibre and matrix. If the Poisson ratios are treated as random, the second order derivatives of the constitutive tensor would generally differ from 0 and the stochastic finite element formulation of the homogenisation procedure would be essentially more complicated.

For the periodicity cell and its discretisation shown in Figure 2.128 elastic properties of the glass fibre and the matrix are adopted as follows: the Young moduli expected values $E[e_1] = 84 \text{ GPa}$, $E[e_2] = 4.0 \text{ GPa}$, while the deterministic Poisson ratios are taken as equal to $\nu_1 = 0.22$ in fibre and $\nu_2 = 0.34$ – in the matrix.

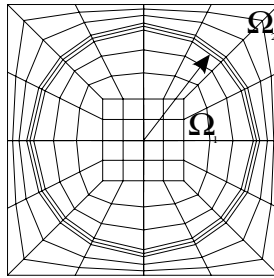


Figure 2.128. Periodicity cell tested

Five different sets of Young moduli coefficients of variation are analysed according to Table 2.21 – various values between 0.05 and 0.15 have been adopted to verify the influence of the component data randomness on the respective probabilistic moments of the homogenised elasticity tensor. The finite difference numerical technique has been employed to determine the relevant derivatives with respect to the input random variables adopted.

Table 2.21. The coefficient of variation of the input random variables

Test number	$\alpha(e_1)$	$\alpha(e_2)$
1	0.050	0.050
2	0.075	0.075
3	0.100	0.100
4	0.125	0.125
5	0.150	0.150

The cross-sectional fibre area equals to about a half of the total periodicity cell area. The results in the form of expected values and coefficients of variation of the homogenised tensor components obtained from four computational tests are shown in Table 2.22 and compared against the corresponding values obtained by using the MCS technique for the total number of random trials taken as 10^3 .

Table 2.22. Coefficients of variation for the effective elasticity tensor

Test	$\alpha(C_{1111}^{(eff)}(\omega))$		$\alpha(C_{1122}^{(eff)}(\omega))$	
	SFEM	MCS	SFEM	MCS
1	0.0410	0.0516	0.7152	0.0517
2	0.0622	0.0777	0.1073	0.0777
3	0.0830	0.1037	0.1430	0.1037
4	0.1036	0.1297	0.1788	0.1297
5	0.1244	0.1557	0.2146	0.1557

It is seen that the results of the SFEM-based computations are slightly smaller than those resulting from the Monte Carlo simulations in the case of $\alpha(C_{1111}^{(eff)}(\omega))$; the opposite trend is observed for $\alpha(C_{1122}^{(eff)}(\omega))$. The differences between both models are acceptable for very small input coefficients of variation and above the value 0.1 (second order approach limitation) they enormously increase. It is also observed that the coefficients from the MCS analysis are equal with each other, while the SFEM returns different values for both effective tensor components. It follows the fact that the first partial derivatives of both components with respect to Young moduli of the fibre and matrix are different. These derivatives are included in the SFEM equations for the second order moments and, in the same time, they do not influence the MCS homogenisation model at all. Furthermore, a linear dependence between the results obtained and the input coefficients of variation of the components Young moduli is observed.

The main reason for numerical implementation of the SFEM equations for modelling of the homogenisation problem is a decisive decrease in computation time in comparison to that necessary by the MCS technique. It should be mentioned that the Monte Carlo sampling time can be approximated as a product of the following times:

- (a) a single deterministic cell problem solution,
- (b) the total number of homogenisation functions required (three functions $\chi_{(11)}$, $\chi_{(12)}$ and $\chi_{(22)}$ in this plane strain analysis),
- (c) the total number of random trials performed.

There are some time consuming procedures in the MCS programs such as random numbers generation, post-processing estimation procedure and the subroutines for averaging the needed parameters within the RVE, which are not included, however their times are negligible in comparison with the routines pointed out before.

On the other hand, the time for Stochastic Finite Element Analysis can be approximated by multiplication of the following procedure times: (a) the SFE solution of the cell problem (with the same order of the cost considered as the deterministic analysis) and the total number of necessary homogenisation functions. Taking into account the remarks posed above, the difference in computational time between MCS and SFEM approaches to the homogenisation problem is of the order of about $(n-1)\tau$ provided that n is the total number of MCS samples and τ stands for the time of a deterministic problem solution. Observing this and considering negligible differences between the results of both these

methods for smaller random dispersion of input variables, the stochastic second order and second moment computational analysis of composite materials should be preferred in most engineering problems. The only disadvantage is the complexity of the equations, which have to be implemented in the respective program as well as the bounds dealing with randomness of input variables (the coefficients of variation should be generally smaller than about 0.15).

2.3.4 Upper and Lower Bounds for Effective Characteristics

Let us consider the coefficients of the following linear second order elliptic problem [65]:

$$- \operatorname{div}(\mathbf{C}^\varepsilon \boldsymbol{\varepsilon}(\mathbf{u}^\varepsilon)) = \mathbf{f}; \quad x \in \Omega \quad (2.230)$$

$$\boldsymbol{\varepsilon}_{ij}(\mathbf{u}^\varepsilon) = \frac{1}{2}(u_{i,j}^\varepsilon + u_{j,i}^\varepsilon); \quad x \in \Omega \quad (2.231)$$

$$\mathbf{C}^\varepsilon = \psi^{\varepsilon(p)}(x) \mathbf{C}^{\varepsilon(p)} \quad (2.232)$$

with boundary conditions

$$\mathbf{u}^\varepsilon = 0; \quad x \in \partial\Omega \quad (2.233)$$

In the above equations \mathbf{u}^ε , $\boldsymbol{\varepsilon}(\mathbf{u}^\varepsilon)$ and \mathbf{f} denote the displacement field, strain tensor and vector of external loadings, respectively. As was presented in Sec. 2.3.3.2, the effective (homogenised) tensor \mathbf{C}^0 is such a tensor that replacing \mathbf{C}^ε and \mathbf{C}^0 in the above system gives \mathbf{u}^0 as a solution, which is a weak limit of \mathbf{u}^ε with scale parameter tends to 0. It should be mentioned that without any other assumptions on Ω microgeometry the bounded set of effective properties is generated. Moreover, it can be proved that there exist such tensors $\inf(C_{ijkl})$ and $\sup(C_{ijkl})$ that

$$\inf(C_{ijkl}) \leq C_{ijkl}^0 \leq \sup(C_{ijkl}) \quad (2.234)$$

It is well known that the theorem of minimum potential energy gives the upper bounds of the effective tensor, whereas the minimum complementary energy approximates the lower bounds. Thanks to the Eshelby formula the explicit equations are as follows:

$$\begin{cases} \sup \kappa = \left[\sum_{r=1}^N C_r (\kappa_u + \kappa_r)^{-1} \right]^{-1} - \kappa_u \\ \sup \mu = \left[\sum_{r=1}^N C_r (\mu_u + \mu_r)^{-1} \right]^{-1} - \mu_u \end{cases} \quad (2.235)$$

where κ_u, μ_u have the following form:

$$\begin{cases} \kappa_u = \frac{4}{3} \mu_{\max} \\ \mu_u = \frac{3}{2} \left(\frac{1}{\mu_{\max}} + \frac{10}{9\kappa_{\max} + 8\mu_{\max}} \right)^{-1} \end{cases} \quad (2.236)$$

Further, lower bounds for the elasticity tensor are obtained as

$$\begin{cases} \inf \kappa = \left[\sum_{r=1}^N C_r (\kappa_l + \kappa_r)^{-1} \right]^{-1} - \kappa_l \\ \inf \mu = \left[\sum_{r=1}^N C_r (\mu_l + \mu_r)^{-1} \right]^{-1} - \mu_l \end{cases} \quad (2.237)$$

where it holds that

$$\begin{cases} \kappa_l = \frac{4}{3} \mu_{\min} \\ \mu_l = \frac{3}{2} \left(\frac{1}{\mu_{\min}} + \frac{10}{9\kappa_{\min} + 8\mu_{\min}} \right)^{-1} \end{cases} \quad (2.328)$$

and n is a total number of composite constituents where $c_r, 1 \leq r \leq n$ denote their volume fractions. It should be noted that

$$\kappa = \frac{e}{3(1-2\nu)} \quad (2.239)$$

$$\mu = \frac{e}{2(1+\nu)} \quad (2.240)$$

$$\lambda = \kappa - \frac{2}{3} \mu \quad (2.241)$$

$$C_{ijkl} = \delta_{ij} \delta_{kl} \lambda + (\delta_{ik} \delta_{jl} + \delta_{il} \delta_{jk}) \mu \quad (2.242)$$

From the engineering point of view the most interesting is the effectiveness of such a characterisation of C_{ijkl} , which can be approximated as the difference between upper and lower estimates and, on the other hand, sensitivity of the

effective tensor with respect to material characteristics of the constituents. The Monte Carlo simulation technique has been used to compute probabilistic moments of the effective elasticity tensor components for the periodic superconductor analysed before. The superconducting cable consists of fibres made of a superconductor placed around a thin-walled pipe (tube) covered with a jacket and insulating material. Experimental data describing elastic characteristics of the composite constituents are collected in Table 2.23.

Table 2.23. Probabilistic elastic characteristics of the superconductor components

Material	$E[e]$	$\sigma(e)$	$E[v]$	$\sigma(v)$
316LN	205 GPa	8 GPa	0.265	0.010
Incoloy 908 'annealed'	182 GPa	-	0.303	-
	'cold worked'	184 GPa	-	0.299
Titanium	126 GPa	12 GPa	0.311	0.012
Insulation G10-CR	36 GPa	-	0.21	-

Because of negligible differences in the elastic properties of Incoloy (between the 'annealed' and 'cold worked' state) the 'annealed' state of the superconductor is considered further. All the results obtained in the computational experiments have been collected in Table 2.24 and Figures 2.129–2.137. Because of the fact that the expected values appeared to be rather insensitive to the total number of random trials in the Monte Carlo simulations, results of the relevant convergence tests have been omitted in the tables and presented further in the figures. The expected values considered have been collected in Table 2.24 for $M=10,000$ random trials.

Table 2.24. Effective elasticity tensor components and their expected values (in GPa)

Effective property type	Analysis type					
	Deterministic			probabilistic		
	$C_{JJJ}^{(eff)}$	$C_{JKKJ}^{(eff)}$	$C_{JKJK}^{(eff)}$	$C_{JJJ}^{(eff)}$	$C_{JKKJ}^{(eff)}$	$C_{JKJK}^{(eff)}$
sup-VR	189.56	81.83	53.86	189.94	82.30	53.82
Sup	178.44	76.07	51.18	178.57	76.37	51.10
Inf	156.99	62.70	47.14	156.68	62.61	47.03
Inf-VR	137.93	51.86	43.03	137.54	51.71	42.92

Effective properties collected in this chapter (*sup*, *inf* in Table 2.24) have been compared with the Voigt–Reuss ones (*sup-VR*, *inf-VR* in Table 2.24). Considering the results obtained, it should be noted that these first approximators are generally more restrictive than the Voigt–Reuss ones. Further, it can be observed that deterministic values are, with acceptable accuracy, equal to the corresponding expected values. Thus, for relatively small standard deviations of the input elastic characteristics, the randomness in the effective characteristics can be neglected.

Finally, it can be noted that more restrictive bounds can be used to determine the effective elasticity tensor in a more efficient way. Taking as a basis the arithmetic average of the upper and lower bounds, the difference between these bounds is in the range of 13% for $C_{JJJ}^{(eff)}$ bound component, 19% for $C_{JKJK}^{(eff)}$ bound component and 8% for $C_{JKKJ}^{(eff)}$ bound component.

The following figures contain the results of the convergence analysis of the coefficient of variation, asymmetry and concentration with respect to increasing total number of Monte Carlo random trials. All these coefficients are presented for $C_{JJJ}^{(eff)}$ bounds in Figures 2.129, 2.132 and 2.135, for $C_{JKJK}^{(eff)}$ bounds in Figures 2.130, 2.133 and 2.136 and for $C_{JKKJ}^{(eff)}$ in Figures 2.131, 2.134 and 2.137. On the horizontal axes of these figures the total number of Monte Carlo random trials M is marked, while the vertical is used for the coefficient of variation.

General observation here is that the $C_{JKJK}^{(eff)}$ bounds are the most sensitive with respect to the randomness of input elastic characteristics. These coefficients for $C_{JKJK}^{(eff)}$ bounds appeared to be the greatest and then we obtain the coefficients for $C_{JJJ}^{(eff)}$ and $C_{JKKJ}^{(eff)}$, respectively. Next, it can be mentioned that the estimators of the coefficients of variation show fast convergence to their limits. Efficient approximation of final coefficients for various components of the tensor $C_{ijkl}^{(eff)}$ bounds is obtained for M equal to about 2,500 random trials. Generally, it is observed that the coefficients of variation of effective elasticity tensor fulfil the inequalities detected in case of the expected values. The greatest coefficients are obtained for Reuss bounds, next the upper and lower bounds proposed in this chapter, and the smallest for the Voigt lower bounds.

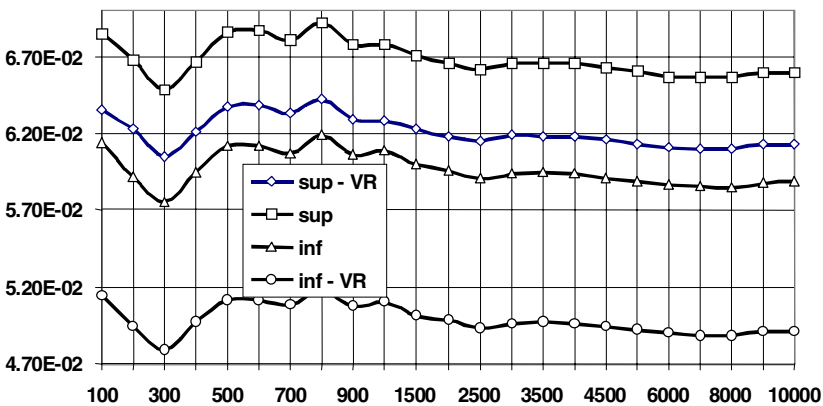


Figure 2.129. The coefficients of variation of $C_{JJJ}^{(eff)}$ bounds

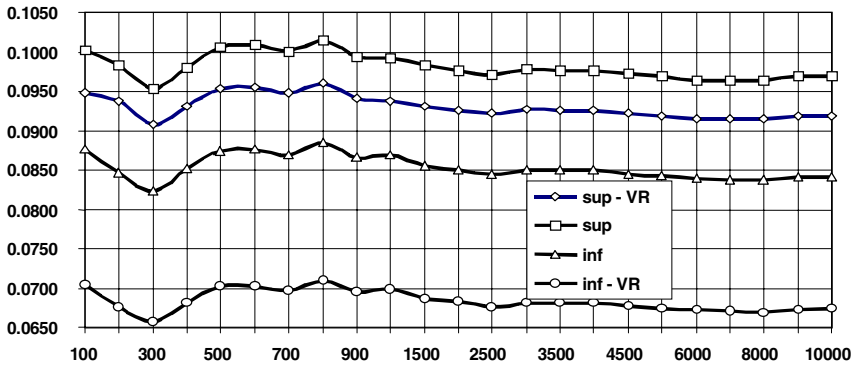


Figure 2.130. The coefficients of variation of $C_{JKJK}^{(eff)}$ bounds

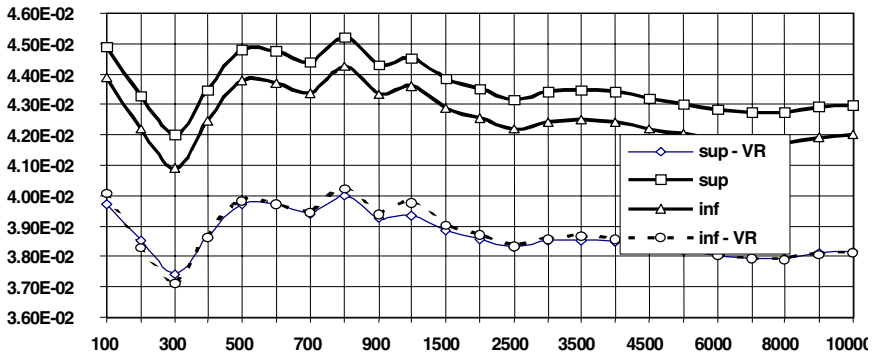


Figure 2.131. The coefficients of variation of $C_{JKKJ}^{(eff)}$ bounds

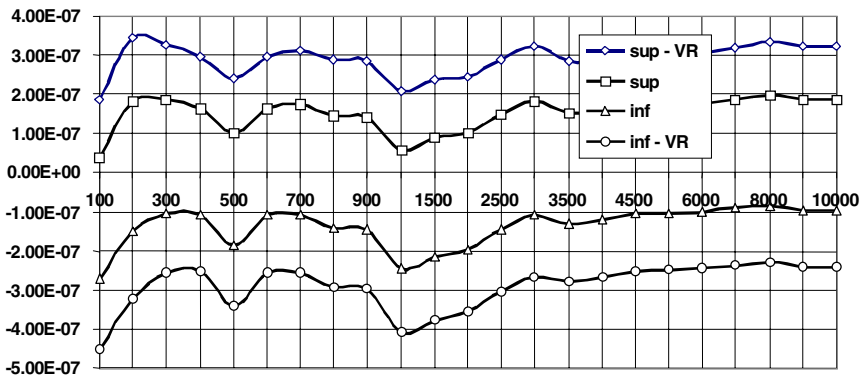


Figure 2.132. The coefficients of asymmetry of $C_{JJJJ}^{(eff)}$ bounds

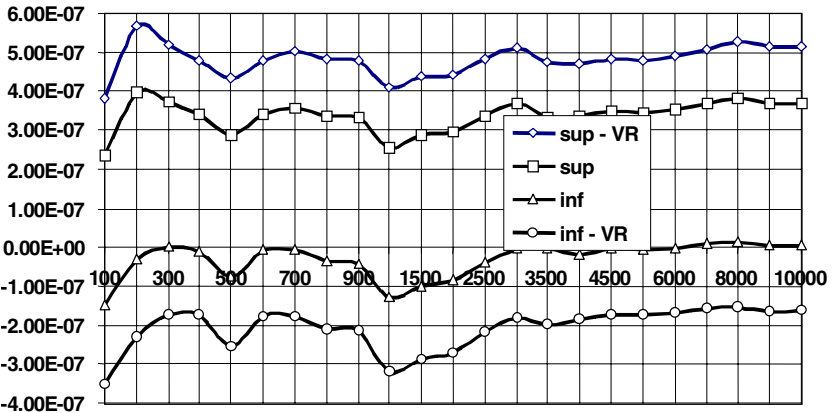


Figure 2.133. The coefficients of asymmetry of $C_{JKJK}^{(eff)}$ bounds

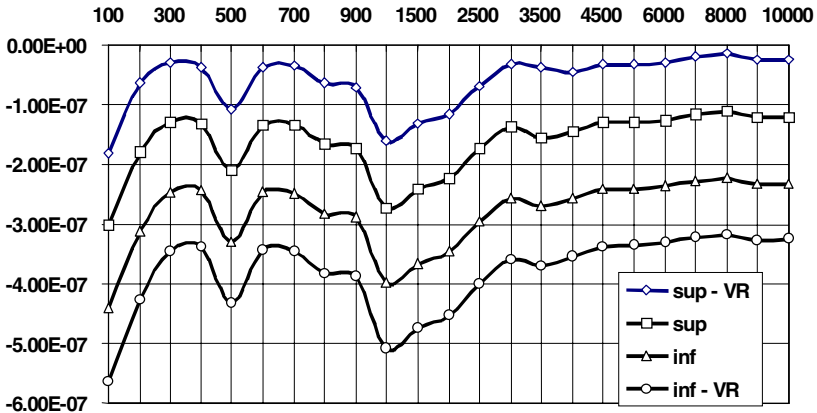


Figure 2.134. The coefficients of asymmetry of $C_{JKKJ}^{(eff)}$ bounds

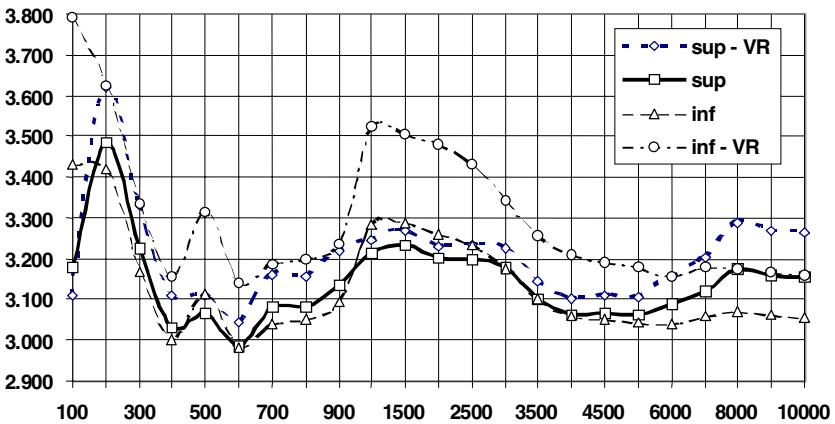


Figure 2.135. The coefficients of concentration of $C_{JJJ}^{(eff)}$ bounds

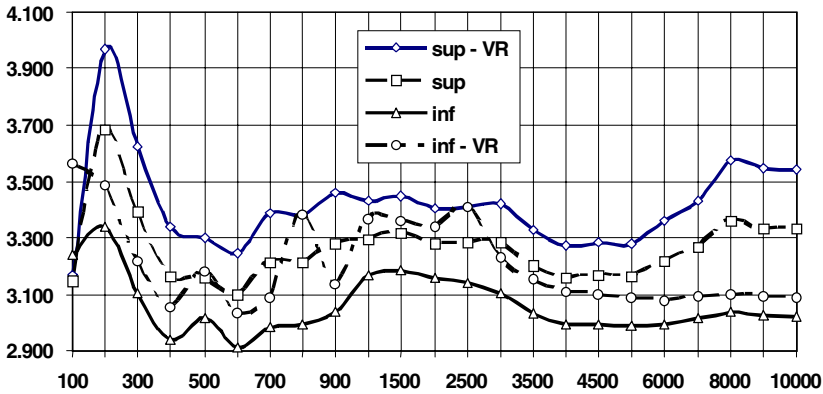


Figure 2.136. The coefficients of concentration of $C_{JKJK}^{(eff)}$ bounds

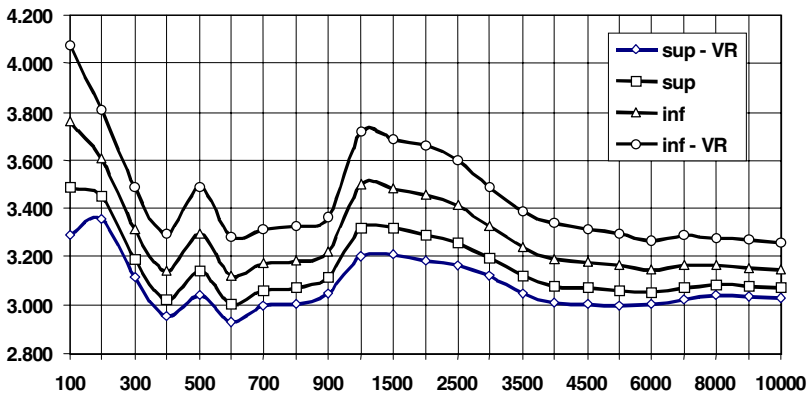


Figure 2.137. The coefficients of concentration of $C_{JKKJ}^{(eff)}$ bounds

Observing the results presented in Figures 2.132 and 2.134 it can be observed that all coefficients of asymmetry of $C_{ijk}^{(eff)}$ verified tend to 0 with increasing total number of random trials. Comparing $C_{JJJ}^{(eff)}$ and $C_{JKJK}^{(eff)}$ against $C_{JKKJ}^{(eff)}$ bounds it can be stated that the first two variables have minimum positive asymmetry, while the last have a negative one. It should be mentioned that for such probabilistic distributions with non-zero coefficients of asymmetry, the expected value is not equal to the most probable one.

Moreover, taking into account the convergence of coefficients of asymmetry it is seen that they are generally more slowly convergent than coefficients of variation estimators. M larger than 5,000 is required to compute these estimators with satisfactory accuracy. Analogous to the coefficients of variation, the hierarchy of the expected values of $C_{ijk}^{(eff)}$, which has been discussed above, is fulfilled.

Figures 2.135–2.137 present the coefficients of concentration for different components of the effective elasticity tensor. The estimator convergence analysis proves that M equal to almost 10,000 is needed to compute these coefficients properly. The convergence of these estimators is more complex than the previous ones, but generally their values are greater than 3, which is characteristic for the Gaussian variables. Thus it can be stated that the $C_{ijkl}^{(eff)}$ probabilistic distributions obtained are more concentrated around their expected values than the Gaussian variables, but this difference is no greater than a maximum of 15% for the $C_{JKJK}^{(eff)}$ bounds.

Figures 2.138–2.140 illustrate the probability density functions of the upper and lower bounds for $C_{JJJJ}^{(eff)}$, $C_{JKJK}^{(eff)}$ and $C_{JKKJ}^{(eff)}$ components of the effective elasticity tensor. On the horizontal axes of these figures the values computed for these components are marked, while on the vertical axes the relevant probability density function (PDF) is given.

The PDFs for the tensor $C_{ijkl}^{(eff)}$ computed together with the additional coefficients of asymmetry and concentration β , γ show that these functions have distributions quite similar to the bell-shaped Gaussian distribution curve. Thus, in further analyses proposed in the conclusions, we assume that for the input random variables being elastic characteristics (Young moduli and Poisson ratios) being Gaussian uncorrelated random variables, the upper and lower bounds computed having also a Gaussian distribution, which essentially simplifies further estimation and related numerical analyses.

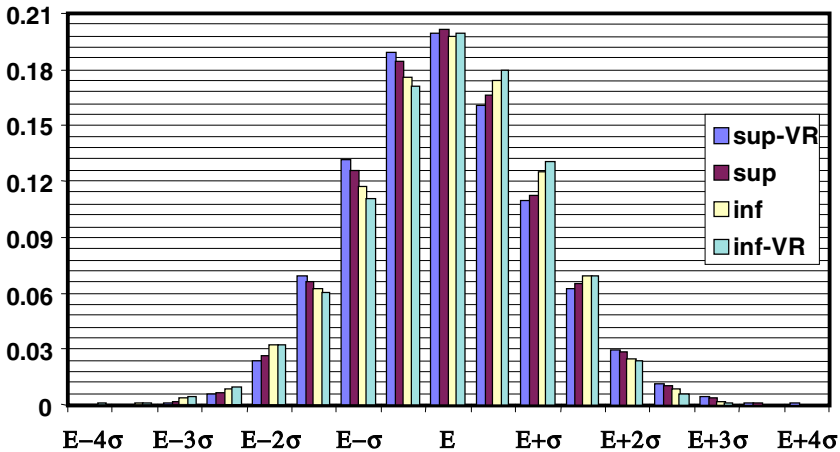


Figure 2.138. The probability densities of $C_{JJJJ}^{(eff)}$ bounds

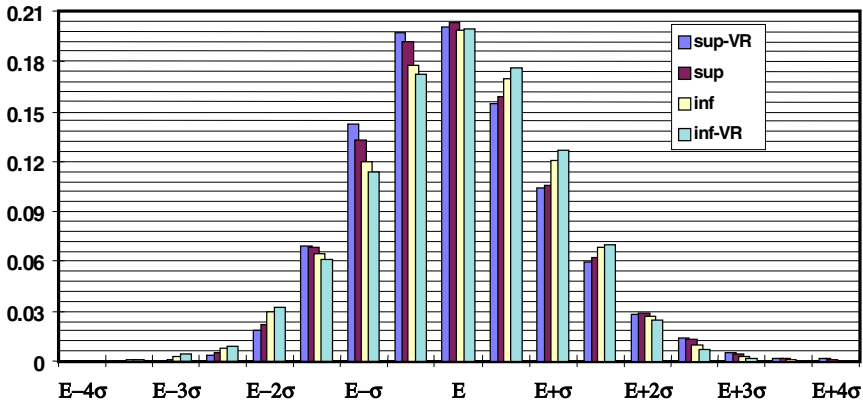


Figure 2.139. The probability densities of $C_{JKK}^{(eff)}$ bounds

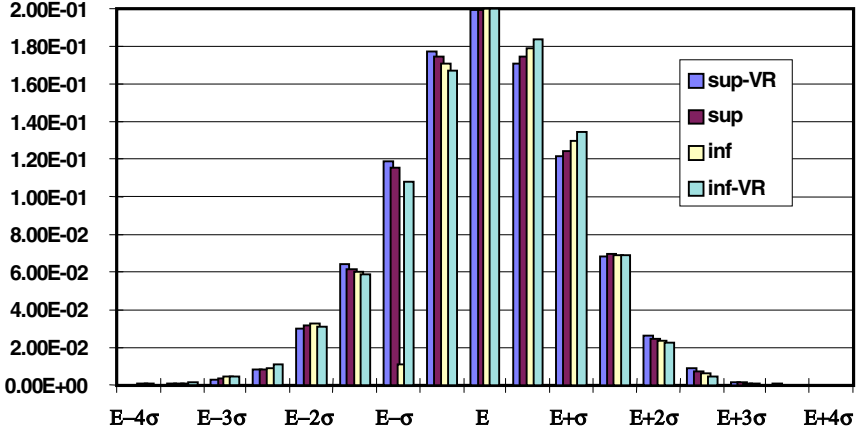


Figure 2.140. The probability densities of $C_{JKK}^{(eff)}$ bounds

The results of numerical tests performed lead us to the conclusion that the probabilistic upper and lower bounds of the effective elasticity tensor may be very efficient in the characterisation of superconducting composites with randomly defined elastic characteristics because of negligible relative differences between the upper and lower bounds. Considering the computational time cost they appear to be much more useful in engineering practice than other FEM-based direct methods.

Computational experiments carried out prove that the coefficients of variation of the bounds computed are in the range of the input random variables of the problem. Considering further analyses of homogenised superconducting coils, this fact confirms the need for the application of the SFEM in such computations, which is important for essential time savings in comparison with the simulation methods.

The probabilistic sensitivity of the effective elastic characteristics with respect to the probabilistic material parameters should be verified computationally in

further analyses as an effect of regression test, for instance. Such an analysis enables us to find out these parameters of composite constituent elastic characteristics, which are the most influencing for global superconductor behaviour.

The procedure for effective elastic properties approximation seems to be the only method, which can be successfully applied to the homogenisation of stochastic interface defects. Such an approach will make the elastic properties of the interphases much more sensitive to the presence of structural defects than was in case of the Probabilistic Averaging Method. Considering this, the bounds presented should be implemented in numerical analysis of stochastic structural defects into the artificial composite interphases.

2.3.5 Effective Constitutive Relations for the Steel Reinforced Concrete Plates

The homogenisation method proposed for composite plates analysis is not based on any mathematical model. However it seems to be very effective for high contrast steel–reinforced concrete plates [160]. The next main reason to apply this model is that the composite plate need not be periodic in the applied approach, which perfectly reflects the civil engineering needs. To get the effective characterisation for the elasticity tensor, Eshelby theorem can be used since upper and lower bounds for this tensor are determined. However it is proved by comparison with collected experimental results, either lower and upper bounds are very effective in computational modelling of a real plate. Both of them can be used to calculate the zeroth, first and second order stiffness matrix and the resulting probabilistic moments of displacements and stresses for the composite plate during the SFEM analysis. It decisively simplifies the numerical analysis in comparison to the traditional FEM modelling of such structures (where reinforcement discretisation is complicated); more accurate results, especially in terms of thin periodic plate vibration analysis, are shown in [155]. Finally, it should be mentioned that the homogenised effective characteristics for composite shells can be derived analogously, following considerations presented in [227,338].

Numerical test deals with the homogenisation of steel–reinforced concrete plates characterised by the data collected in Table 2.25; the coefficients of variation randomized Young moduli are taken as 0.1 as in all previous experiments. The concrete rectangular plate with horizontal dimensions 0.90 m x 0.90 m and thickness 0.045 m, supported at its corners and loaded by the vertical concentrated force is examined and Table 2.26 contains the deterministic and probabilistic homogenisation output. It can be observed that, as in previous examples, the deterministic and expected values are close to each other, respectively, and the resulting coefficients of variation are obtained as smaller or equal to those taken for input random variables.

Table 2.25. Material data of the composite plate

Material properties	Steel	Concrete
Young modulus	200.0 GPa	28.6 GPa
Poisson ratio	0.30	0.15
Volume fraction	0.0367	0.9633
Yield stress	345.0 GPa	20.68 GPa

Table 2.26. Effective materials characteristics

Effective elasticity tensor components	Deterministic	Expected value	Variation
$E[\text{inf}(C_{1111})]$	42.53 GPa	42.52 GPa	0.0985
$E[\text{sup}(C_{1111})]$	44.84 GPa	44.84 GPa	0.0905
$E[\text{inf}(C_{1212})]$	13.13 GPa	13.12 GPa	0.0982
$E[\text{sup}(C_{1212})]$	13.88 GPa	13.88 GPa	0.0896
$E[\text{inf}(C_{1122})]$	16.27 GPa	16.28 GPa	0.0991
$E[\text{sup}(C_{1122})]$	17.09 GPa	17.09 GPa	0.0896

The most important observation is that the lower and upper bounds are almost equal for any of the effective elasticity tensor components. Thus it does not matter which of them are used in the approximation of the real composite structure. Hence, the very complicated discretisation process of this particular concrete structure type (ABAQUS) can be replaced with an analysis of the homogeneous plate with elasticity tensor components calculated as proposed above. After successful verification of other reinforced concrete plates with various combinations of input parameters, such formulas for the effective elasticity tensor could be incorporated in the finite element stiffness formation process to speed up the FEM modelling procedures for these structures.

The variability analysis for expected values and the coefficients of variation of the effective elasticity tensor is presented in Figures 2.141 and 2.142 as a function of Young moduli expectations of the steel and concrete. It is seen that the Young modulus of the concrete matrix is detected as a crucial parameter for both probabilistic moments. It is due to the fact that the matrix is the dominating component (in the volumetric context) while the equations for homogenised tensor are rewritten as functions of the volume ratios of the composite components.

Considering the above, the behaviour of a real composite is compared against the homogenised one, cf. Figure 2.143. It is seen that the central deflection increments for both models are almost equal in the elastic range and, further, some expressions for the nonlinear range should be proposed and verified.

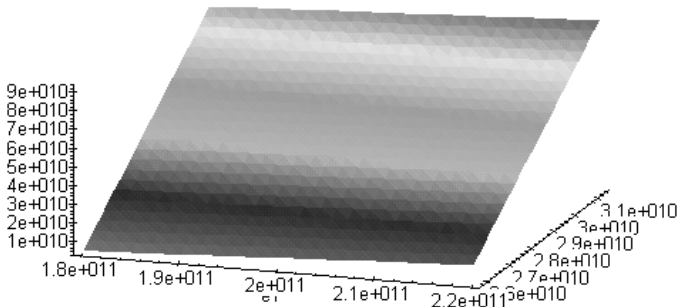


Figure 2.141. Expected value of upper bound for the component C_{1111}

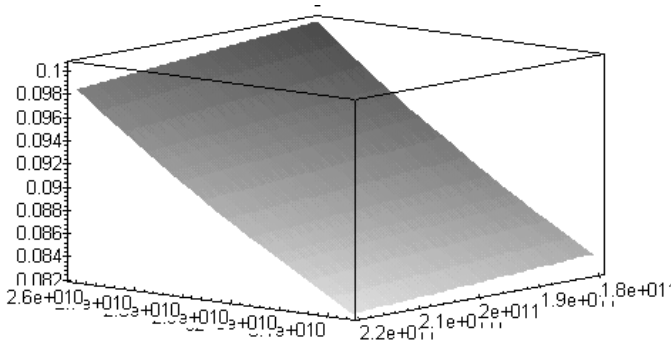


Figure 2.142. Coefficient of variation of upper bound for the component C_{1111}

A very broad discussion on theoretical and numerical modelling concepts in reinforced concrete structures have been presented in [22] – fracture analysis contained in this study can be incorporated into the SFEM using the approach described in [33]. Future analyses devoted to the application of homogenisation technique in reinforced plates modelling should focus on incorporation of the microcracks appearing in real matrices. It can be done using initial homogenisation of the cracks into the matrix [92,266,321] to find equivalent homogeneous medium; further homogenisation follows the above considerations.

Taking into account all the results of this test as well as the previous analyses on the homogeneous plates with random parameters, the application of the Stochastic Finite Element Method for the homogenised plate should approximate the probabilistic moments of displacements [63] in linear elastic range for the real plate very well. The expected values and variances of the effective elasticity tensor can be obtained for this purpose by using symbolic MAPLE computations analogous to those presented above.

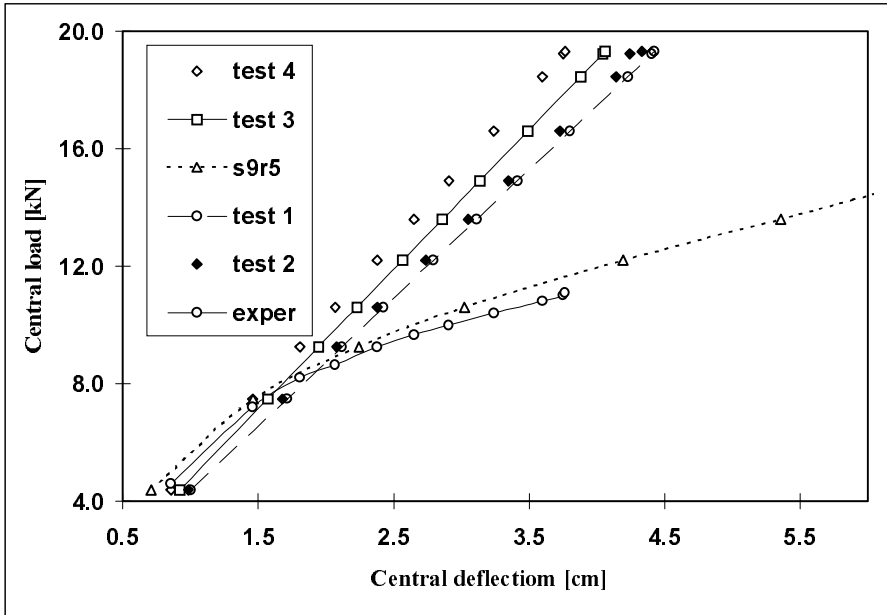


Figure 2.143. Vertical displacements of the composite plate centre

2.4 Conclusions

The main advantage of the homogenisation approach proposed is that any randomness in geometry or elasticity of the composite structures is replaced by a single effective random variable of the elasticity tensor components characterising such a structure. Hence, computational studies of engineering composites with different random variables using a homogeneous one with deterministically defined geometry and equivalent probability density function of the elastic properties can be carried out. It is observed that using an analytical expression for the homogenised elastic properties, the randomness in geometry for the periodicity cell can be introduced and can result in random fluctuations of the effective parameters only. Furthermore, even if the composite structure is not periodic, the results of homogenisation method application are satisfactory, i.e. the probabilistic response of the structure homogenised approximates very well the real composite model; analytical solution in the correlative approach for random quasi-periodic structures can be found in [278].

The basic value of the proposed homogenisation method is that the equations for the expected values and covariances of effective characteristics do not depend on the PDF type of the input random fields. However, in case of greater values of higher order probabilistic moments related to the first two as well as the lack of the

PDFs symmetry, a higher order version of the perturbation method is recommended. It is important since the probability density function of the input may not always be assumed properly, while in most experimental cases it is a subject of the statistical approximation only. Application of a stochastic higher order perturbation technique is relatively easy for closed form homogenisation equations considering the symbolic differentiation approach. It should be emphasised that, taking into account the capability of MAPLE links with FORTRAN routines, the program can be used in further SFEM computations as an intermediate procedure for symbolic homogenisation and sequential order perturbation derivation.

It should be underlined that the method proposed can find its application in stochastic reliability studies (SOSM approach) for various composite structures. This homogenisation technique makes it possible to reduce significantly the total number of degrees of freedom for such a structure, while the expected values and covariances of displacements and stresses enable one to estimate the second order second moment reliability (SORM) index or even third order reliability coefficients (W-SOTM). In the same time, both probabilistic methodologies have [171,175,180] and can find further applications in determination of effective heat conductivity coefficients in various models [216,294] including fibre-reinforced structures with some interfacial thermal resistance [303].

Due to the satisfactory accuracy of the homogenisation approach in modelling of composite structures, the model worked out can be treated as the first step for so-called self-homogenising finite elements, where the computer program automatically homogenises the entire structure using original material composite characteristics and finally calculates the displacements and stresses probabilistic moments for an equivalent homogeneous medium. On the other hand, the stochastic perturbation homogenisation procedure can be further modified for elastoplastic composite structures using Transformation Field Analysis (TFA) or Fast Fourier Transform (FFT) approaches. In the same time, the study of stochastic elastodynamic effective behaviour is recommended since the still growing range of composites has possible engineering applications.

2.5 Appendix

We prove, in the context of the composite model introduced in this chapter, that $\mathbf{u}(\mathbf{x}, \mathbf{y})$ being a solution of problem (2.121) is constant in the region Ω . For this purpose, let us consider $\mathbf{u}(\mathbf{y})$ being a Ω -periodic displacement function and the solution of the following boundary value problem:

$$\left\{ \begin{array}{l} -\frac{\partial}{\partial y_j} \sigma_{ij} = F_i(\mathbf{y}), \mathbf{x} \in \Omega \\ \sigma_{ij} = C_{ijkl}(\mathbf{y}) \varepsilon_{kl}(\mathbf{u}), \mathbf{x} \in \Omega_1 \cup \Omega_2 \\ |\sigma_N| = g(\mathbf{y}), \mathbf{x} \in \Gamma_r, r = 1, \dots, m \end{array} \right. \quad (\text{A2.1})$$

where $g(\mathbf{y})$ are given functions defined on Ω or Γ_r , $r=1, \dots, m$ with m being the total number of various interface boundaries. The variational formulation of (A2.1) may be stated as follows:

$$-\sum_{r=1}^m \int_{\Gamma_r} \sigma_{ij} n_j v_i d\Gamma + \sum_{a=1}^n \int_{\Omega_a} \sigma_{ij} \varepsilon_{ij}(\mathbf{v}) d\Omega = \int_{\Omega} f_i v_i d\Omega \quad (\text{A2.2})$$

for $\mathbf{v} \in V$ being the following space:

$$V = \left\{ v_i; v_i \in [H^1(\Omega_i)]^3; [v_i] = 0 \text{ on } \Gamma_r; r = 1, \dots, m \right\} \quad (\text{A2.3})$$

while the corresponding components of the vector \mathbf{v} are equal on the two opposite faces of Ω . Taking into account these conditions and neglecting body forces, we arrive at the well-known relation, cf. (2.121):

$$a(\mathbf{u}, \mathbf{v}) = L(\mathbf{v}) \quad (\text{A2.4})$$

If $v_i = c$ is taken, which belongs to the set C of vectors constant on Ω , there holds for all $c \in C$

$$L(c) = 0 \quad (\text{A2.5})$$

Thus, if $g(\mathbf{y})$ from (A2.1) is such that $L(c) \neq 0$, there is no solution for the problem (A2.1). Next, let us introduce the space $S=V/C$ and let us denote by $\|\cdot\|_k$ the norm in $[H^1(\Omega_k)]^3$ and by $\|\cdot\|_k$ the norm in $L^2(\Omega_k)$. Let us observe that

- (1) V is a subspace of $\tilde{V} : [H^1(\Omega_1)]^3 \times [H^2(\Omega_2)]^3$;
- (2) \tilde{V} is a Hilbert space for the norm

$$\|\mathbf{v}\| = \left(\|v_1\|_1^2 + \|v_2\|_2^2 \right)^{\frac{1}{2}} \quad (\text{A2.6})$$

- (3) There holds

$$\|\mathbf{v}\|_k^2 = \sum_{i,j} |\varepsilon_{ij}(\mathbf{v})|_k^2 + \sum_i |v_i|_k^2 \quad (\text{A2.7})$$

(4) (A8) may be written equivalently as

$$\|\mathbf{v}\| = \left(\|v_1\|_1^2 + \sum_{i,j} |\varepsilon_{ij}(v_2)|_2^2 \right)^{\frac{1}{2}} \quad (\text{A2.8})$$

(5) It can be proved that S is an Hilbert space for the norm

$$\|\mathbf{v}\| = \operatorname{Inf}_{c \in C} \|\mathbf{v} + c\| \quad (\text{A2.9})$$

(6) The norm equivalent to (A2.9) on space S may be rewritten as

$$N(\mathbf{v}) = \left(\sum_{i,j} |\varepsilon_{ij}(\mathbf{v})|_1^2 + \sum_{i,j} |\varepsilon_{ij}(\mathbf{v})|_2^2 \right)^{\frac{1}{2}} \quad (\text{A2.10})$$

If we prove the statement (6) thus, due to the fact that $N(\mathbf{v})$ is continuous as well as coercive on space S and, further, applying the Lax–Millgram theorem we arrive at the conclusion that there exists a unique solution for (A2.1). To show this fact let us note that

$$\|\mathbf{v}\|^2 = \operatorname{Inf}_{c \in C} \|\mathbf{v} + c\|^2 = N^2(\mathbf{v}) + \operatorname{Inf}_{c \in C} \|v_1 + c\|_1^2 \quad (\text{A2.11})$$

where

$$\|\mathbf{v}\|^2 \leq N^2(\mathbf{v}) \quad (\text{A2.12})$$

There exists such a constant c_1 that for all $\mathbf{v} \in W$ that there holds

$$\|\mathbf{v}\|^2 \leq c_1 N^2(\mathbf{v}) \quad (\text{A2.13})$$

Let us introduce the orthogonal projection operator O such that

$$O : (L^2(\Omega_1))^3 \rightarrow C \quad (\text{A2.14})$$

with respect to the scalar product corresponding to $\|\cdot\|_1$. It yields

$$\|\mathbf{v}\|^2 = N^2(\mathbf{v}) + |v_1 - O v_1|_1^2 \quad (\text{A2.15})$$

Equation (A2.15) is true if and only if for all $\mathbf{v} \in V$ there holds

$$|v_1 - O v_1|_1^2 \leq c_1 N^2(\mathbf{v}) \quad (\text{A2.16})$$

We assume that it is possible to improve $\mathbf{v}^n = (v_1^n, v_2^n) \in V$ for any positive n such that

$$\left|v_1^n - Ov_1^n\right|_1^2 = 1, \quad N^2(\mathbf{v}^n) \leq \frac{1}{n} \quad (\text{A2.17})$$

Setting $\mathbf{w}^n = (v_1^n - Ov_1^n, v_2^n - Ov_2^n)$ we get for all $c \in C$ that

$$N^2(\mathbf{w}^n) \leq \frac{1}{n}; \quad |w_1^n|_1 = 1; \quad (w_1^n, c) = 0 \quad (\text{A2.18})$$

Then, $\{\mathbf{w}^n\}$ is bounded in V and there exists such a subsequence $\{\mathbf{w}^m = (w_1^m, w_2^m)\}$, which converges weakly to w_0 in V . Since that, w_1^m converges strongly in $(L^2(\Omega_1))^3$

$$|w_1^0|_1 = 1 \quad (\text{A2.19})$$

Due to the lower semi-continuity there holds

$$N^2(\mathbf{w}^0) \leq \underline{\lim} N^2(\mathbf{w}^m) = 0 \quad (\text{A2.20})$$

Finally, it is obtained that

$$\varepsilon_{ij}(w_1^0) = 0; \quad \varepsilon_{ij}(w_2^0) = 0 \quad (\text{A2.21})$$

which gives as the result

$$w_1^0 = w_2^0 = c \in C \quad (\text{A2.22})$$